

Group-based approaches to space-time multiuser detection in WCDMA

Benoît Pelletier



Department of Electrical & Computer Engineering
McGill University
Montréal, Canada

October 2007

A thesis submitted to McGill University in partial fulfillment of the requirements for the degree of Doctor of Philosophy.

© 2007 Benoît Pelletier

Abstract

Mobile telephony has now become a commodity in most industrialized countries. While voice communications still dominate, data services are expected to be prevalent in the future. Efficient use of the radio spectrum is essential to offer voice and data wireless mobile communications services at a competitive price. Third Generation cellular systems are based on code-division multiple access technology and suffer from multiple-access interference, which limits system capacity. Several approaches exist to mitigate this interference, including multiuser detection and beamforming. To reduce the complexity of the space-time multiuser detection, it has been proposed recently to exploit the spatial dimension offered by an antenna array at the receiver, by forming groups of users and apply detection individually to each group.

In this work, new space-time receiver structures derived from the group-optimal minimum mean square error (MMSE) linear detector are proposed and studied for the up-link. In particular, the optimal group-based linear space-time multiuser detection block-receiver with and without beamforming is derived. The family of group-based multiuser detection structures introduces inter-group-interference (IGI), which is caused by the non-orthogonality between groups. To overcome this limitation, new multistage group-based receiver structures based on successive interference cancellation and parallel interference cancellation are derived and studied. In addition, it is proposed to take advantage of the full computational capabilities of practical receiver structures by introducing non-mutually exclusive grouping. Furthermore, the computational complexity of the proposed structures is studied in details. Finally, the computer simulation results demonstrate that the proposed reduced-complexity group-based approaches proposed provide a bit error rate performance close to that of the full linear MMSE multiuser detector, at a fraction of the computational cost.

Sommaire

La téléphonie sans fil mobile est maintenant devenue monnaie courante dans la plupart des pays industrialisés. Malgré la prédominance actuelle des communications vocales, les services de données numériques devraient les surpasser d'ici quelque temps. Dans ce contexte, une utilisation pleine et efficace du spectre radio devient essentielle afin d'offrir ces services à prix compétitif. Les systèmes de communications cellulaires de troisième génération (3G) sont fondés sur la technologie utilisant l'accès multiple par répartition en code (AMRC). La capacité de ces systèmes est limitée par le brouillage d'accès multiple (BAM). Plusieurs techniques existent afin de réduire les effets non désirés du BAM, notamment la détection multi-usagers (DMU) et le filtrage spatial. Afin de réduire la complexité du calcul reliée à la DMU, certains chercheurs ont récemment suggéré d'exploiter la dimension spatiale grâce aux réseaux d'antennes au récepteur. Les usagers mobiles sont partagés en groupes, et chaque groupe est détecté individuellement avec un récepteur de DMU.

Dans ce mémoire, de nouvelles structures de récepteurs spatio-temporels fondées sur le filtrage linéaire optimal, minimisant l'erreur quadratique moyenne (MEQM), sont étudiées. En particulier, le récepteur en bloc spatio-temporel, optimisé pour la détection par groupe d'usagers, avec et sans filtrage spatial indépendant, est suggéré et étudié. Comme toute structure fondée sur le groupage, cette structure crée du brouillage inter-groupe (BIG), dû à la non-orthogonalité des signaux entre les groupes. Afin de réduire ce BIG, de nouvelles structures de récepteurs dérivées de l'annulation d'interférence par succession et de la cancellation d'interférence en parallèle sont étudiées. De plus, en permettant le partage des usagers entre groupes par groupage non exclusif, il devient possible d'exploiter au maximum la capacité de calcul des récepteurs et d'y améliorer la performance. Ensuite, la complexité des calculs des diverses structures est étudiée en détail. Finalement, les résultats provenant des simulations informatiques démontrent que les structures par groupe étudiées donnent un taux d'erreur sur les bits similaire à celui du filtre MEQM sans groupage, et ce à moindre coût en terme de calculs.

Acknowledgments

The completion of this thesis would not have been possible without the advice, guidance and support of my supervisor, Prof. Benoît Champagne to which I am forever grateful. I would like to thank the Natural Sciences and Engineering Research Council of Canada (NSERC), the Fonds de recherche sur la nature et les technologies (FQRNT), InterDigital Canada Ltée., and the Communications Research Center for providing the financial support to carry this research. Also, I would like to thank the CLUMEQ Supercomputer Center and its dedicated staff for providing the computational resources and support necessary to complete this work.

I would like to thank Prof. Tho Le-Ngoc and Prof. Xiao-Wen Chang, members of my Ph.D. committee, for their feedback and suggestions.

During my stay at McGill University, I have met many dedicated students, faculty and staff who have contributed to make this experience memorable. I am particularly grateful to my fellow graduate students in the Telecommunications and Signal Processing Laboratory, and especially to François and Joachim, for their companionship and for creating such an exciting work environment. I would also like to thank my research assistant, Jim Huang.

I am forever indebted to my family for their love, support and encouragement throughout my life. Foremost, my deepest gratitude goes to my wife Kim for her unconditional love, understanding and patience throughout my studies.

Contents

1	Introduction	1
1.1	Overview of receiver technology for cellular systems	1
1.2	Group-based receivers combining MUD and beamforming	5
1.3	Research objectives and methodology	6
1.4	Contributions and claim of originality	8
1.5	Thesis organization	10
2	Background	13
2.1	Overview of cellular systems	13
2.1.1	The cellular concept	13
2.1.2	The mobile channel	17
2.2	Received signal model	22
2.3	Conventional receiver	25
2.4	Equivalent matrix-based signal model	29
2.5	Space-time multiuser detection	33
3	Group-based approaches to multiuser detection	39
3.1	Motivation	39
3.2	Group-based linear MUD	40
3.2.1	Group-based linear MUD with beamforming	45
3.2.2	Optimal MMSE group-based linear space-time MUD	50
3.3	Non-mutually exclusive grouping: user sharing	54
3.4	Complexity analysis	60
3.4.1	Full STMUD	61
3.4.2	GRP-STMUD-BF	63

3.4.3	GRP-STMUD	65
3.4.4	User sharing with MMSE combining	67
3.4.5	Summary	69
4	Group-based multistage receiver structures	71
4.1	Motivation	71
4.2	Group-based successive interference cancellation	72
4.2.1	Single-stage group-based SIC	72
4.2.2	Multistage group-based SIC	76
4.2.3	Convergence analysis	80
4.3	Group-based parallel interference cancellation	83
4.3.1	Multistage group-based PIC	83
4.3.2	Convergence analysis	91
4.3.3	Multistage group-based PIC with weighting	95
4.4	Complexity analysis	97
4.4.1	Single-stage GRP-SIC	97
4.4.2	MS-GRP-SIC	98
4.4.3	MS-GRP-PIC	99
4.4.4	Summary	101
5	Grouping algorithms	103
5.1	Motivation	103
5.2	Grouping cost function	105
5.2.1	Grouping notation	106
5.2.2	MSE-based cost function	106
5.2.3	Simplified cost function	107
5.3	Proposed grouping algorithms	110
5.3.1	Grouping criterion	110
5.3.2	Mutually exclusive grouping	113
5.3.3	Grouping with user sharing	114
5.4	Group ordering for SIC	118
5.5	Complexity analysis	119
5.5.1	Mutually exclusive grouping	119

5.5.2	Non-mutually exclusive grouping	121
5.5.3	Summary	122
6	Results	125
6.1	Methodology	126
6.1.1	Space-time channel model	126
6.1.2	Group-based receiver parameters	129
6.1.3	BER measurements	129
6.2	BER performance comparison	130
6.2.1	GRP-STMUD-BF	130
6.2.2	GRP-STMUD with user sharing	132
6.2.3	Iterative and multistage receiver structures	136
6.3	Grouping algorithms	143
6.4	Complexity comparison	146
7	Summary and conclusion	153
7.1	Summary of the work	153
7.2	Concluding remarks	155
7.3	Future work	156
A	Derivation of the various MMSE linear filters	159
A.1	Optimal MMSE linear filter for the GRP-STMUD-BF receiver	159
A.2	Optimal MMSE linear filter for the GRP STMUD receiver	161
A.3	Optimal MMSE linear combining weights for user sharing	162
A.4	Optimal MMSE linear weights for the single-stage GRP-SIC	164
B	Complexity analysis	167
B.1	Block Toeplitz Cholesky factorization	168
B.2	Block triangular backsubstitution	170
C	Exact bit-error probability for BPSK	173
	References	175

List of Figures

1.1	Group-based STMUD receiver with beamforming.	5
2.1	Example of a cellular network.	14
2.2	Radio wave reflection.	19
2.3	Simulated channel small scale fading.	21
2.4	Spatial dispersion and angular spread.	22
2.5	Conventional CDMA receiver block diagram.	27
2.6	Block diagram for the full STMUD receiver.	34
3.1	Conceptual diagram for group-based linear MUD receiver structures.	40
3.2	Linear group detection module for the GRP-STMUD-BF receiver.	46
3.3	Linear group detection module for the GRP-STMUD receiver.	53
3.4	GRP-STMUD receiver with MMSE combining.	58
3.5	GRP-STMUD with selective combining.	60
4.1	Block diagram for the GRP-SIC receiver.	73
4.2	Block diagram for the MS-GRP-SIC receiver.	77
4.3	Block diagram for the MS-GRP-PIC receiver.	88
5.1	Flow diagram for the grouping algorithm without sharing.	115
5.2	Flow diagram for the grouping algorithm extension for user sharing.	117
6.1	GRP-STMUD-BF receiver average BER performance.	131
6.2	GRP-STMUD receiver average BER performance.	133
6.3	User cross-correlation power.	134
6.4	GRP-STMUD receiver BER performance for user # 8	135

6.5	GRP-STMUD receiver average BER with a single dominant user.	136
6.6	GRP-SIC and MS-GRP-SIC BER performance.	137
6.7	MS-GRP-SIC BER convergence.	138
6.8	MS-GRP-PIC receiver BER performance for Config-1.	139
6.9	MS-GRP-PIC weighting strategies	140
6.10	BER convergence of the MS-GRP-PIC receiver with Chebyshev weighting .	141
6.11	CDF of SNR gain when using user sharing with MS-GRP-PIC receiver. . .	143
6.12	BER convergence for MS-GRP-PIC for users in extended groups	144
6.13	Normalized MSE difference of grouping algorithms.	147
6.14	Complexity comparison for group-based receivers.	148
6.15	Complexity comparison for multistage receivers.	149

List of Tables

2.1	Typical system parameter values for UTRA/TDD.	25
3.1	Relevant system parameters for the complexity analysis.	61
3.2	Full STMUD receiver complexity.	62
3.3	GRP-STMUD-BF receiver complexity.	64
3.4	GRP-STMUD receiver complexity.	66
3.5	MMSE combining complexity.	68
3.6	Receiver structures complexity summary.	69
4.1	Typical grouping example with conventional and shared users	84
4.2	GRP-SIC receiver complexity.	98
4.3	MS-GRP-SIC receiver complexity.	99
4.4	MS-GRP-PIC receiver complexity.	100
4.5	Multistage receiver structures complexity summary.	101
5.1	Number of possibilities for different grouping configurations.	104
5.2	Comparison of normalized and non-normalized grouping criteria.	112
5.3	IGI power for each grouping scenario.	113
5.4	Grouping algorithm complexity.	122
6.1	Vehicular channel A power-delay profile.	128
6.2	Receiver structure hardware configurations.	129
6.3	User DOA and grouping	131
6.4	Grouping obtained from experimental data.	133
6.5	Chebyshev weighting coefficients estimation parameters.	142
6.6	Grouping algorithm performance statistics.	146

6.7 Complexity comparison of MS-GRP-PIC with full STMUD. 150

Glossary of Acronyms

3G	Third Generation
3GPP	Third Generation Partnership Project
AWGN	Additive white Gaussian noise
BER	Bit error rate
BF	Beamforming
BPSK	Binary Phase Shift Keying
CDMA	Code division multiple access
CDF	Cumulative distribution function
CIR	Channel impulse response
CFLOPS	Complex floating point operations
DOA	Direction of arrival
DPA	Dynamic phase array
DS-CDMA	Direct-sequence CDMA
DSP	Digital signal processing
EVD	Eigenvalue decomposition
FDD	Frequency-division duplexing
FDMA	Frequency-division multiple access
GSM	Global system for mobile communications
IF	Intermediate frequency
IGI	Inter-group interference
ISI	Inter-symbol interference
LSS	Linear system solution

MAI	Multiple access interference
MF	Match filter
ML	Maximum likelihood
MMSE	Minimum mean square error
MPDR	Minimum power distortionless response
MRC	Maximal-ratio combining
MSC	Mobile switching center
MSE	Mean square error
MUD	Multiuser detection
OFDM	Orthogonal frequency-division multiplexing
OPS	Operations
OVSF	Orthogonal variable spreading factor
PCF	Partial cancellation factor
PCS	Personal communication services
PIC	Parallel interference cancellation
PSK	Phase Shift Keying
PSTN	Public Switched Telephone Network
QPSK	Quadrature Phase Shift Keying
RF	Radio Frequency
RG	Random Grouping
SA	Smart antenna
SDMA	Space-division multiple-access
SIC	Successive interference cancellation
SINR	Signal to interference plus noise ratio
SNR	Signal to noise ratio
ST	Space-time
STMUD	Space-time multiuser detection
SVD	Singular value decomposition
TDD	Time-division duplex

TDMA	Time-division multiple access
TRP	Time-resolvable path
UMTS	Universal Mobile Telecommunications System
UTRA	Universal Terrestrial Radio Access
WCDMA	Wideband CDMA
ZF	Zero forcing

Notation

\mathbb{C}	Set of complex numbers
\mathbb{R}	Set of real numbers
a^*	Complex conjugate of scalar a
\mathbf{a}	Column vector
a_n	Element n of vector \mathbf{a}
\mathbf{A}	Matrix
$[\mathbf{A}]_{n,m}$	Element (n, m) of matrix \mathbf{A}
\mathbf{I}_N	Identity matrix of dimension $N \times N$
$\mathbf{0}_{N \times M}$	Zero matrix of dimension $N \times M$
$\text{tr}(\cdot)$	Matrix trace operator
$\text{diag}(\cdot)$	Diagonal matrix operator
$\ \mathbf{a}\ $	Vector norm
$\ \mathbf{A}\ $	Matrix 2-norm
$\ \mathbf{A}\ _F$	Frobenius norm
$(\cdot)^T$	Transpose operator
$(\cdot)^H$	Complex conjugate transpose operator
\otimes	Kronecker matrix product
$\text{vec}(\cdot)$	Matrix vectorization operator
$E(\cdot)$	Statistical expectation operator
$\text{Var}(\cdot)$	Statistical variance operator
$\text{Re}(\cdot)$	Real component operator
$\text{Im}(\cdot)$	Imaginary component operator

$\text{sgn}(\cdot)$	Signum function (returns the sign of the argument)
$\text{sinc}(\cdot)$	sinc function ($\sin(x)/x$)
$\text{rect}(\cdot)$	Rectangular pulse function
$\text{erf}(\cdot)$	Error function
$\text{erfc}(\cdot)$	Complementary error function

Chapter 1

Introduction

Mobile telephony has now become a commodity in most industrialized countries. This commercial success is due in great part to the advances in telecommunication technology that made the products reliable, portable and accessible to the masses. While voice communications still dominate, data services such as Internet, e-mail, instant messaging, and others have already become a reality to most service providers and are expected to be prevalent in the future. With the arrival of Third Generation (3G) cellular technology, data services have already become an integral part of the service offering.

1.1 Overview of receiver technology for cellular systems

Cellular service providers operate with a limited radio bandwidth, a fundamental resource for radio communications. Part of the spectrum licensed to digital wireless personal communications services (PCS) is usually obtained at a premium, sometimes auctioned by governmental authorities such as Spectrum Management and Telecommunications in Canada or the Federal Communications Commission (FCC) in the United States. The other elemen-

tary resource of radio communications is the transmitting power, which is also regulated. It is usually limited to confine the coverage to a given geographical area.

From the perspective of service providers, it is imperative that the resources be used as efficiently as possible, so that more users can share the cost while benefiting from a reliable and affordable service. To remain competitive and at the same time offer data services such as e-mail, file sharing, Internet browsing, video and music streaming, as supported by the new mobile terminals, it becomes even more important to exploit the available bandwidth to its fullest potential.

Most of the current and 3G cellular systems are based on direct-sequence (or direct-sequence) code-division multiple-access (DS-CDMA) technology. In DS-CDMA, the multiple users are assigned a code or a specific *signature sequence* that spreads the signal over a large bandwidth. Because of the inherent channel distortion and code non-orthogonality, the users interfere with each other, creating multiple-access interference (MAI). The capacity of DS-CDMA systems is known to be interference-limited; to increase the bandwidth usage, it is essential to reduce the impact of MAI. Fortunately, several techniques exist to mitigate MAI and improve the bandwidth efficiency. Of particular interest to 3G systems, spatial filtering or beamforming with antenna arrays (or smart antennas) and multiuser detection (MUD) have both shown promising results. Note that the DS-CDMA technology used in most 3G systems is often referred to as *wideband* CDMA (WCDMA), indicating the larger spectrum it requires when compared to second generation systems.

Beamforming

Beamforming provides a spatial filtering means for separating users based on angular characteristics. Indeed, filtering in the spatial domain by using an antenna array allows the separation of spectrally and temporally overlapping signals originating from different users

with unique spatial signature. In addition to reducing interference, a definite advantage for WCDMA systems, beamforming can also allow the same channel (frequency, timeslot or code) to be allocated to different users in the same cell, effectively increasing spectral efficiency. For these reasons, beamforming is considered a key technology for capacity increase for present and future wireless cellular systems (see e.g. [GHB00, LPO02, LGH00]).

Numerous algorithms for the design of *beamformers* exist [VT02, God97]. The simplest form is based on a set of pre-determined weights; for each signal of interest, the receiver determines which “beam” to use. This *switched beam* technique has the advantage that it can be implemented in hardware at intermediate frequency (IF) using the so-called Butler matrix. Several beams may also be selected and combined for signal detection [GHB00].

Another well-known technique for beamforming makes use of dynamic phase arrays (DPA) and is often referred to as conventional beamforming [God97]. The weight design here is trivial but requires an estimate of the direction-of-arrival (DOA). Alternatively, the weights may be computed optimally for improved interference reduction [VT02]. This approach however often necessitates matrix inversion and requires more elaborate and costly hardware.

Multuser detection

Likewise, multuser detection is known to be a particularly effective technique for interference-limited systems (see e.g. [KKB96, BCMW00]). By performing joint detection of all users known in the system, the mutual interference is taken into account, resulting in higher quality symbol estimates. This improvement is achieved at the expense of a considerable increase in computational complexity compared to conventional detectors. Indeed, optimal MUD takes the form of trellis decoding and is very complex due to the size of the search space which increases exponentially with the number of users and sequence

length [Ver98]. Implementing MUD with the Viterbi algorithm in this context would represent a considerable challenge for real-time operation.

To reduce MUD complexity, several sub-optimal techniques have been proposed in the literature, including relaxation and heuristic search methods [TR04]. Linear filtering approaches such as minimum mean square error (MMSE) and zero forcing (ZF) have also generated extensive interest, due to their good performance and relatively low complexity. The actual linear filter may be obtained with knowledge of the channel coefficients and signature sequences through a matrix inversion [VHG01, KKB96]. Several improvements and variations of the basic linear receiver structure, such as the MMSE multiuser detector with decision-feedback proposed in [WRHR02], can be found in the literature.

While the complexity of these linear MUD receivers structures is significantly lower than that of the optimal MUD receiver, these techniques require the solution of a system of linear equations, which typically have polynomial complexity in the number of users. Using traditional techniques for matrix inversion for example, the complexity is proportional to the number of users cubed (see e.g.: [GVL96]). For large numbers of users, these approaches still represent a considerable challenge for real-time applications.

Since matrix inversion can be a costly operation, alternative techniques have been developed such as parallel interference cancellation (PIC) [DSR98, MVU01, GRSL00, BMV⁺01] and successive interference cancellation (SIC) [PH94, ZB03, And05]. Both PIC and SIC provide symbol estimates through a finite number of iterations, in a way very similar to Jacobi and Gauss-Seidel iterations for matrix inversion [RLJ00, GRSL00]. Improvements to the basic SIC and PIC structures such as the insertion of partial cancellation factors (PCF) [DSR98, HW05, CBW99, XWLNT99], the introduction of different linear filters for de-spreading and re-spreading operations [LS03], and the evolution to space-time iterative structures [MVU01] can be found in the literature.

1.2 Group-based receivers combining MUD and beamforming

Receiver structures combining beamforming with MUD have also been widely studied [UM99, GL03, KGNH99]. Of particular interest in [YYU02], several approaches to filtering in space and time separately and jointly are compared. A switched-beam approach followed by linear MUD is studied in [KYL00], and it is shown in [RC02] that in the presence of clustered users, switched beams followed by multiuser detection performs better than adaptive beamforming followed by multiuser detection.

To further reduce the MUD complexity, it has been proposed to exploit the spatial dimension available when using an antenna array at the base station [HSMGT00, PK00, LLC05]. With beamforming, users can be “separated” into spatial equivalence classes or groups, as illustrated in Fig. 1.1. Each group is then detected using a separate and inde-

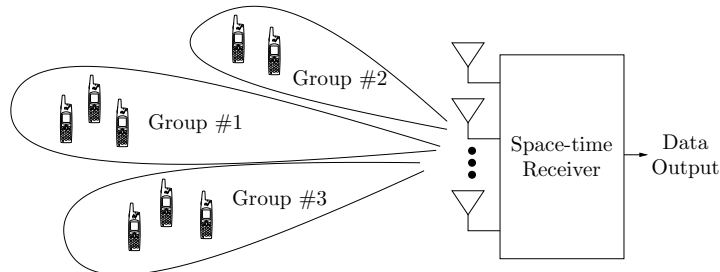


Fig. 1.1 Group-based STMUD receiver with beamforming.

pendent multiuser detector. Since the number of users for each MUD receiver is reduced, and since the complexity is polynomial in the number of users, this approach has the potential to reduce the complexity significantly. However, because of the inherent group non-orthogonality, this reduced complexity approach introduces *inter-group interference* (IGI). This interference degrades the performance of the receiver when compared to the full space-time multiuser detection (STMUD) receiver, which operates on all the users jointly.

In most of the existing literature on group-based space-time MUD, the inter-group interference is often disregarded based on the assumption that the spatial filtering provides sufficient attenuation (see e.g.: [HSMTG00, PK00]). In practice, because the maximum number of users per group is limited by hardware constraints and because of the non-orthogonality among groups, the IGI may become an important factor of performance degradation.

The IGI can be reduced by choosing the grouping properly. The grouping in [HSMTG00, PK00, LLC05] is based on a threshold approach of the normalized cross-correlation between user array signatures. Alternatively, the grouping can be based on the received signal direction-of-arrival or according to the received power (see [LLC05] and [SB00b], respectively). An optimal grouping algorithm for a group decision-feedback detector for synchronous CDMA is proposed in [LPWL03]. In [MG00], users with the same processing gain or data-rate are grouped together, an approach only applicable to multi-rate systems. Similarly in [HBP03], the grouping is based on the code orthogonal variable spreading factor (OVSF) tree and does not consider channel distortion. In [BSZ06], a grouping algorithm based on re-ordering of the effective signature correlation matrix for group-based SIC approaches is proposed.

Finally, the concept of group-based multiuser detection for single antenna systems has been studied in [Var95, Var96] and more recently in [JR98, BZSS03, BZSB07]. Note that a different kind of grouping is studied in [WHM99], where the users with known and unknown spreading sequences are grouped separately for detection and interference suppression, respectively.

1.3 Research objectives and methodology

The main objective of this research work is to develop new space-time receiver structures that provide a performance comparable to that offered by the linear multiuser detection receiver, at a lower complexity level.

This is achieved by improving upon existing space-time group-based MUD receiver structures. In light of the discussion in Section 1.2, it can be concluded that a number of elements in those existing receiver structures can be considered for possible improvements. In particular, the following elements are studied in detail in this work:

1. Beamforming and spatio-temporal filtering:

Most of the existing space-time group-based receiver structures require a separate beamforming unit. In practice it might be more advantageous to have a single spatio-temporal filtering unit.

2. Inter-group interference:

In existing space-time group-based receivers, the interference from the outside groups is usually ignored in the filter design. However, IGI can significantly degrade the performance of group-based receivers and should be mitigated.

3. Grouping algorithm:

In a practical system, the number of resources are limited. Most of the existing grouping algorithms for space-time systems are based on thresholding and do not take the finite limitations of the hardware into consideration. More practical algorithms should be developed.

The proposed improved receiver structures will be studied and compared using analytical and experimental approaches. The experiments measuring the bit error rate (BER)

performance of each receiver structure will be carried out using computer simulations. A complete analysis of the complexity associated to each receiver structure studied is to be provided; this is an essential consideration yet such an analysis is currently missing in the literature on group-based receiver structures.

1.4 Contributions and claim of originality

In this work, new group-based space-time receiver structures for cellular systems are derived and studied. New approaches for inter-group interference reductions are proposed, including multistage approaches and the innovative concept of user sharing.

Through computer simulations, it is shown that the proposed group-based techniques provide a BER performance that can approach the full STMUD receiver BER performance. User sharing is shown to improve not only the BER performance of the group-based MUD receiver, but also the convergence rate of the multistage PIC approach. Moreover, the complexity analysis demonstrates that the proposed multistage PIC approach requires only a fraction of the computational complexity associated to the full STMUD receiver to achieve essentially the same BER performance.

To complete the study, new algorithms for both mutually and non-mutually exclusive grouping are proposed. The performance in terms of mean square error (MSE) of the proposed mutually exclusive grouping algorithm is shown to be comparable to the MSE of the optimal grouping. Yet, the proposed algorithm does not require a costly exhaustive search.

Together, these improvements to the group-based structures provide a means to achieve the performance of the full STMUD receiver at a lower complexity cost. The main original contributions of this research work can be summarized as follows:

- i. Derivation of the optimal group-based linear space-time multiuser detection block-receiver with and without beamforming;
- ii. Development of a new group-based linear space-time MUD receiver with *user sharing*;
- iii. Development of new multistage group-based receiver approaches for IGI reduction with user sharing;
- iv. Proof of the convergence of the new multistage group-based linear MUD receiver with parallel interference cancellation to the full linear MMSE space-time MUD receiver;
- v. Derivation of the complexity associated to the full linear space-time MUD receiver and the proposed group-based linear space-time MUD receivers;
- vi. Development of new mutually exclusive and non-mutually exclusive grouping algorithms respecting hardware constraints and justification of the simplified cost criterion.

These contributions lead to a number of publications in peer-reviewed journals and refereed conferences. The following is a list of publications resulting from this Thesis work:

Journal papers

- J-1 B. Pelletier and B. Champagne, "*Group-based multistage MMSE PIC space-time receiver with user sharing*," IEEE Transactions on Vehicular Technology, to appear in 2008.
- J-2 B. Pelletier and B. Champagne, "*Group-based space-time multiuser detection with user sharing*," IEEE Transactions on Wireless Communications, vol. 6, no. 6, pp. 2034-2039, June 2006.

Conference papers

- C-1 B. Pelletier and B. Champagne, "*Group-based block linear successive interference cancellation for DS-CDMA*," in Proc. IEEE Globecom Conference, San Francisco, California, USA, November 2006.
- C-2 B. Pelletier and B. Champagne, "*Group-based linear parallel interference cancellation for DS-CDMA systems*," in Proc. IEEE Vehicular Technology Conference, Montréal, Canada, September 2006.
- C-3 B. Pelletier and B. Champagne, "*Group optimal linear space-time multiuser detection*," in Proc. IEEE Canadian Conference on Electrical and Computer Engineering, Ottawa, Canada, pp. 1761–1765, May 2006.
- C-4 B. Pelletier and B. Champagne, "*Group optimal space-time MUD with beamforming*," in Proc. IEEE Vehicular Technology Conference, vol. 2, pp. 1323–1327, Stockholm, Sweden, May 2005.
- C-5 B. Pelletier, J. Mao, and B. Champagne, "*Comparative study of uplink and downlink beamforming algorithms in UTRA/TDD*," in Proc. IEEE Vehicular Technology Conference, vol. 2, pp. 1162–1166, Milan, Italy, May 2004.

1.5 Thesis organization

An overview of cellular systems and the description of the signal model is given in Chapter 2, along with the derivation of the full space-time linear multiuser detection receiver. In Chapter 3, group-based approaches to multiuser detection in space-time systems are studied. The group-based linear MUD receiver with beamforming is derived along with the

new optimal MMSE group-based linear space-time MUD receiver. The innovative concept of user sharing or non-mutually exclusive grouping is described. Finally, the computational complexity of each approach is derived.

Multistage receiver structures are derived in Chapter 4. In particular, the proposed multistage group-based MUD receiver with parallel interference cancellation is shown to converge, as the number of stages increases, to the full STMUD receiver. The computational complexity of each proposed multistage receiver structure is also derived. In Chapter 5, the grouping problem is addressed. New algorithms for both mutually and non-mutually exclusive grouping are developed. The proposed algorithms take into consideration practical hardware limitations. Furthermore, the computational complexity of each grouping algorithm is derived and analyzed.

The methodology and the results of the computer experiments are described in Chapter 6 and concluding remarks are presented in Chapter 7. The derivation of the linear weights associated to the different receiver structures studied is detailed in Appendix A. In Appendix B, the complexity associated with solving a complex linear system with a block Toeplitz and Hermitian structure is derived. Finally, details of the exact BER expression for a linear receiver are documented in Appendix C.

Chapter 2

Background

In this Chapter, the conceptual and mathematical frameworks for the remainder of this Thesis are established. In Section 2.1, a general overview of cellular systems from the wireless communications point-of-view is presented. Multiuser communications and the mechanisms of radio propagation in a typical cellular environment are discussed. The mathematical signal model for the WCDMA received signal is developed in Section 2.2. The conventional receiver structure for CDMA is presented in Section 2.3, along with the RAKE receiver. A discrete-time matrix-vector signal model formulation is presented in Section 2.4. This convenient formulation is used in Section 2.5 to derive the full space-time MUD receiver.

2.1 Overview of cellular systems

2.1.1 The cellular concept

Wireless telephony is based on the *cellular* principle. Because the radio resource is scarce and expensive, it must be shared efficiently by the mobile subscribers. In practice, this

is achieved by partitioning the resource (e.g.: frequency spectrum) into smaller parts and *re-using* them at regular intervals in space. To cover a large area, several *cells* are used; since each cell has a finite effective coverage radius, its resources can be re-used by another cell further away [Rap02].

Each cell contains a *base station* providing the radio links to its associated mobile subscribers. The base stations within the entire coverage area are connected to the *mobile switching center* (MSC) to form a *cellular network*, a concept illustrated in Fig. 2.1. The MSC coordinates the activities of all the base stations and connects the cellular systems to the public switched telephone network (PSTN).

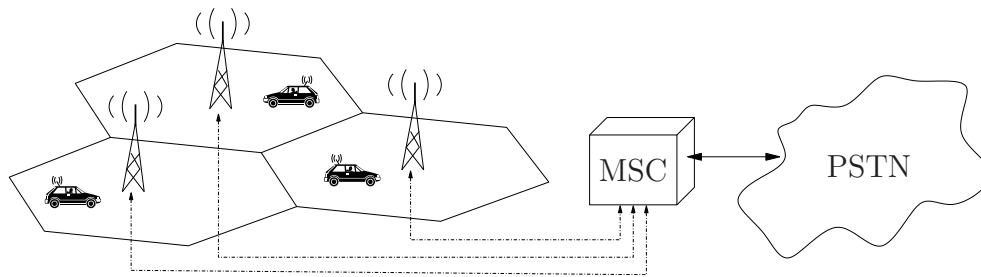


Fig. 2.1 Example of a cellular network.

Duplexing

The radio link from the base station to the mobile subscriber is referred to as the *downlink*, while the radio link from the mobile subscriber to the base station is called the *uplink*. This terminology originates from the fact that the base station antennas are usually located higher than the mobile terminals, often on a tower or building. Note that the downlink and uplink are sometimes referred to as the forward link and reverse link, respectively.

There are two different approaches to share the spectrum between the downlink and the uplink. In the first approach, frequency-division duplexing (FDD), the spectrum is

partitioned in two; one part of the spectrum is allocated to the downlink while the other is allocated to the uplink. This approach requires the use of good duplexing filters at both the mobile and base station since both transmission and reception take place simultaneously.

In the second approach, time-division duplexing (TDD), the access to the whole spectrum is shared in time-alternations between the downlink and the uplink. This approach is advantageous since it is possible to allocate more time to the downlink than the uplink (or the reverse); a definite advantage for asymmetric data services. TDD is usually used in smaller cells because of synchronization difficulties with large propagation delays.

Some of the Third Generation systems specifications include both TDD and FDD operations mode. This is the case for example of the Third Generation Partnership Project (3GPP) Universal Terrestrial Radio Access (UTRA) [3GPb].

Multiple access

There are four main approaches to share the available bandwidth among users in a communications system. First, in *frequency-division multiple access* (FDMA), the spectrum is partitioned in frequency so that users can simultaneously access part of the resource for radio transmission. FDMA has been the method of choice for older generations analog mobile phones because it allocates a fixed frequency slot that is used by a single user at a time. Because of the necessity of building sharp radio frequency (RF) filters within the mobiles, FDMA can be costly to implement.

Second, in *time-division multiple access* (TDMA), time is divided in a number of small *timeslots*. Each user is assigned to a fixed timeslot and uses the whole bandwidth during that short period of time. TDMA is used in several Second Generation cellular technologies such as Global System for Mobile communications (GSM). One of the main difficulty with TDMA is the synchronization of the different mobiles on the uplink.

The third approach used to share the radio resources among users is based on *code-division multiple-access* (CDMA). In CDMA, each user is assigned a different code sequence, often chosen from a pre-determined set or generated in real-time using a shift register with linear feedback (e.g.: see [Pro01]). The code sequence is used to *spread* the transmitted signal so that the whole bandwidth is occupied. All the users transmit simultaneously, and at the receiving end the signal is *de-spread* using the same code sequence. If the sequences are orthogonal, then in the absence of noise the signal from each user can be recovered exactly. The code sequences are usually assigned by the base station to the mobile terminal through a control channel and are thus known to both transmitter and receiver. Most cellular systems use direct-sequence code-division multiple-access (DS-CDMA), where the access code modulates the transmitted symbols in time.

The last approach to share the available bandwidth consists of *space-division multiple-access* (SDMA). In SDMA, the users are separated according to the directional characteristics of their received signal. In practice this is achieved at the base station using beamforming with narrow beam width.

All multiple access methods suffer from multiple-access interference. For FDMA, this interference is caused by non-ideal filters and frequency offsets. For TDMA, non-ideal synchronization causes the signals to overlap in time. For DS-CDMA, the small cross-correlation among codes results in a residual interference component in the de-spread signal. This multiple-access interference is known to limit the capacity of DS-CDMA systems. Finally for SDMA, non-ideal spatial filtering causes signals originating from different directions to interfere with each other at the base station.

Most 3G systems use DS-CDMA as the multiple access scheme. The 3GPP UTRA TDD mode uses short code sequences that are repeated every symbol, while the FDD mode uses long spreading sequences that have a period of several symbols although it can also be

configured to use short spreading code sequences as well. Because of the larger bandwidth used in 3G, those systems are referred to as *wideband*-CDMA or WCDMA.

2.1.2 The mobile channel

In a wireless communication system, the information signal is transmitted to the receiver in the form of radio waves that propagate through space via the so-called *propagation channel*. This channel distorts the signal in an unpredictable way, so that the receiver can only *estimate* the signal being transmitted. The distortion can be described by the physics of the propagation environment.

The wireless mobile channel is characterized by a time-variant impulse response. To exactly describe a practical wireless channel would be very difficult due to the large number of variables involved. Fortunately, several statistical models based on physical properties of wave propagation have been developed to describe such phenomenon.

Large scale fading

Large scale fading designates the average signal power attenuation over large areas [Pro01, Skl97]. The total signal attenuation caused by wave propagation along a transmission path is often referred to as *path loss*. The first cause of path loss is the free-space propagation. In free-space, the power received by a receiver antenna is given by Friis free-space equation, which establishes that the power falls off as the square of the transmitter-receiver distance [Rap02].

In a typical cellular wireless channel, however, the propagation does not occur in pure free-space. Besides free-space propagation loss, *reflection*, *diffraction* and *scattering* also affect propagation. These three mechanisms cause, to different degree, large-scale signal attenuation. In addition, the transmission path may be obstructed by foliage, buildings,

hills and other elements that are part of the terrain. These obstructive elements, combined with the propagation mechanisms listed above, cause the received signal to have a larger attenuation than what is predicted by Friis formula alone. While difficult to calculate exactly, the actual path loss is often modeled as a function of the distance between the transmitter and receiver raised to the *path loss exponent*.

In practice, the obstacles can be very different from one location to the next. The actual path loss measurements may thus vary greatly from the average. Experimental data suggests that the path loss measured at any location is random and distributed log-normally around a mean path loss value with a given standard deviation. This random variation is often referred to as log-normal *shadowing*. Typical values for the path loss exponent and the log-normal shadowing standard deviation have been tabulated for different environments, based on experimental measurements (see e.g. [Hat80, Rap02]).

These long-term channel variations can usually be tracked by power-control algorithms. In a cellular system the transmitting power is usually limited, and consequently the path loss essentially determines the size of each cell. The larger the exponent index and log-normal fading standard deviation, the smaller the cell, which in turn leads to more important operating costs.

Small scale fading

Small scale fading designates the ensemble of rapid variations in received signal characteristics over a short time interval or small mobile terminal displacement. Fading is caused by two or more versions of the transmitted signal arriving at the receiver with slightly different time delay, amplitude, and phase. Because of those *multipaths*, and depending on their characteristics, the resulting signal may vary significantly in amplitude. These variations are usually described using well-accepted statistical models [Pro01, Skl97].

The cellular system transmission environment often includes urban objects and structures that act as *reflectors* and *scatterers*. As illustrated in Fig. 2.2 for the uplink case, the transmitted signal is often reflected on structures that may be largely separated. If the transmission path lengths are sufficiently different, the multiple signal copies may be *resolvable* or *differentiable* in time, i.e.: the copies can be separated in time at the receiver. In this work, each of these paths is referred to as a *time-resolvable path* (TRP).

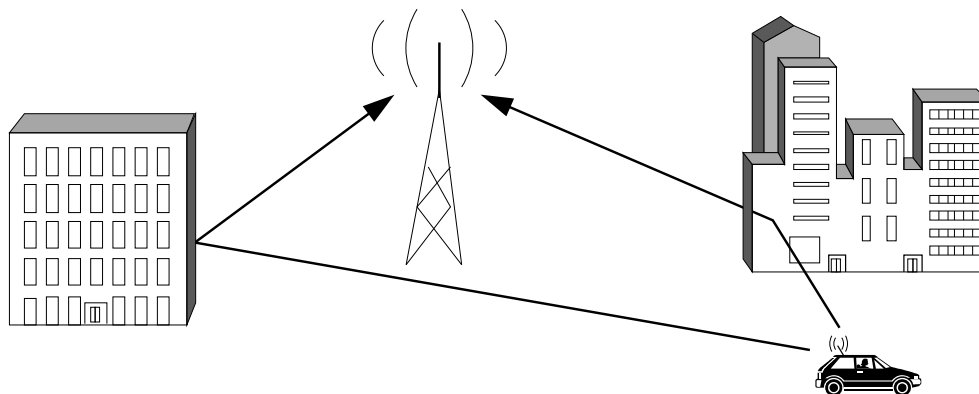


Fig. 2.2 Radio wave reflection.

Reflections on rough surfaces, or surfaces with dimensions on the order of the transmission wavelength or smaller cause the signal energy to be spread out in different directions. This *scattering* creates multipath fading *within* each resolvable path.

When the received signal amplitude for each path is modeled as a zero-mean complex-valued Gaussian random variable, it follows that its envelope is Rayleigh distributed and the channel is then said to be *Rayleigh fading*. If there is a significant line-of-sight component in the path, then the envelope may be modeled as a Rician random variable in which case the channel is said to be *Rician* [Pro01].

If the total channel time dispersion or *delay spread* is much smaller than the symbol duration, the channel is said to be *frequency flat*. On the other hand, if the channel time

dispersion is larger than the symbol duration, then the channel is said to be *frequency selective*.

Naturally, motion of the mobile terminal and/or its surrounding environment causes the channel characteristics to change with time, which in turn causes the fading amplitude to also change with time. When the rate of change of the channel is small compared to the transmitted symbol rate, then the channel is said to be *slow fading*. Alternatively, when the channel rate of change is large compared to the symbol rate, then the channel is said to be *fast fading*.

The rate of change of the channel is directly related to the speed of the mobile terminal or the speed of the various elements in its surrounding environment. This motion induces a time-varying Doppler shift on the multipath components. Because different multipath components have different relative speeds, the received signal will be composed of several frequency-shifted versions of the transmitted signal, resulting in an overall spreading in frequency, thus increasing at the same time the signal bandwidth. The channel *coherence time*, which essentially defines the largest time difference for which two transmitted signals will be strongly correlated, is often used to characterize the rate of change of time-varying channels.

Another important measure for the wireless mobile channel is its *coherence bandwidth*. It essentially defines the maximum frequency difference for which two signals transmitted through the mobile wireless channel are strongly correlated. The coherence bandwidth is related to the multipath structure of the channel. In general, if the transmitted signal bandwidth is much larger than the channel coherence bandwidth, then the signal will experience distortion. Conversely, if the transmitted bandwidth is much smaller than the channel coherence bandwidth, the transmitted signal will experience little distortion. Further details on fading channel properties, including a complete mathematical formulation,

can be found in e.g. [Sk197, Pro01].

Figure 2.3 shows the impact of small scale fading on the magnitude squared of the channel amplitude over time. It is clear that the channel suffers from a large number of very deep fades.

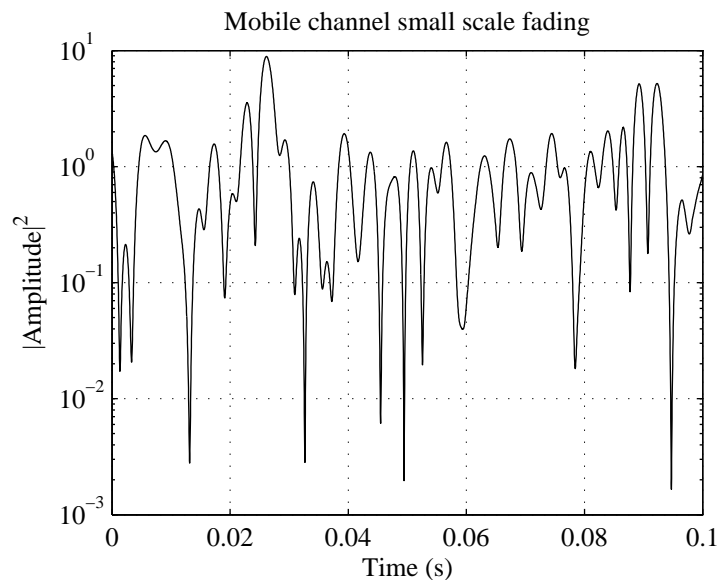


Fig. 2.3 Simulated channel small scale fading at mobile velocity $v = 30m/s$, and carrier frequency $f_c = 2GHz$.

Spatial dispersion

In a space-time channel, the received signal is not only sampled in time, but also in space with an antenna array, as illustrated in Fig. 2.4 for the uplink. The angular information of the received signal, also called direction-of-arrival or DOA, and denoted by θ in the figure, can be used to help improve detection.

The DOA at the receiver for each resolvable path depends on the direction of the direct path or the location of the different reflectors. Because of scattering, the received signal for each path may also experience *angular spreading*. Angular spreading, denoted by $\Delta\theta$

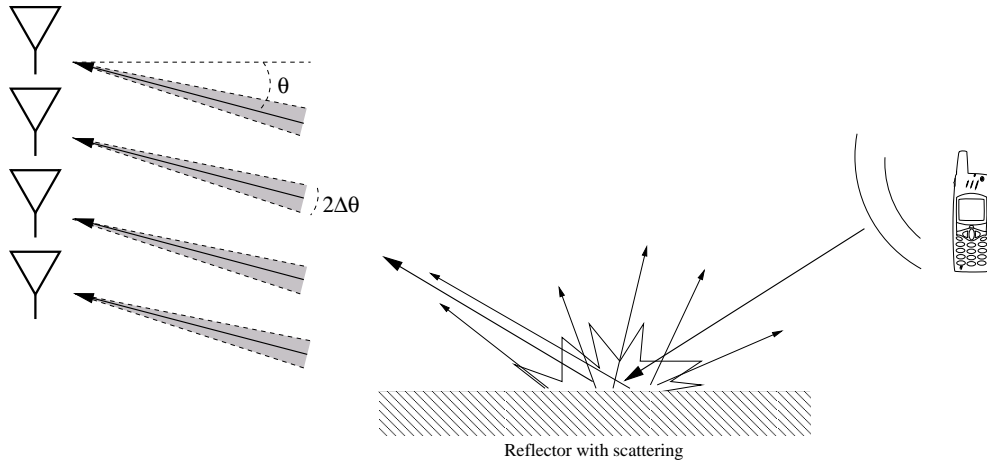


Fig. 2.4 Spatial dispersion and angular spread.

in Fig. 2.4, is due to the propagation wave being scattered by a large surface (or a number of small elements over a large area).

Several statistical models exist for space-time channels (see e.g.: [ECS⁺98]) with various degrees of complexity and realism. Fortunately, there exists techniques to efficiently simulate such space-time channels with temporal fading [SC00].

2.2 Received signal model

While most of the receiver structures developed in this work can also be used for the downlink, it is more natural for a receiver with multiple antennas to be located at the base station than at the mobile terminal. For this reason, the uplink of a multiuser wireless communications system is considered.

The signal transmitted by each mobile terminal is modulated at a carrier frequency f_c . To simplify the mathematical formulation of the signal model, it is convenient to use the complex envelope. This approach leads to a simpler equivalent complex signal model, where the modulation is abstracted [Pro01]. Let $d_k(m) \in \mathcal{A}_s$ be the m^{th} data symbol transmitted

from user k , where \mathcal{A}_s is the symbol alphabet (e.g.: for binary phase shift keying (BPSK) $\mathcal{A}_s = \{-1, 1\}$), which in general may be complex-valued. The WCDMA spread signal output for user k then becomes

$$g_k(t) = \sum_{m=-\infty}^{\infty} d_k(m)s_k(t - mT_s), \quad -\infty < t < \infty, \quad (2.1)$$

where T_s is the symbol duration and $s_k(t)$ is the spreading signal or *signature waveform* for user k . The signature waveform can be expressed in general as

$$s_k(t) = \sum_{n=0}^{Q-1} c_k(n)p(t - nT_c), \quad -\infty < t < \infty, \quad (2.2)$$

where $c_k(n)$ is the n^{th} “chip” of the DS-CDMA *code sequence* of user k , $p(t)$ is the pulse function, T_c is the chip interval, $Q \triangleq T_s/T_c$ is the so-called *spreading factor* or bandwidth expansion factor and indicates the number of chips per symbol in the spreading sequence.

The code sequence, also called *signature sequence*, is known to both the transmitter and receiver. The elements of the sequence are chosen from a finite chip alphabet \mathcal{A}_c , typically $\mathcal{A}_c = \{\pm 1\}$ or $\mathcal{A}_c = \{\pm \frac{1}{\sqrt{2}}, \pm \frac{j}{\sqrt{2}}\}$ in the complex case. The sequence $c_k(n)$ itself can be chosen from a set of OVSF sequences as in UTRA/TDD, or generated using a shift register with linear feedback such as m -sequences and Gold sequences [Pro01].

In general, the pulse function $p(t)$ is specified by the transmission specifications and often takes the form of a raised cosine (e.g. see [3GPa]) so that the spectrum is band-limited. To simplify the development, the pulse function in this work is the rectangular pulse, specifically:

$$p(t) = \begin{cases} \frac{1}{\sqrt{Q}}, & 0 < t < T_c \\ 0, & \text{otherwise.} \end{cases} \quad (2.3)$$

where the $1/\sqrt{Q}$ factor normalizes the signature waveforms in (2.2) to unit energy, i.e.: $\int_{-\infty}^{\infty} |s_k(t)|^2 dt = 1$.

As outlined in the previous section, the multipath components in the channel distort the received signal. Let $\xi_{k,l}(t)$ and $\tau_{k,l}(t)$ be the time-varying complex amplitude and delay at the receiver, respectively, for the l^{th} path of user k . Note that $\xi_{k,l}(t)$ incorporates both the large scale and small scale fading effects. Also, let W_k be the maximum number of paths in the received signal for user k . Then the received signal at the base station, which consists of the contribution of the K active users and additive noise, can be expressed as:

$$x(t) = \sum_{k=1}^K \sum_{l=1}^{W_k} \xi_{k,l}(t) g_k(t - \tau_{k,l}(t)) + v(t), \quad -\infty < t < \infty, \quad (2.4)$$

where $v(t)$ is the additive white Gaussian (AWGN) noise term with instantaneous power $E(|v(t)|^2) = \sigma^2$, where $E(\cdot)$ denotes the statistical expectation operator. The type of mobile channel determines the statistics of $\xi_{k,l}(t)$ and $\tau_{k,l}(t)$. Assuming a slowly fading and frequency selective channel, $\xi_{k,l}(t)$ and $\tau_{k,l}(t)$ become approximately fixed for the duration of a block of symbols or *frame*. The received signal then becomes

$$x(t) = \sum_{k=1}^K \sum_{l=1}^{W_k} \xi_{k,l} g_k(t - \tau_{k,l}) + v(t), \quad 0 < t < NT_s + \tau_{\max}, \quad (2.5)$$

where N is the number of consecutive symbols in a transmission block, $\tau_{k,l} > 0, \forall(k, l)$, and the maximum delay is given by

$$\tau_{\max} = \max_{k,l} \tau_{k,l}. \quad (2.6)$$

It is assumed in (2.5) that there is a period of silence (with no transmission) between

adjacent frames. This period of time is often referred to as the *guard period*. The guard period duration T_G must be long enough to avoid inter-frame interference due to channel dispersion (i.e.: $T_G > \tau_{\max}$).

Table 2.1 indicates typical values of some of the system parameters introduced above for a UTRA/TDD system. As it can be observed, the chip rate ($1/T_c$) is fixed at 3.84Mcps while the spreading factors may take different values. This approach leads to different possible combinations of symbol rates and numbers of users. More details on UTRA/TDD can be found in [HKK⁺00, CB04] and in the 3GPP specifications [3GPb].

Parameter	Symbol	Typical value
Carrier frequency	f_c	2GHz
Chip rate	$1/T_c$	3.84Mcps
Number of simultaneous users	K	up to 16
Spreading factor	Q	1,2,4,8, or 16
Guard period	T_G	0.025ms

Table 2.1 Typical system parameter values for UTRA/TDD.

2.3 Conventional receiver

One of the simplest receiver structure for WCDMA signals essentially consists of a bank of correlators; one for each user or code sequence. This so-called *conventional* receiver structure is shown in block diagram form in Fig. 2.5. To illustrate its operation, consider the simpler case of synchronous WCDMA with 1 path for each user, i.e. $W_k = 1, \forall k$. In this context the relative time delay for the single path is assumed to be zero so that $\tau_{k,1} = 0$, and the complex amplitude for the unique path can be expressed as $\xi_k \equiv \xi_{k,1}$. In this framework, the output of the correlator for user k at the symbol index m can be expressed

as

$$y_k(m) = \int_{mT_s}^{(m+1)T_s} x(t) s_k^*(t - mT_s) dt \quad (2.7)$$

$$= \sum_{k'=1}^K \sum_{m'=0}^N \xi_{k'} d_{k'}(m') \int_{mT_s}^{(m+1)T_s} s_{k'}(t - m'T_s) s_k^*(t - mT_s) dt + \nu_k(m) \quad (2.8)$$

$$= \xi_k d_k(m) + \sum_{\substack{k'=1 \\ k' \neq k}}^K \xi_{k'} d_{k'}(m) \varphi_{k',k} + \nu_k(m), \quad (2.9)$$

where the superscript $*$ denotes complex conjugation, $\varphi_{k',k} \equiv \varphi_{k',k}(0)$, where $\varphi_{k',k}(\tau)$ is the cross-correlation function between the signatures of users k' and k , defined as

$$\varphi_{k',k}(\tau) \triangleq \int_0^{T_s} s_{k'}(t) s_k^*(t + \tau) dt, \quad (2.10)$$

and the noise term is given by

$$\nu_k(m) \triangleq \int_{mT_s}^{(m+1)T_s} v(t) s_k^*(t - mT_s) dt. \quad (2.11)$$

The first term in (2.9) is the signal of interest, the second is the multiple access interference and the last term is the AWGN noise. It can also be observed from (2.9) that the cross-correlation $\varphi_{k',k}$ plays a central role in the MAI.

In the conventional receiver, the decision variable or soft estimate for the symbol m of user k is given by $y_k(m)$ in (2.9). The hard symbol estimate is obtained through the decision device, represented by the function $\mathcal{Q}(\cdot)$ in Fig. 2.5. In general, this decision or quantization function is designed to minimize the probability of making an incorrect decision and depends on the modulation. For BPSK, the decision device is usually a simple

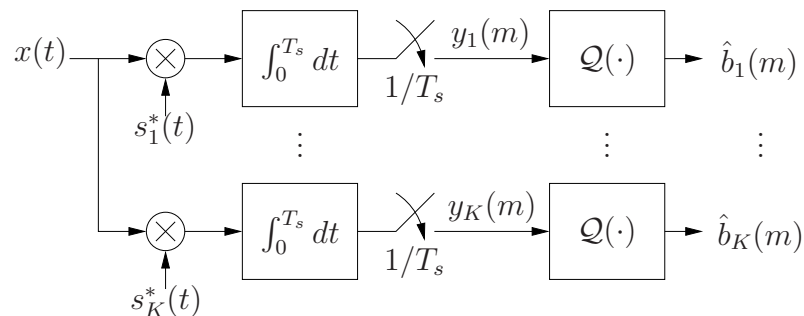


Fig. 2.5 Conventional CDMA receiver block diagram.

hard limiter taking the form

$$\hat{d}_k(m) = \text{sgn}(\text{Re}(y_k(m))), \quad (2.12)$$

where $\text{sgn}(\cdot)$ and $\text{Re}(\cdot)$ are the sign and real part of the corresponding argument, respectively. If the signature waveforms' cross-correlations $\varphi_{k',k}$ ($k' \neq k$) are zero or negligible, then the single-user detector in (2.12) will provide a BER performance close to the single-user bound.

In the presence of multipath fading with one or more paths (i.e.: $W_k \geq 1, \forall k$), the conventional receiver may suffer from significant performance degradation, especially when the main path undergoes a deep fade. When the channel has several paths, the received signal at the output of the correlator for user k at the symbol index m can be expressed

using (2.5) and (2.7) as

$$y_k(m) = \sum_{k'} \sum_l \xi_{k',l} \int_{mT_s}^{(m+1)T_s} g_{k'}(t - \tau_{k',l}) s_k^*(t - mT_s) dt + \nu_k(m) \quad (2.13)$$

$$\begin{aligned} &= \int_{mT_s}^{(m+1)T_s} \sum_{l=1}^{W_k} \xi_{k,l} g_k(t - \tau_{k,l}) s_k^*(t - mT_s) dt \\ &+ \sum_{k' \neq k} \int_{mT_s}^{(m+1)T_s} \sum_l \xi_{k',l} g_{k'}(t - \tau_{k',l}) s_k^*(t - mT_s) dt + \nu_k(m), \end{aligned} \quad (2.14)$$

where the first term in (2.14) contains all the signal contribution from user k only, the second term contains the multiple access interference, and the last term is the additive noise term. It can be observed in (2.14) that for user k , W_k delayed versions of the transmitted signal are available at the receiver. These delayed signal replicas cause consecutive symbols to overlap in time at the receiver; this type of interference is referred to as *inter-symbol interference* (ISI).

With the conventional receiver, if the main path undergoes a deep fade, the signal for the user of interest is lost regardless of how many signal replicas are available. To maintain signal detection the conventional receiver must lock onto a new time-resolvable path, possibly losing data and synchronization in the process.

One of the approaches to recover the energy and take advantage of the diversity offered by all multipaths consists of combining the signal replicas coherently using maximal-ratio combining (MRC). The receiver structure achieving this is referred to as the RAKE receiver [Rap02].

The conventional and RAKE receiver structures suffer from the *near-far* effect that arises from varying received powers of the users. Without proper power control, the signal from the users close to the base station may be received with much more power than the signal from users located at the edge of the cell. Due to the inherent code non-orthogonality,

the strong users may *mask* the weaker users. Detection then becomes difficult due to the excessive MAI. In general, multiuser detection receivers do not suffer from these drawbacks and perform much better.

2.4 Equivalent matrix-based signal model

To derive the conventional linear multiuser detection receiver and the proposed group-based linear multiuser detection receivers, which are the subject of this work, it is convenient to use an equivalent matrix-based signal model. The model was originally derived in [VHG01] to represent the received signal at the antenna array receiver of a UTRA/TDD WCDMA system. It is based on a matrix-vector equation which is sufficiently general to be applicable not only to WCDMA and other DS-CDMA based systems, but also to many other types of multiuser systems. As opposed to the continuous-time (analog) model of the previous section, the matrix-based model is suitable for use in the context of digital signal processing.

Consider the uplink of a synchronous WCDMA communication system with K users transmitting simultaneously through a dispersive channel to a common multi-antenna receiver. At each antenna, the received signal is converted to baseband, matched filtered to the transmission pulse and sampled at the “chip” rate of $1/T_c$, where T_c denotes the chip duration. To simplify and to maintain the equivalence with the continuous-time model of the previous section, assume that the pulse shaping function $p(t)$ in (2.3) is band-limited to $1/T_c$ and that the channel time-delays $\tau_{k,l}$ are exact multiples of the sampling interval T_c . Furthermore, let

$$W \triangleq \max_{k,l} \frac{\tau_{k,l}}{T_c} \quad (2.15)$$

be the maximum channel delay in terms of number of samples. Without loss of generality, it can be assumed that the channel for each user has a finite impulse response of length

W , with some paths having zero amplitude. In this context, the RAKE receiver consists of multiple correlators set to different delays in units of T_c .

For a block of N consecutive symbols followed by an appropriately long guard period, the observed signal at the receiver consists of a complex-valued vector of length $NQ+W-1$, where $Q = T_s/T_c$ is the symbol expansion factor (or spreading factor), T_s is the symbol duration, and W is the finite impulse response channel length.

Let M be the number of antennas and $\mathbf{x}^{(m)} \in \mathbb{C}^{(NQ+W-1) \times 1}$ for $m = 1, \dots, M$, be the received signal vector for the m^{th} antenna element. Following the linear model described in [VHG01], it is convenient to represent the complete set of observations in vector form as

$$\mathbf{x} = \text{vec}([\mathbf{x}^{(1)} \ \dots \ \mathbf{x}^{(M)}]^T) \in \mathbb{C}^{M(NQ+W-1) \times 1}, \quad (2.16)$$

where superscript T denotes matrix transposition and $\text{vec}(\cdot)$ is an operation that sequentially concatenates the columns of a matrix into a column vector of appropriate dimension.

Similarly, the vector of NK information symbols transmitted by the K users can be represented as

$$\mathbf{d} = \text{vec}([\mathbf{d}^{(1)} \ \dots \ \mathbf{d}^{(K)}]^T) \in \mathcal{A}_s^{NK \times 1}, \quad (2.17)$$

where $\mathbf{d}^{(k)} \in \mathcal{A}_s^{N \times 1}$ is the vector of information symbols for user k and \mathcal{A}_s is the finite symbol alphabet. The information symbols are assumed to be independent, identically distributed (iid) and normalized such that $E[\mathbf{d}\mathbf{d}^H] = \mathbf{I}_{NK}$, where superscript H represents Hermitian transposition and \mathbf{I}_{NK} is the identity matrix of dimension $NK \times NK$.

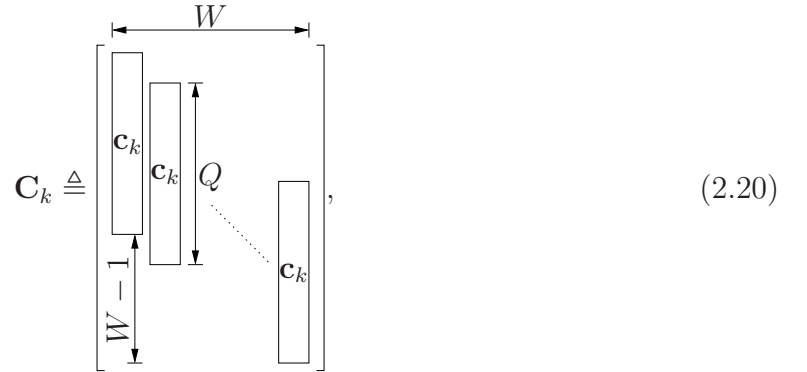
In this model, the channel is assumed to be fixed for the duration of at least one block of data symbols. Let the complex-valued channel impulse response (CIR) from the user k

to antenna element m be given by $h_k^{(m)}(n)$ for $1 \leq n \leq W$, and define

$$\mathbf{h}_k^{(m)} \triangleq [h_k^{(m)}(1), \dots, h_k^{(m)}(W)]^T. \quad (2.18)$$

The effect of the channel impulse response and the CDMA code sequence can be combined into the so-called *effective signature* vector. For the m^{th} antenna element, this effective signature vector has dimension $(Q + W - 1) \times 1$ and can be expressed as

$$\mathbf{v}_k^{(m)} = \mathbf{C}_k \mathbf{h}_k, \quad (2.19)$$



$$\mathbf{C}_k \triangleq \begin{bmatrix} \mathbf{c}_k & \mathbf{c}_k & \mathbf{c}_k \end{bmatrix}, \quad (2.20)$$

where \mathbf{c}_k is the $Q \times 1$ CDMA code sequence vector given by

$$\mathbf{c}_k \triangleq [c_k(1), \dots, c_k(Q)]^T. \quad (2.21)$$

The total space-time effective signature vector for user k , combining the contributions from all the W antenna elements, can finally be expressed as

$$\mathbf{v}_k = \text{vec} \left([\mathbf{v}_k^{(1)}, \dots, \mathbf{v}_k^{(M)}]^T \right) \in \mathbb{C}^{M(Q+W-1) \times 1}. \quad (2.22)$$

In effect, the effective signature \mathbf{v}_k represents the space-time response to a single sym-

bol of unit value transmitted by user k , as observed by the multi-antenna receiver after demodulation, sampling and vector formatting as described above. Finally, define

$$\mathbf{V} = [\mathbf{v}_1 \ \dots \ \mathbf{v}_K] \in \mathbb{C}^{M(Q+W-1) \times K} \quad (2.23)$$

as the effective signature *matrix* for the K users.

The total received vector at the antenna array may then be conveniently expressed in matrix form as

$$\mathbf{x} = \mathbf{T}\mathbf{d} + \mathbf{n}, \quad (2.24)$$

where $\mathbf{T} \in \mathbb{C}^{M(NQ+W-1) \times NK}$ is a block-Toeplitz¹ matrix. In particular, assuming a relatively short channel delay-spread so that symbols interfere only with their adjacent neighbors, i.e. $W < Q$, the matrix \mathbf{T} takes the special form [VHG01]

$$\mathbf{T} = \begin{bmatrix} \boxed{\mathbf{V}} & & & \\ & \boxed{\mathbf{V}} & & \\ & & \ddots & \\ & & & \boxed{\mathbf{V}} \end{bmatrix}. \quad (2.25)$$

The vector $\mathbf{n} \in \mathbb{C}^{M(NQ+W-1) \times 1}$ in (2.24) contains white circular complex Gaussian noise samples with covariance matrix $\mathbf{R}_{\mathbf{n}} \triangleq E[\mathbf{n}\mathbf{n}^H] = \sigma^2 \mathbf{I}_{M(NQ+W-1)}$, where σ^2 is the AWGN noise power.

¹The entries of a Toeplitz matrix are constant down the diagonals parallel to the main diagonal [HJ90]. Similarly for a block-Toeplitz matrix, the blocks are constant down the diagonals parallel to the main diagonal.

Notice that the above model and ensuing results can be generalized to account for colored noise and to support the asynchronous case. For the latter, over-sampling may be required for robustness against timing offsets, in which case the structure of the system equations needs to be slightly modified.

The model can also support variable data rate scenarios with no modifications. This is achieved by splitting the higher data rate sources into multiple streams, each providing new information at the basic symbol rate of $1/T_s$. Each stream can be associated to a unique space-time effective signature. These different data streams can also be interpreted as originating from different “virtual users” sharing the same channel.

2.5 Space-time multiuser detection

The purpose of the receiver is to obtain reliable estimates of the data symbol vector \mathbf{d} from the space-time observation vector \mathbf{x} in (2.24). As discussed in Section 2.3, the conventional single-user receiver suffers from the near-far effect and MAI because it does not take into consideration this interference created by the other users.

Multiuser detection refers to an ensemble of techniques to jointly detect the NK information symbols simultaneously [Mos96]. A MUD receiver attempts to recover the information symbols by considering in its calculation the interference caused by all users simultaneously. In the particular case of the maximum-likelihood optimal MUD receiver, this is achieved by solving a combinatorial problem of exponential dimension with respect to the total number of symbols considered.

Linear receivers provide an attractive alternative to the optimal MUD receiver because of their lower complexity and adequate performance. The zero-forcing (ZF) (or decorrelator) and minimum mean square error (MMSE) linear receiver structures have been shown

to perform significantly better than the conventional receiver, in addition to providing near-far resistance [MH94, KKB96]. In particular, the optimal MMSE MUD receiver is known to perform better in the presence of noise than the ZF MUD receiver, and it also provides a means for reducing the impact of inter-group interference; a potentially considerable advantage for group-based receivers. For these reasons, the main focus of this work is on the MMSE receiver.

In this work, the effective signature for each user is assumed to be known by the receiver, as it is commonly presumed in papers on linear MUD (see e.g.: [VHG01, KKB96, Mos96]). In the context of the matrix-based signal model of Section 2.4, this assumption means that matrix \mathbf{V} (and consequently \mathbf{T} by definition) is known. For a WCDMA system, this generally implies that the code signatures from the different users are known and that the channel coefficients have been estimated with sufficient accuracy. Channel estimation can be achieved for instance by using the training sequences provided by the transmission format of wireless cellular systems standards such as UTRA/TDD (see e.g.: [HKK⁺00, SB93]).

The basic structure for the space-time multiuser detection receiver is illustrated in Fig. 2.6. The receiver consists essentially of four different sections: the RF front-end, which provides the observation vector \mathbf{x} , the matched filter, the MMSE linear MUD filter, and the hard decision (quantization) device.

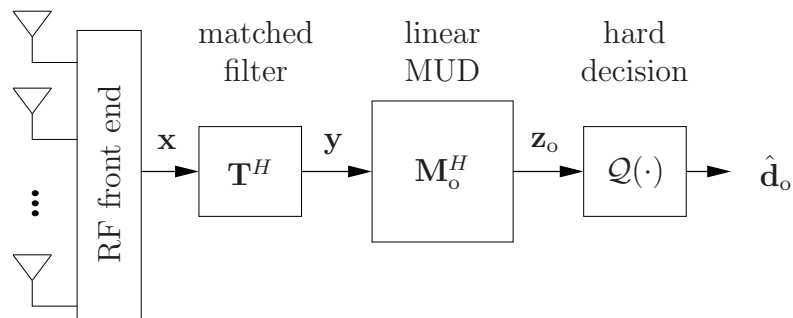


Fig. 2.6 Block diagram for the full STMUD receiver.

Due to the large dimension of the observation vector, it is common to apply the MMSE MUD filter at the output of the matched filter [Ver98]. For the specific case of MMSE filtering, this so-called *symbol-rate* approach leads to the same symbol estimate as the symbol estimate obtained using the more complex *chip-rate* approach which, as its name implies, requires the entire sampled observation vector (see e.g.: [FFT04]).

According to the formulation in (2.24), the joint matched filter (MF) output for the observation signal \mathbf{x} can be expressed as

$$\begin{aligned}\mathbf{y} &= \mathbf{T}^H \mathbf{x} \\ &= \mathbf{T}^H \mathbf{T} \mathbf{d} + \mathbf{T}^H \mathbf{n}.\end{aligned}\tag{2.26}$$

Thus the input of the MUD filter has dimension reduced from $M(NQ + W - 1) \times 1$ to $NK \times 1$, which corresponds to the total number of symbols to estimate.

To obtain the multiuser detection soft symbol estimate, the MF output in (2.26) is processed by the MMSE linear filter. The soft symbol estimate can be expressed as

$$\mathbf{z}_o = \mathbf{M}_o^H \mathbf{y},\tag{2.27}$$

where $\mathbf{M}_o \in \mathbb{C}^{NK \times NK}$ is the optimal filter matrix that minimizes the MMSE cost function

$$J(\mathbf{M}) = E \|\mathbf{d} - \mathbf{M}^H \mathbf{y}\|^2,\tag{2.28}$$

where $\|\cdot\|$ denotes the vector norm. The optimal weights can be expressed as (see

e.g.: [Ver98])

$$\mathbf{M}_o = \arg \min_{\mathbf{M}} J(\mathbf{M}) \quad (2.29)$$

$$= (\mathbf{T}^H \mathbf{T} + \sigma^2 \mathbf{I})^{-1}, \quad (2.30)$$

where \mathbf{I} is the identity matrix of appropriate dimensions. Furthermore, the minimum achievable cost in (2.28) is given by

$$J(\mathbf{M}_o) = \text{tr}[\mathbf{I} - \mathbf{R}^H (\mathbf{R} + \sigma^2 \mathbf{I})^{-1}], \quad (2.31)$$

where $\mathbf{R} \triangleq \mathbf{T}^H \mathbf{T}$, and $\text{tr}(\cdot)$ is the matrix trace operator. From (2.25), it can be seen that the correlation matrix \mathbf{R} takes the form of a block Toeplitz matrix with two off-diagonal blocks:

$$\mathbf{R} = \begin{bmatrix} \boxed{\mathbf{V}^H \mathbf{V}} & \boxed{\mathbf{V}_L^H \mathbf{V}_U} & & & \\ \boxed{\mathbf{V}_U^H \mathbf{V}_L} & \boxed{\mathbf{V}^H \mathbf{V}} & & & \\ & & \ddots & & \\ & & & \boxed{\mathbf{V}_L^H \mathbf{V}_U} & \\ & & & & \boxed{\mathbf{V}^H \mathbf{V}} \end{bmatrix}, \quad (2.32)$$

where $\mathbf{V}_L \in \mathbb{C}^{M(W-1) \times K}$ is formed from the last $M(W-1)$ rows of \mathbf{V} and its K columns, and $\mathbf{V}_U \in \mathbb{C}^{M(W-1) \times K}$ is formed from the first $M(W-1)$ rows of \mathbf{V} and its K columns.

As shown in Fig. 2.6, the soft symbol estimate vector \mathbf{z}_o is finally quantized or mapped

to provide the hard symbol estimates:

$$\begin{aligned}\hat{\mathbf{d}}_o &= \mathcal{Q}(\mathbf{z}_o) \\ &= \mathcal{Q}(\mathbf{M}_o^H \mathbf{y}),\end{aligned}\tag{2.33}$$

where $\mathcal{Q}(\cdot)$ is a non-linear mapping or decision device. For BPSK, the decision function is the sign of the real part of the filter output i.e. $\mathcal{Q}(\cdot) = \text{Re}(\text{sgn}(\cdot))$, where both $\text{Re}(\cdot)$ and $\text{sgn}(\cdot)$ functions operate here element-wise on their respective vector argument. Because it estimates the symbols from all the users jointly, the receiver structure illustrated in Fig. 2.6 and described by equations (2.26)-(2.33) is referred to in this work as the *full STMUD* receiver.

Note that the output of the MF can also be used for detection, in which case the hard symbol estimate becomes

$$\hat{\mathbf{d}}_{\text{mf}} = \mathcal{Q}(\mathbf{y}).\tag{2.34}$$

This sub-optimal receiver structure is referred to in this work as the *matched filter* receiver. It can be interpreted as the discrete-time equivalent to the continuous-time RAKE receiver presented in Section 2.3. Alternatively, it can also be interpreted as a discrete-time form of conventional receiver, in which case the entire effective signature itself must be interpreted as the code sequence.

Chapter 3

Group-based approaches to multiuser detection

3.1 Motivation

The full STMUD receiver presented in Section 2.5 is optimal in the MMSE sense but requires the solution of a $NK \times NK$ linear system; a costly operation. As discussed in Section 1.1, by separating the users in groups it is possible to reduce the overall complexity, at the expense of a small performance degradation.

In this Chapter, the group-based approach to multiuser detection in the context of WCDMA is studied. In Section 3.2, new receiver structures for reduced complexity group-based MUD are derived. By exploiting the potentially unused computing resources available, it is possible to improve the performance of group-based receivers. This new concept, referred to as *user sharing*, is detailed in Section 3.3. Finally in Section 3.4, the computational complexity of the receiver structures studied is derived.

3.2 Group-based linear MUD

The receiver structures presented in this Section can be described conceptually by the generic block diagram in Fig. 3.1. The proposed receiver structures essentially consist of a RF front-end, which converts the received radio waves to baseband so that the received signal can be represented by the matrix signal model of Section 2.4, a set of G linear group multiuser detection filters, a grouping algorithm block, a symbol ordering block to sort the symbol estimates in the expected order, and a decision device. The two approaches presented in this Section differ only in the linear group multiuser detection blocks.

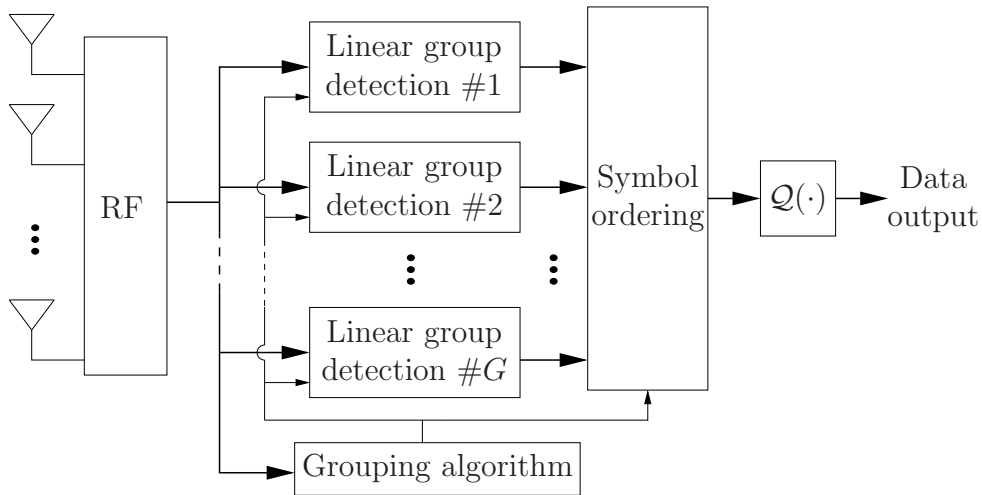


Fig. 3.1 Conceptual diagram for group-based linear space-time multiuser detection receiver structures.

The linear filters in each linear group detection block in Fig. 3.1 depend in general on the grouping, which is normally performed at startup, when a new user is introduced in the system, or when the channel characteristics change significantly. Let $\mathcal{G} = \{\mathcal{G}_1, \dots, \mathcal{G}_G\}$ be the system grouping and let $\mathcal{G}_j \subseteq \mathcal{S}$ be the set of user indices belonging to group $j \in \{1, \dots, G\}$, where $G = |\mathcal{G}|$ is the number of groups and $\mathcal{S} = \{1, \dots, K\}$ is the set of all

user indices. Let $g_{j,l} \in \mathcal{G}_j$ be the index of the l^{th} user of group j , then

$$\mathcal{G}_j = \{g_{j,1}, \dots, g_{j,K_j}\}, \quad (3.1)$$

where $K_j = |\mathcal{G}_j|$ is the number of users in group j . Also let $\bar{\mathcal{G}}_j$ be the complement of \mathcal{G}_j such that $\mathcal{G}_j \cup \bar{\mathcal{G}}_j = \mathcal{S}$ and $\mathcal{G}_j \cap \bar{\mathcal{G}}_j = \emptyset, \forall j$. If $\bar{g}_{j,l} \in \bar{\mathcal{G}}_j$ denotes the index for the l^{th} user of the complement of group j , then

$$\bar{\mathcal{G}}_j = \{\bar{g}_{j,1}, \dots, \bar{g}_{j,K-K_j}\}. \quad (3.2)$$

Each user typically belongs to at least one group so that $\bigcup_{j=1}^G \mathcal{G}_j = \mathcal{S}$. If the groups are mutually exclusive then $\mathcal{G}_j \cap \mathcal{G}_i = \emptyset$, for any $j \neq i$, and it follows that $K = \sum_j K_j$.

In general, the criterion for selecting the groups also depends on the actual linear filters; thus there is a need for a joint grouping and filter design approach. Since symbol detection is performed independently among groups and the choice of weights for a given group does not affect the other groups, it is reasonable to define the cost function associated to group j for a given set of user grouping as $J(\mathbf{M}_j, \mathcal{G}_j)$, where \mathbf{M}_j is the MUD linear filter for group j , and define the total cost as the sum of the individual cost from each group. The set of optimal filters and grouping may thus be expressed as

$$(\mathbf{M}_1^o, \dots, \mathbf{M}_G^o, \mathcal{G}^o) = \arg \min_{\forall (\mathbf{M}_1, \dots, \mathbf{M}_G, \mathcal{G})} \sum_{j=1}^G J(\mathbf{M}_j, \mathcal{G}_j). \quad (3.3)$$

Due to the discrete nature of \mathcal{G} , finding a solution for (3.3) may be a very difficult task for real-time operations. Indeed, grouping problems are in general NP-hard; although some techniques exist for finding sub-optimal solutions, there is no known polynomial time complexity algorithm that is guaranteed to provide an optimal grouping. There exists

different approaches for finding sub-optimal solutions such as genetic algorithms [Fal98], however these methods are usually too complex or too slow for the application considered here.

For this reason, the optimization problem is carried out in two separate steps: the first step consists of determining the grouping itself, and the second step consists of computing the MUD filter coefficients based on the grouping provided. Consequently, it is assumed for the remaining of this work that the grouping is available for the filter weight design. The grouping problem is discussed separately in Chapter 5.

In order to simplify the presentation on group-based systems, some new definitions need to be introduced. Let the term *selection matrix* designate an $n \times m$ ($n \geq m$) matrix containing exactly one entry of value 1 in each column and no more than one such entry per row; all other entries take value 0. Furthermore, define the $n \times m$ *selection matrix complement* as a selection matrix of dimension $n \times (n - m)$ such that $\mathbf{P}_{\text{perm}} = [\mathbf{P} \ \bar{\mathbf{P}}]^T$ is a permutation matrix¹, where \mathbf{P} and $\bar{\mathbf{P}}$ are the selection matrix and the selection matrix complement, respectively.

According to the above definitions, the $K \times K_j$ selection matrix associated to the symbols for the users of group j can thus be expressed as

$$\mathbf{P}^{(j)} = [\mathbf{e}_{g_{j,1}}, \dots, \mathbf{e}_{g_{j,K_j}}], \quad (3.4)$$

where $\mathbf{e}_{g_{j,t}}$ is the elementary vector of dimension $K \times 1$ containing zeros except at position

¹An $n \times n$ matrix \mathbf{A} is called a *permutation matrix* if exactly one entry in each row and column is equal to 1, and all other entries are 0 (see e.g.: [HJ90]).

$g_{j,l}$, where it contains the value 1, i.e.:

$$\mathbf{e}_{g_{j,l}} = \underbrace{[0, \dots, 0]_{g_{j,l}-1}}_{g_{j,l}-1}, \underbrace{[1, 0, \dots, 0]_{K-g_{j,l}}}_{K-g_{j,l}}^T. \quad (3.5)$$

Then the $NK \times NK_j$ selection matrix for all NK_j symbols transmitted by users of group j takes the form

$$\mathbf{P}_j \triangleq (\mathbf{I}_N \otimes \mathbf{P}^{(j)}) = \begin{bmatrix} \mathbf{P}^{(j)} & \dots & \mathbf{0} \\ \vdots & \ddots & \vdots \\ \mathbf{0} & \dots & \mathbf{P}^{(j)} \end{bmatrix}, \quad (3.6)$$

where \otimes denotes the Kronecker matrix product². Similarly, let $\bar{\mathbf{P}}^{(j)}$ be the $K \times (K - K_j)$ selection matrix complement for users of group j . That is, $\bar{\mathbf{P}}^{(j)}$ selects the users outside of group j and takes the form

$$\bar{\mathbf{P}}^{(j)} = [\mathbf{e}_{\bar{g}_{j,1}}, \dots, \mathbf{e}_{\bar{g}_{j,(K-K_j)}}], \quad (3.7)$$

where as in (3.2) $\bar{g}_{j,l}$ is the index of the l^{th} user *not* in group j . Thus, the selection matrix complement for the NK_j symbols of group j can be expressed as

$$\bar{\mathbf{P}}_j \triangleq (\mathbf{I}_N \otimes \bar{\mathbf{P}}^{(j)}) = \begin{bmatrix} \bar{\mathbf{P}}^{(j)} & \dots & \mathbf{0} \\ \vdots & \ddots & \vdots \\ \mathbf{0} & \dots & \bar{\mathbf{P}}^{(j)} \end{bmatrix}. \quad (3.8)$$

²The Kronecker product of matrices \mathbf{A} ($p \times q$) and \mathbf{B} ($m \times n$) is given by $(pm \times qn)$ matrix

$$\mathbf{A} \otimes \mathbf{B} \triangleq \begin{bmatrix} a_{1,1}\mathbf{B} & \dots & a_{1,q}\mathbf{B} \\ \vdots & \ddots & \vdots \\ a_{p,1}\mathbf{B} & \dots & a_{p,q}\mathbf{B} \end{bmatrix}.$$

From (3.6) and (3.8), it can be observed that the vector of NK_j symbols for the users of group j and the $N(K - K_j)$ symbols associated to the users outside of group j are given by

$$\mathbf{d}_j \triangleq \mathbf{P}_j^T \mathbf{d} \quad (3.9)$$

$$\bar{\mathbf{d}}_j \triangleq \bar{\mathbf{P}}_j^T \mathbf{d}, \quad (3.10)$$

respectively. In the same way, the columns of \mathbf{T} associated to users of group j and to users outside of group j can be obtained using (3.6) and (3.8) as

$$\mathbf{T}_j \triangleq \mathbf{T} \mathbf{P}_j, \quad \mathbf{T}_j \in \mathbb{C}^{M(NQ+W-1) \times NK_j} \quad (3.11)$$

$$\bar{\mathbf{T}}_j \triangleq \mathbf{T} \bar{\mathbf{P}}_j, \quad \bar{\mathbf{T}}_j \in \mathbb{C}^{M(NQ+W-1) \times N(K-K_j)}, \quad (3.12)$$

respectively. Note that equations (3.6), (3.8) and (3.9) to (3.12) are used extensively in the remaining of this work to simplify the presentation in the convenient matrix format adopted. Also observe that $\mathbf{P}_j^T \mathbf{P}_j = \mathbf{I}$, $\bar{\mathbf{P}}_j^T \bar{\mathbf{P}}_j = \mathbf{I}$ and $\bar{\mathbf{P}}_j^T \mathbf{P}_j = \mathbf{0}$, so that the matrices $\mathcal{P} \triangleq \mathbf{P}_j \mathbf{P}_j^T$ and $\bar{\mathcal{P}} \triangleq \bar{\mathbf{P}}_j \bar{\mathbf{P}}_j^T$ provide a pair of complementary orthogonal projection matrices that can be used to express the observation vector as the sum of “in-group” and “out-of-group” components (i.e. $\mathcal{P} + \bar{\mathcal{P}} = \mathbf{I}$). As such, the received signal in (2.24) can be conveniently be expressed as

$$\mathbf{x} = \mathbf{T}(\mathcal{P} + \bar{\mathcal{P}})\mathbf{d} + \mathbf{n} \quad (3.13)$$

$$= \mathbf{T}_j \mathbf{d}_j + \bar{\mathbf{T}}_j \bar{\mathbf{d}}_j + \mathbf{n}, \quad (3.14)$$

where the first and second term in (3.14) correspond to the signal contribution from the

users in the group of interest and from the users outside of the group of interest, respectively.

3.2.1 Group-based linear MUD with beamforming

There exists several approaches to group-based linear MUD with beamforming (BF) in the literature. In general, a simplified transmission model is used where the ISI is neglected (see e.g.: [HSMTG00, LLC01]). This assumption simplifies the filter design since the symbols can be processed independently. Unfortunately, the MUD filters may suffer from model mismatch when confronted to the more practical and general model in (2.24). Indeed, while the modeling simplifications and approximations are well-justified for WCDMA systems with long codes, it may not be the case for short code WCDMA such as UTRA/TDD for instance. In fact for the same relative channel delay spread and chip rate, the ISI contribution to each symbol on the received signal is more significant for short codes than for long code WCDMA systems. In general, for the codes of interest, the residual correlation is inversely proportional to the code length.

In this section, a new group-based linear MUD receiver with beamforming that takes into consideration ISI and IGI is derived. The proposed receiver structure incorporates block processing³ and optimal MMSE post-beamforming MUD linear filtering. It can be interpreted as a generalization of existing group-based MUD receiver structures with beamforming. The proposed receiver follows the general structure illustrated in Fig. 3.1, where the specific linear group detection module for each group consists of a set of beamforming weights followed by a multiuser detection device, as illustrated in Fig. 3.2.

Let the beamforming weight vector for the l^{th} user of group j be given by $\mathbf{w}_{j,l} \in \mathbb{C}^{M \times 1}$. The weights are also assumed to be normalized so that $\|\mathbf{w}_{j,l}\| = 1, \forall j, l$. The beamforming

³In this work the term *block processing* indicates that the symbols in the proposed receiver structures are processed in blocks, as opposed to being processed independently.

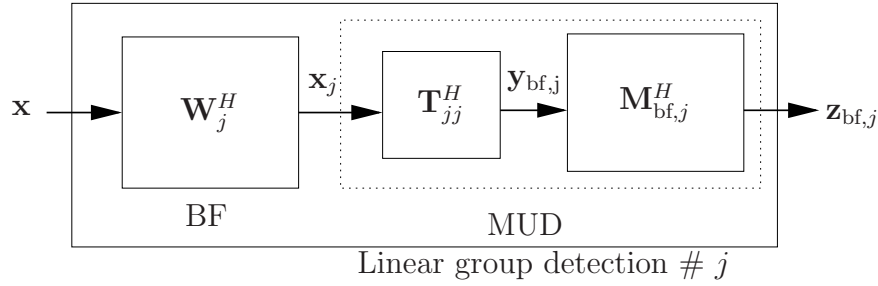


Fig. 3.2 Block diagram for the linear group detection module, which is part of the group-based linear space-time MUD receiver structure in Fig. 3.1, for the optimal group-based space-time MUD receiver with beamforming (GRP-STMUD-BF).

weights can be obtained using one of the multiple existing approaches for spatial filter design (see e.g. [VT02, God97]). Let the beamforming weight matrix for the K_j users of group j be defined as

$$\mathbf{W}^{(j)} \triangleq [\mathbf{w}_{j,1} \ \dots \ \mathbf{w}_{j,K_j}], \quad (3.15)$$

and the beamforming matrix for the $NQ + W - 1$ temporal samples of the observation interval be given by

$$\begin{aligned} \mathbf{W}_j &= \mathbf{I}_{NQ+W-1} \otimes \mathbf{W}^{(j)} \\ &= \begin{bmatrix} \mathbf{W}^{(j)} & & \\ & \ddots & \\ & & \mathbf{W}^{(j)} \end{bmatrix}, \end{aligned} \quad (3.16)$$

where $\mathbf{W}_j \in \mathbb{C}^{M(NQ+W-1) \times K_j(NQ+W-1)}$. Then the vector output of the beamforming module can be expressed as

$$\mathbf{x}_j = \mathbf{W}_j^H \mathbf{x}, \quad \mathbf{x}_j \in \mathbb{C}^{K_j(NQ+W-1) \times 1}. \quad (3.17)$$

To simplify the derivation of the MMSE MUD filter weights, it is convenient to define the following matrices:

$$\mathbf{T}_{jj} \triangleq \mathbf{W}_j^H \mathbf{T}_j, \quad \mathbf{T}_{jj} \in \mathbb{C}^{K_j(NQ+W-1) \times NK_j} \quad (3.18)$$

$$\bar{\mathbf{T}}_{jj} \triangleq \mathbf{W}_j^H \bar{\mathbf{T}}_j, \quad \bar{\mathbf{T}}_{jj} \in \mathbb{C}^{K_j(NQ+W-1) \times N(K-K_j)}, \quad (3.19)$$

where \mathbf{T}_j and $\bar{\mathbf{T}}_j$ have been defined in (3.11) and (3.12), respectively. Matrices \mathbf{T}_{jj} and $\bar{\mathbf{T}}_{jj}$ contain the columns of \mathbf{T} *after* beamforming with the spatial filters associated to group j , for users of group j and users outside of group j , respectively.

The beamformer output for group j can then be expanded to take the convenient form

$$\mathbf{x}_j = \mathbf{T}_{jj} \mathbf{d}_j + \bar{\mathbf{T}}_{jj} \bar{\mathbf{d}}_j + \mathbf{n}_j, \quad (3.20)$$

where the first term corresponds to the signal coming from the users of group j , the second term is the inter-group interference and the last term corresponds to the AWGN noise vector given by

$$\mathbf{n}_j \triangleq \mathbf{W}_j^H \mathbf{n}. \quad (3.21)$$

The noise term in (3.20) is colored by the beamformer and the corresponding noise covariance matrix is given by

$$\begin{aligned} \mathbf{R}_{\mathbf{nn}} &\equiv E[\mathbf{n}_j \mathbf{n}_j^H] = \sigma^2 \mathbf{W}_j^H \mathbf{W}_j \\ &= \sigma^2 (\mathbf{I}_{NQ+W-1} \otimes \mathbf{W}^{(j)H} \mathbf{W}^{(j)}). \end{aligned} \quad (3.22)$$

Notice that the beamformer output \mathbf{x}_j has dimension $K_j(NQ + W - 1) \times 1$, which can be very large even for moderate values of N and Q . In the context of MUD filtering, it is

more practical to use the output of a filter matched to the output signal of the beamformer. This approach can also be justified by the fact that the matched filter provides a set of sufficient statistics [Ver98].

Based on this observation, the group MUD linear filter weights are therefore applied to the output of the matched filter, after beamforming. Let $\mathbf{y}_{\text{bf},j}$ be the matched filter output after beamforming, defined here as

$$\mathbf{y}_{\text{bf},j} = \mathbf{T}_{jj}^H \mathbf{x}_j \quad (3.23)$$

$$= \mathbf{T}_{jj}^H \mathbf{T}_{jj} \mathbf{d}_j + \mathbf{T}_{jj}^H \bar{\mathbf{T}}_{jj} \bar{\mathbf{d}}_j + \mathbf{T}_{jj}^H \mathbf{n}_j, \quad (3.24)$$

where \mathbf{T}_{jj} is defined in (3.18) and \mathbf{x}_j is given in (3.20). The MMSE cost function for the output of the linear filter for group j can therefore be expressed as

$$J_{\text{bf},j}(\mathbf{M}) = E \|\mathbf{d}_j - \mathbf{M}^H \mathbf{y}_{\text{bf},j}\|^2. \quad (3.25)$$

The linear filter matrix minimizing the cost function in (3.25) is given by the solution of the following optimization problem:

$$\mathbf{M}_{\text{bf},j} = \arg \min_{\mathbf{M}} J_{\text{bf},j}(\mathbf{M}), \quad (3.26)$$

and the filter matrix $\mathbf{M}_{\text{bf},j}$ is the MMSE linear estimator after beamforming for the symbols belonging to users of group j .

In deriving the MMSE linear estimator, it is assumed that only the symbols belonging to users of group j are to be estimated; the signal contribution from the users outside of group j is considered random and is not estimated.

Proposition 1. *The solution to (3.26), giving the optimal MMSE weights for the group-based linear receiver after beamforming is given by the $NK_j \times NK_j$ matrix*

$$\mathbf{M}_{\text{bf},j} = (\mathbf{R}_{jj}\mathbf{R}_{jj}^H + \mathbf{C}_{jj}\mathbf{C}_{jj}^H + \mathbf{T}_{jj}^H\mathbf{R}_{\text{nn}}\mathbf{T}_{jj})^{-1}\mathbf{R}_{jj}^H, \quad (3.27)$$

where

$$\mathbf{R}_{jj} \triangleq \mathbf{T}_{jj}^H\mathbf{T}_{jj}, \quad (3.28)$$

$$\mathbf{C}_{jj} \triangleq \mathbf{T}_{jj}^H\bar{\mathbf{T}}_{jj}. \quad (3.29)$$

Proof. The proof is detailed in Appendix A.1. □

It is important to recognize that the optimality of (3.27) is with respect to the pre-determined grouping and beamforming weights. Joint optimization for grouping, beamforming, and linear weight design for data estimation would be very complex and is not considered in this work.

Notice that the matrix inversion in (3.27) has dimension $NK_j \times NK_j$, reduced from the full space-time MUD in (2.30) with dimension $NK \times NK$. Depending on the grouping, this may represent a considerable reduction in complexity.

The block diagram in Fig. 3.2 illustrates the linear group detection module, part of the group-based receiver in Fig. 3.1, for the optimal MMSE group-based linear MUD with beamforming. The input of the group detection module as shown in Fig. 3.2 is the observation signal from the antenna array output (\mathbf{x}), and the output is the soft symbol estimate vectors for the symbols of group j , given here by

$$\mathbf{z}_{\text{bf},j} \triangleq \mathbf{M}_{\text{bf},j}^H\mathbf{y}_{\text{bf},j}. \quad (3.30)$$

This group-based linear MUD block is part of the larger group-based receiver illustrated in Fig. 3.1. The complete receiver structure, combining the linear group detection of Fig. 3.2 with the general receiver structure in Fig. 3.1, will be referred to in this work as the *GRP-STMUD-BF* receiver.

3.2.2 Optimal MMSE group-based linear space-time MUD

The new GRP-STMUD-BF receiver structure derived in the previous section requires a dedicated and independent beamforming unit, as shown in Fig. 3.2. While beamforming has the potential to reduce inter-group interference, it provides a suboptimal observation signal to the multiuser detection filter. Indeed, since the multiuser detection unit has no control over the weights matrix \mathbf{W}_j , the signal \mathbf{y}_j in (3.17) does not necessarily provide a sufficient statistic for the desired user information contained in the input signal vector \mathbf{x} to the MUD device. Thus, in addition to requiring extra hardware complexity for the beamforming weight design, the approach in Section 3.2.1 does not necessarily provide the best symbol estimates.

Moreover, it can be observed from Fig. 3.2 that even though the structure contains a beamforming unit (BF), the MUD block still requires a matched filter to reduce the dimension of the observation vector to a practical size and to combine the multipaths. Thus spatial and temporal filtering are essentially being performed separately. Compared to the full space-time MUD in (2.30), where space-time filtering is performed by the matched filter simultaneously providing a set of sufficient statistics to the MUD filter, the separate beamforming unit adds complexity and leads to a potential loss of information, depending on how the weights are designed.

In this section, a new optimal MMSE group-based linear space-time MUD approach that does not require a dedicated beamforming unit is proposed. The new structure is

based on the full STMUD receiver structure.

Using the selection matrices defined in (3.6) and (3.8), the received signal in (2.24) can be expressed as in (3.14), repeated here for convenience:

$$\mathbf{x} = \mathbf{T}_j \mathbf{d}_j + \bar{\mathbf{T}}_j \bar{\mathbf{d}}_j + \mathbf{n}, \quad (3.31)$$

where j is the index of the group of interest, and where \mathbf{d}_j , $\bar{\mathbf{d}}_j$, \mathbf{T}_j and $\bar{\mathbf{T}}_j$ are defined in (3.9)-(3.12), respectively.

The proposed linear group detection structure consists of a matched filter followed by a group-based multiuser detection linear filter. The matched filter outputs for the users of each group are selected as inputs to the linear MUD filter. The matched filter output for users of group j can be expressed as

$$\mathbf{y}_j \triangleq \mathbf{P}_j^T \mathbf{y} \quad (3.32)$$

$$= \mathbf{P}_j^T \mathbf{T}^H \mathbf{x} \quad (3.33)$$

$$= \mathbf{T}_j^H \mathbf{T}_j \mathbf{d}_j + \mathbf{T}_j^H \bar{\mathbf{T}}_j \bar{\mathbf{d}}_j + \mathbf{T}_j^H \mathbf{n}, \quad (3.34)$$

where \mathbf{y} is the matched filter output defined in (2.26). Equation (3.34) is obtained by applying matched filtering to the observation signal expressed in its expanded form in (3.31).

The group MUD filter weights are designed according to the MMSE criterion. The proposed cost function for the group-based linear filter is given by

$$J_{\text{grp},j}(\mathbf{M}) = E \|\mathbf{d}_j - \mathbf{M}^H \mathbf{y}_j\|^2. \quad (3.35)$$

The optimal MMSE weights matrix is the solution to the following optimization problem:

$$\mathbf{M}_{\text{grp},j} = \arg \min_{\mathbf{M}} J_{\text{grp},j}(\mathbf{M}). \quad (3.36)$$

Let the group signature autocorrelation block matrix \mathbf{R}_j be defined as

$$\mathbf{R}_j \triangleq \mathbf{T}_j^H \mathbf{T}_j, \quad \mathbf{R}_j \in \mathbb{C}^{NK_j \times NK_j}. \quad (3.37)$$

As its name implies, the elements of \mathbf{R}_j can be interpreted as the correlation between the symbols associated to users of group j . Similarly, define the group signature cross-correlation block matrix \mathbf{C}_j as

$$\mathbf{C}_j \triangleq \mathbf{T}_j^H \bar{\mathbf{T}}_j, \quad \mathbf{C}_j \in \mathbb{C}^{NK_j \times N(K-K_j)}. \quad (3.38)$$

It can be observed from the definition that the elements of \mathbf{C}_j can be interpreted as the correlation between symbols associated to users of group j and the symbols associated to users in the interfering groups.

Proposition 2. *The solution to the group MMSE linear weights optimality criterion of (3.36) is given by the $NK_j \times NK_j$ matrix*

$$\mathbf{M}_{\text{grp},j} = (\mathbf{R}_j \mathbf{R}_j^H + \mathbf{C}_j \mathbf{C}_j^H + \sigma^2 \mathbf{R}_j)^{-1} \mathbf{R}_j^H. \quad (3.39)$$

Proof. The proof is in Appendix A.2. □

Notice that the proposed MUD linear filter in (3.39) takes into consideration the contribution from the IGI via the term $\mathbf{C}_j \mathbf{C}_j^H$. As a result, the filter has a slightly more complex form than the full space-time MUD of (2.30).

Figure 3.3 illustrates the block diagram of the proposed optimal MMSE linear group detection module, which is integrated in the general receiver structure shown in Fig. 3.1. The input is the observation signal from the antenna array, and the output is the soft symbol estimate for group j . As illustrated, the soft symbol estimate is obtained by applying the group-based multiuser detection linear weights of (3.39) to the output of the group matched filter in (3.32). The soft symbol estimate for users of group j is thus given by

$$\mathbf{z}_{\text{grp},j} = \mathbf{M}_{\text{grp},j}^H \mathbf{T}_j^H \mathbf{x}. \quad (3.40)$$

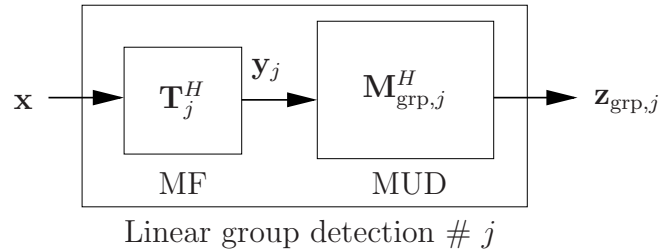


Fig. 3.3 Block diagram for linear group detection module, part of the group-based linear space-time MUD receiver structure in Fig. 3.1, for the optimal group-based linear MUD (GRP-STMUD).

The receiver described by (3.39) and (3.40), and illustrated in Fig. 3.3 (which is part of the larger receiver block diagram of Fig. 3.1) is referred to in this work as the group space-time MUD (GRP-STMUD) receiver.

Based on the above discussion, it can be observed that the GRP-STMUD receiver structure in Fig. 3.3 is simpler than the GRP-STMUD-BF receiver structure in Fig. 3.2. Moreover, it can be noted that the beamforming in the GRP-STMUD-BF represents a redundant filtering step that reduces the observation space provided to the MUD linear filter.

3.3 Non-mutually exclusive grouping: user sharing

In a practical receiver, the resources are limited by the hardware, which is typically designed to support a given maximum load. For a group-based receiver the concept is similar; a practical design would support a limited number of groups G_{\max} , and each group would support a maximum number of users K_{grp} .

Depending on the total number of active users and on the actual grouping, some groups may not have all their resources occupied. For a given group $j \in \{1, \dots, G_{\max}\}$, this situation corresponds to the case $K_j < K_{\text{grp}}$; the extra $K_{\text{grp}} - K_j$ available resources can be used to improve the detection. This may be accomplished by *sharing* users among groups. This new approach can be advantageous when, for example, a given user belonging to group j interferes severely with users of a different group $l \neq j$. If the two groups are too large to be merged into a single one, i.e. $K_j + K_l > K_{\text{grp}}$, and if one or both groups have unused resources available so that either $K_j < K_{\text{grp}}$, $K_l < K_{\text{grp}}$ or both, then user sharing can be used to improve detection.

When some users are shared, the groups are no longer mutually exclusive; the signal from each shared user is processed by multiple groups simultaneously. If a user belongs to multiple groups, one symbol estimate vector for that user will be available for each of the linear group detection units that “share” the user. To further improve the detection of that shared user, the symbol soft estimates from the different groups can be combined. This can be achieved using different techniques; to maintain uniformity with previous development, the focus here is on MMSE linear combining. The low complexity and efficient selective combining approach will also be discussed.

As for the case of group-based receiver design discussed in the previous section, the combining weight design and non-mutually exclusive grouping are carried out separately.

An algorithm for non-mutually exclusive grouping is proposed in Section 5.3.3.

MMSE combining

In MMSE combining, the outputs from the groups sharing a given user are linearly weighted to provide the vector of soft symbol estimates for that shared user. Assume, without loss of generality, that user k is shared among groups 1 to N_k , $N_k \leq G$. Let $\mathbf{z}_j^{(k)} \in \mathbb{C}^{N \times 1}$ be the vector of soft symbol estimates for user k , obtained at the output of the linear MUD filter of group $j \in \{1, \dots, N_k\}$. Using the GRP-STMUD receiver derived in Section 3.2.2 as a basis for the group-based receiver with sharing, $\mathbf{z}_j^{(k)} \in \mathbb{C}^{N \times 1}$ can be expressed as

$$\begin{aligned} \mathbf{z}_j^{(k)} &= (\mathbf{I}_N \otimes \mathbf{e}_{u_{j,k}})^T \mathbf{z}_j \\ &= (\mathbf{I}_N \otimes \mathbf{e}_{u_{j,k}})^T \mathbf{M}_{\text{grp},j}^H \mathbf{T}_j^H \mathbf{x}, \end{aligned} \quad (3.41)$$

where $\mathbf{e}_{u_{j,k}}$ is the elementary vector of dimension $K_j \times 1$ taking value 1 at position $u_{j,k}$, and $u_{j,k}$ is the index of user k within group j . Note that for different groups, the k^{th} user index within the group may change and in general $u_{j,k} \neq u_{j',k}$ for $j \neq j'$. Also, define the concatenated vector of soft symbol estimates for user k , containing the linear MUD filter outputs from all $N_k \in \{1, \dots, G\}$ groups sharing user k , as follows:

$$\tilde{\mathbf{z}}^{(k)} \triangleq \begin{bmatrix} \mathbf{z}_1^{(k)} \\ \vdots \\ \mathbf{z}_{N_k}^{(k)} \end{bmatrix}, \quad \tilde{\mathbf{z}}^{(k)} \in \mathbb{C}^{N_k N \times 1}. \quad (3.42)$$

Using (3.42) the cost function for MMSE linear combining of the $N_k > 1$ multiple

information symbol estimates for user k can be expressed as

$$J_c^{(k)}(\mathbf{M}_c) = E\|\mathbf{d}^{(k)} - \mathbf{M}_c^H \tilde{\mathbf{z}}^{(k)}\|^2, \quad (3.43)$$

where $\mathbf{d}^{(k)}$ is the vector of N transmitted symbols from user k and $\mathbf{M}_c \in \mathbb{C}^{NN_k \times N}$. The optimal MMSE linear estimator here is the weight matrix \mathbf{M}_c that solves the following optimization problem:

$$\mathbf{M}_{c,o}^{(k)} = \arg \min_{\mathbf{M}_c} J_c^{(k)}(\mathbf{M}_c). \quad (3.44)$$

Proposition 3. *The optimal MMSE weight matrix that minimizes the cost in (3.43) is given by*

$$\begin{aligned} \mathbf{M}_{c,o}^{(k)} &= [\mathbf{M}_{\text{grp}}^{(k)H} (\mathbf{T}\mathbf{T}^H + \sigma^2\mathbf{I}) \mathbf{M}_{\text{grp}}^{(k)}]^{-1} \mathbf{M}_{\text{grp}}^{(k)H} \mathbf{T}^{(k)} \\ &= [\mathbf{M}_{\text{grp}}^{(k)H} \mathbf{T}\mathbf{T}^H \mathbf{M}_{\text{grp}}^{(k)} + \sigma^2 \mathbf{M}_{\text{grp}}^{(k)H} \mathbf{M}_{\text{grp}}^{(k)}]^{-1} \mathbf{M}_{\text{grp}}^{(k)H} \mathbf{T}^{(k)}, \end{aligned} \quad (3.45)$$

where $\mathbf{T}^{(k)} \triangleq \mathbf{T}(\mathbf{I}_N \otimes \mathbf{e}_k) \in \mathbb{C}^{M(NQ+W-1) \times N}$ contains the columns of \mathbf{T} corresponding to user k only, with \mathbf{e}_k being the elementary vector of dimension $K \times 1$ with value 1 at position k , and

$$\mathbf{M}_{\text{grp}}^{(k)H} \triangleq \begin{bmatrix} (\mathbf{I}_N \otimes \mathbf{e}_{u_{1,k}})^T \mathbf{M}_{\text{grp},1}^H \mathbf{T}_1^H \\ \vdots \\ (\mathbf{I}_N \otimes \mathbf{e}_{u_{N_k,k}})^T \mathbf{M}_{\text{grp},N_k}^H \mathbf{T}_{N_k}^H \end{bmatrix}, \quad \mathbf{M}_{\text{grp}}^{(k)H} \in \mathbb{C}^{NN_k \times M(NQ+W-1)}. \quad (3.46)$$

Proof. The proof is given in Appendix A.3. □

Noting that MMSE combining is not necessary for $N_k = 1$, the vector of N soft symbol

estimates for user k takes the form

$$\mathbf{z}_c^{(k)} = \mathbf{M}_{\text{comb}}^{(k)H} \tilde{\mathbf{z}}^{(k)}, \quad \text{where} \quad (3.47)$$

$$\mathbf{M}_{\text{comb}}^{(k)} \triangleq \begin{cases} \mathbf{M}_{c,o}^{(k)}, & N_k > 1 \\ \mathbf{I}_N, & N_k = 1. \end{cases} \quad (3.48)$$

The soft symbol estimates for all users can be obtained by concatenating $\mathbf{z}_c^{(k)}$ for all K users into a single vector:

$$\mathbf{z}_c \triangleq \text{vec}([\mathbf{z}_c^{(1)}, \dots, \mathbf{z}_c^{(K)}]^T). \quad (3.49)$$

Finally, as for all receiver structures discussed in this Chapter, the hard estimate is obtained via non-linear mapping:

$$\hat{\mathbf{d}}_c^{(k)} = \mathcal{Q}(\mathbf{z}_c). \quad (3.50)$$

Figure 3.4 on page 58 illustrates the proposed approach in block diagram form. Note that the block that selects the output from the different GRP-STMUD filters and the re-ordering block do not require computing resources. On the other hand, resources are required for computing the combining matrices $\mathbf{M}_{c,o}^{(k)}$ in (3.45), and to linearly combine the symbol estimates in (3.47) for every users with $N_k > 1$.

In general, not all users are to be shared and the extra processing required for MMSE combining applies to only a few users. In this context, the diagram in Fig. 3.4 illustrates the worst case scenario; in practice, not all users would require combining.

Selective combining

The MMSE combining approach presented in the previous section is optimal in the linear sense, but is costly to implement. The selective combining approach proposed here uses only

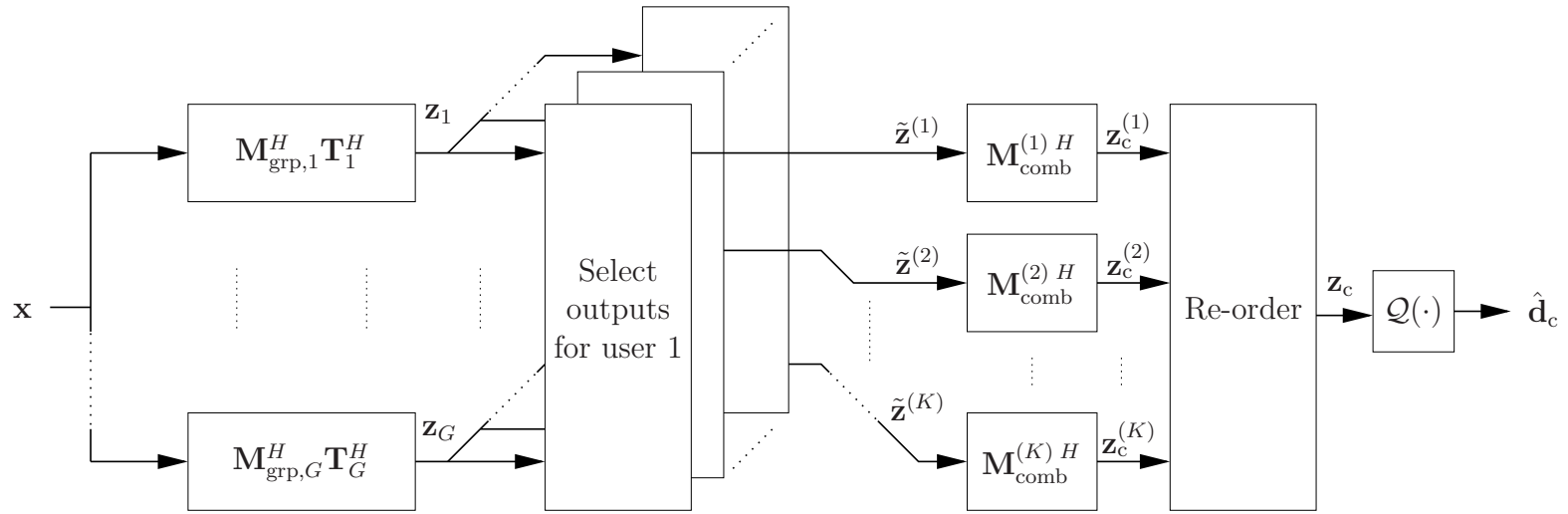


Fig. 3.4 Block diagram for the GRP-STMUD receiver with sharing using MMSE linear combining.

a single group output for detection, chosen among the multiple groups sharing the given user, and thus does not require significant additional computing resources to implement.

To select the group output for detection, several criteria may be used. In this work, the selection is based on the grouping algorithm cost criterion. Essentially, the group output that provides the lowest interference level for a given user, measured using the squared magnitude of the cross-correlation between effective signature waveforms, is selected for detection. The exact form of the selection criterion will be discussed in Chapter 5.

Let user k be shared by multiple groups. Assume that the MUD linear filter output of group j is selected for symbol detection of user k . Then the vector of soft symbol estimates for the selective combiner becomes

$$\begin{aligned}\mathbf{z}_s^{(k)} &\triangleq (\mathbf{I}_N \otimes \mathbf{e}_{u_{j,k}})^T \mathbf{z}_j \\ &= (\mathbf{I}_N \otimes \mathbf{e}_{u_{j,k}})^T \mathbf{M}_{\text{grp},j}^H \mathbf{T}_j^H \mathbf{x},\end{aligned}\tag{3.51}$$

where $u_{j,k}$ is the index of user k within group j , and $\mathbf{e}_{u_{j,k}}$ is the corresponding elementary vector of dimension $K_j \times 1$. As for the MMSE combining receiver, the vector of soft symbol estimates for all users can be expressed as

$$\mathbf{z}_s \triangleq \text{vec}([\mathbf{z}_s^{(1)}, \dots, \mathbf{z}_s^{(K)}]^T),\tag{3.52}$$

and the hard symbol estimate is given by

$$\hat{\mathbf{d}}_s \triangleq \mathcal{Q}(\mathbf{z}_s).\tag{3.53}$$

The block diagram of the proposed GRP-STMUD receiver with user sharing and selective combining is illustrated in Fig. 3.5. This structure is similar to the structure for MMSE

combining illustrated in Fig. 3.4, but since there is only a single group output selected per user, there is no need for linear combining.

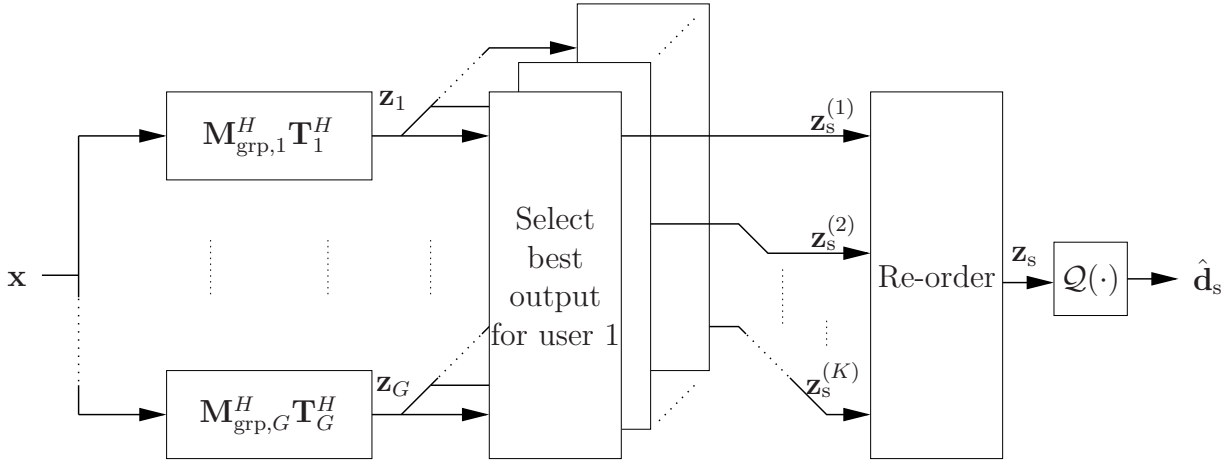


Fig. 3.5 Block diagram for the GRP-STMUD receiver with user sharing using selective combining.

3.4 Complexity analysis

Along with the BER performance, computational complexity is an important factor in the design process of any receiver, and for this reason, it is essential to quantify it. In this section, the complexity of the GRP-STMUD-BF and GRP-STMUD receiver structures is analyzed and compared to that of the full STMUD receiver.

To compare the complexity between the different receiver structures, the number of complex floating point operations (CFLOPS) is counted for the different parts of the equations describing each structure. All the computations involved in computing the vector of soft symbol estimates from the observation signal \mathbf{x} are taken into consideration. Whenever possible, the structure in the matrices is exploited to save on computations. This is the case for instance in operations involving \mathbf{T} in (2.25), which is highly structured. The cost expressed in most cases is approximated by neglecting smaller order terms.

All the receiver structures considered require the solution of an inverse system, which takes the form of a matrix inverse (see (2.30), (3.27), and (3.39)). In practice, since only the system solution is of interest, computing the actual filter weights matrix for each receiver is not required. Thus, to obtain the soft vector estimate, it is more practical to use Cholesky decomposition and back-substitution to solve the inverse problem [GVL96]. Note that this approach leads to an exact solution; it is also possible to use lower-complexity techniques that provide approximate solutions [VHG01].

The complexity figures are expressed in terms of a number of system parameters. For convenience, the relevant parameters and their associated meaning are summarized in Table 3.1. To simplify the complexity expressions obtained in this section, it is assumed that the channel length is much smaller than the spreading factor, i.e. $W \ll Q$.

Parameter	Meaning
N	Block size (number of symbols per user per frame)
K	Total number of users
M	Number of antenna elements
Q	Spreading factor
W	Channel length (in # of chips)
K_j	Number of users in group j
N_k	Number of groups sharing user k

Table 3.1 Relevant system parameters for the complexity analysis.

3.4.1 Full STMUD

The full STMUD receiver, described in Section 2.5 and illustrated in Fig. 2.6, is used as a reference for comparison purposes. To obtain the vector of soft symbol estimates provided by the full STMUD, three steps are essentially required. The first step consists of matched filtering and it is described by (2.26). The second step consists of observation signal independent calculations, a set of operations designated as *intermediate calculations*

in this work. These intermediate calculations are required to prepare the matrices for linear system solution and other processing. The last step consists of computing the linear system solution, an operation described by (2.27) and (2.30). This is achieved here using Cholesky decomposition and backsubstitution. Table 3.2 summarizes the cost for each of the steps related to the full STMUD receiver.

Category	Operation	Label	Approximate cost (in CFLOPS)
Matched filter	$\mathbf{T}^H \mathbf{x}$	\mathcal{C}_{mf}	$2NKM(Q + W - 1)$
Intermediate calculations	$\mathbf{T}^H \mathbf{T} + \sigma^2 \mathbf{I}$	$\mathcal{C}_{\text{icalc}}$	$MK^2(Q + 3W)$
Linear system solution	Cholesky factorization	$\mathcal{C}_{\text{chol}}$	$\frac{10NK^3}{3}$
	Backsubstitutions	\mathcal{C}_{bs}	$6NK^2$

Table 3.2 Approximate complexity (in CFLOPS) for the different steps of the full STMUD receiver.

In Appendix B, the cost associated to computing the Cholesky factorization of a matrix with the general structure of $\mathbf{T}^H \mathbf{T}$ is derived, along with the cost associated to backsubstitution. Note that the structure of the system matrix ($\mathbf{T}^H \mathbf{T} + \sigma^2 \mathbf{I}$) corresponds to the generic case presented in Appendix B with one off-block diagonal. For conciseness, the derivation of the complexity associated to the other operations is not explicitly documented in this work.

The total cost associated to the full STMUD receiver of Section 2.5 is given by

$$\mathcal{C}_{\text{STMUD}} = \mathcal{C}_{\text{mf}} + \mathcal{C}_{\text{icalc}} + \mathcal{C}_{\text{chol}} + \mathcal{C}_{\text{bs}}. \quad (3.54)$$

For large N , and dropping the lower order terms in (3.54), the total cost can be approxi-

mated as

$$\mathcal{C}_{\text{STMUD}} \approx 2NKMQ + \frac{10NK^3}{3}. \quad (3.55)$$

3.4.2 GRP-STMUD-BF

The GRP-STMUD-BF receiver has the general structure illustrated in Fig. 3.1. It is described in details in Section 3.2.1 and the corresponding linear group detection block diagram is illustrated in Fig. 3.2. The operations involved in getting the vector of soft symbol estimates consist of essentially five steps for each group, described by equations (3.17), (3.27), and (3.30).

The first step consists of beamforming (BF), an operation described by (3.17). It is assumed, for the purpose of the complexity analysis, that the beamforming weights are pre-calculated. The second step consists of the *intermediate calculations*, which consist in this case of computing the matrix to invert in (3.27) and other matrix elements required for matched filtering and post-processing. The third step consists of group-based matched filtering (after beamforming), an operation expressed by the right-most multiplicative matrix term in (3.27). The fourth operation is the actual solution of the linear system, and the last operation, referred to here as *post-processing*, consists of multiplying the solution vector defined here as

$$\mathbf{z}'_{\text{bf},j} \triangleq (\mathbf{R}_{jj}\mathbf{R}_{jj}^H + \mathbf{C}_{jj}\mathbf{C}_{jj}^H + \mathbf{T}_{jj}^H\mathbf{R}_{\text{nn}}\mathbf{T}_{jj})^{-1}\mathbf{T}_{jj}^H\mathbf{x}_j \quad (3.56)$$

by the matrix \mathbf{R}_{jj} , as indicated by (3.27). Table 3.3 summarizes the cost for each of the steps related to the GRP-STMUD-BF receiver.

By combining the costs associated to the overhead in Table 3.3, the total overhead cost

Category	Operation	Label	Approximate cost (in CFLOPS)
Beamforming	$\mathbf{W}_j^H \mathbf{x}, \quad \forall j$	\mathcal{C}_{bf}	$2NKMQ$
Intermediate calculations	$\mathbf{T}_{jj}, \bar{\mathbf{T}}_{jj}$	$\mathcal{C}_{\mathbf{T}_{jj}, \bar{\mathbf{T}}_{jj}}$	$(2M - 1)K_j K(Q + W - 1)$
	$\mathbf{R}_{jj} = \mathbf{T}_{jj}^H \mathbf{T}_{jj}$	$\mathcal{C}_{\mathbf{R}_{jj}}$	$K_j^3(Q + 3W)$
	$\mathbf{C}_{jj} = \mathbf{T}_{jj}^H \bar{\mathbf{T}}_{jj}$	$\mathcal{C}_{\mathbf{C}_{jj}}$	$2K_j^2(K - K_j)(Q + 3W)$
	$\mathbf{R}_{jj} \mathbf{R}_{jj}^H$	$\mathcal{C}_{\mathbf{R}_{jj} \mathbf{R}_{jj}^H}$	$9K_j^3 + \frac{5}{2}K_j^2$
	$\mathbf{C}_{jj} \mathbf{C}_{jj}^H$	$\mathcal{C}_{\mathbf{C}_{jj} \mathbf{C}_{jj}^H}$	$9K_j^2(K - K_j) + \frac{5}{2}K_j^2$
	$\mathbf{T}_{jj}^H \mathbf{R}_{nn} \mathbf{T}_{jj}$	$\mathcal{C}_{\sigma^2, j}$	$3MK_j^2(Q + W - 1) + 2K_j M(W - 1)$
	$\mathbf{R}_{jj} \mathbf{R}_{jj}^H + \mathbf{C}_{jj} \mathbf{C}_{jj}^H + \mathbf{T}_{jj}^H \mathbf{R}_{nn} \mathbf{T}_{jj}$	$\mathcal{C}_{\text{add-bf}, j}$	$6K_j^2$
Matched filter	$\mathbf{T}_{jj}^H \mathbf{x}_j$	$\mathcal{C}_{\text{mf-bf}, j}$	$2NK_j^2(Q + W - 1)$
Linear system solution	Cholesky factorization	$\mathcal{C}_{\text{chol-bf}, j}$	$\frac{19NK_j^3}{3}$
	Backsubstitutions	$\mathcal{C}_{\text{bs-bf}, j}$	$10NK_j^2$
Post-processing	$\mathbf{R}_{jj} \mathbf{z}'_{\text{bf}, j}$	$\mathcal{C}_{\text{post-bf}, j}$	$6NK_j^2$

Table 3.3 Approximate complexity (in CFLOPS) for the different steps of the GRP-STMUD-BF receiver.

becomes

$$\mathcal{C}_{\text{icalc-bf}, j} = \mathcal{C}_{\mathbf{T}_{jj}, \bar{\mathbf{T}}_{jj}} + \mathcal{C}_{\mathbf{R}_{jj}} + \mathcal{C}_{\mathbf{C}_{jj}} + \mathcal{C}_{\mathbf{R}_{jj} \mathbf{R}_{jj}^H} + \mathcal{C}_{\mathbf{C}_{jj} \mathbf{C}_{jj}^H} + \mathcal{C}_{\sigma^2, j} + \mathcal{C}_{\text{add-bf}, j}. \quad (3.57)$$

Then the total cost in terms of CFLOPS for the GRP-STMUD-BF receiver can be expressed as

$$\mathcal{C}_{\text{GRP-STMUD-BF}} = \mathcal{C}_{\text{bf}} + \sum_{j=1}^G \mathcal{C}_{\text{icalc-bf}, j} + \mathcal{C}_{\text{mf-bf}, j} + \mathcal{C}_{\text{chol-bf}, j} + \mathcal{C}_{\text{bs-bf}, j} + \mathcal{C}_{\text{post-bf}, j}. \quad (3.58)$$

It can be observed from Table 3.3 that the dominant terms for large N in (3.58) are \mathcal{C}_{bf} , $\mathcal{C}_{\text{mf-bf}, j}$, $\mathcal{C}_{\text{chol-bf}, j}$, $\mathcal{C}_{\text{bs-bf}, j}$, and $\mathcal{C}_{\text{post-bf}, j}$. The total complexity may thus be approximated by

dropping the smaller order terms (essentially neglecting the cost associated to the intermediate calculations) in (3.58) as

$$\mathcal{C}_{\text{GRP-STMUD-BF}} \approx 2NKMQ + N \left(\sum_{j=1}^G \frac{19K_j^3}{3} + (16 + 2Q)K_j^2 \right), \quad (3.59)$$

where it is also assumed that $W \ll Q$.

3.4.3 GRP-STMUD

The GRP-STMUD receiver is described in Section 3.2.2. It has the general structure illustrated in Fig. 3.1 with linear group detection block diagram illustrated in Fig. 3.3. The operations involved in getting the vector of soft symbol estimates provided by the GRP-STMUD receiver consist essentially of four different steps.

The first step is matched filtering, described by equation (2.26). The second step consists of computing the elements of the system matrix (the matrix to invert in (3.39)). The third step consists of computing the actual soft symbol estimates by solving the inverse system, an operation described by (3.40). The final step, consists of multiplying the solution vector

$$\mathbf{z}'_{\text{grp},j} \triangleq (\mathbf{R}_j \mathbf{R}_j^H + \mathbf{C}_j \mathbf{C}_j^H + \sigma^2 \mathbf{R}_j)^{-1} \mathbf{y}_j \quad (3.60)$$

by \mathbf{R}_j , an operation that is called post-processing here. Table 3.4 summarizes the cost for each of the steps related to the GRP-STMUD receiver.

Combining all the terms, the total complexity of the GRP-STMUD receiver can be

Category	Operation	Label	Approximate cost (in CFLOPS)
Matched filter	$\mathbf{T}^H \mathbf{x}$	\mathcal{C}_{mf}	$2NKM(Q + W - 1)$
Intermediate calculations	$\mathbf{T}^H \mathbf{T}$	$\mathcal{C}_{\mathbf{T}^H \mathbf{T}}$	$MK^2(Q + 3W)$
	$\mathbf{R}_j \mathbf{R}_j^H + \sigma^2 \mathbf{R}_j$	$\mathcal{C}_{\mathbf{R}_j \mathbf{R}_j^H + \sigma^2 \mathbf{R}_j}$	$9K_j^3 + \frac{5}{2}K_j^2$
	$\mathbf{C}_j \mathbf{C}_j^H$	$\mathcal{C}_{\mathbf{C}_j \mathbf{C}_j^H}$	$9K_j^2(K - K_j) + \frac{5}{2}K_j^2$
	$(\mathbf{R}_j \mathbf{R}_j^H + \mathbf{C}_j \mathbf{C}_j^H + \sigma^2 \mathbf{R}_j)$	$\mathcal{C}_{\text{add},j}$	$\frac{5}{2}K_j^2$
Linear system solution	Cholesky factorization	$\mathcal{C}_{\text{chol},j}$	$\frac{19NK_j^3}{3}$
	Backsubstitutions	$\mathcal{C}_{\text{bs},j}$	$10NK_j^2$
Post-processing	$\mathbf{R}_j \mathbf{z}'_{\text{grp},j}$	$\mathcal{C}_{\text{post-grp},j}$	$6NK_j^2$

Table 3.4 Approximate complexity (in CFLOPS) for the different steps of the GRP-STMUD receiver.

expressed as

$$\begin{aligned} \mathcal{C}_{\text{GRP-STMUD}} = & \mathcal{C}_{\text{mf}} + \mathcal{C}_{\mathbf{T}^H \mathbf{T}} + \\ & \sum_{j=1}^G \mathcal{C}_{\mathbf{R}_j \mathbf{R}_j^H + \sigma^2 \mathbf{R}_j} + \mathcal{C}_{\mathbf{C}_j \mathbf{C}_j^H} + \mathcal{C}_{\text{add},j} + \mathcal{C}_{\text{chol},j} + 2\mathcal{C}_{\text{bs},j} + \mathcal{C}_{\text{post},j}, \end{aligned} \quad (3.61)$$

where it can also be observed that the dominant terms for large N are essentially \mathcal{C}_{mf} , $\mathcal{C}_{\text{chol},j}$, $\mathcal{C}_{\text{bs},j}$, and $\mathcal{C}_{\text{post},j}$. Thus the complexity can be further approximated as

$$\mathcal{C}_{\text{GRP-STMUD}} \approx 2NKMQ + N \left(\sum_{j=1}^G \frac{19K_j^3}{3} + 16K_j^2 \right). \quad (3.62)$$

It can be observed that the cost in (3.62) is very similar to the cost associated to the GRP-STMUD-BF receiver in (3.59). Indeed, the two approaches share the same group MUD structure. The cost of beamforming for the GRP-STMUD-BF receiver is of the same order as the match filtering cost for the GRP-STMUD receiver. However, in addition to beamforming, the GRP-STMUD-BF receiver also requires a matched filter before the MMSE

MUD filter. This additional operation is reflected by the term $2QK_j^2$ in the expression for the GRP-STMUD-BF cost in (3.59).

3.4.4 User sharing with MMSE combining

The operations required to combine the different GRP-STMUD filter output for shared users consist essentially of computing the N_k GRP-STMUD filter weights, computing the elements of the MMSE filter matrix, and applying the MMSE filter to the combined vector of soft estimates.

The cost can be divided in three different categories. The first category, intermediate calculations, essentially includes the cost associated to computing the elements of the matrix to invert in (3.45). The second category includes all the costs associated to solving the linear system described by (3.47) and (3.45). The last category, called post-processing, consists of multiplying the linear system solution vector

$$\bar{\mathbf{z}}^{(k)'} \triangleq (\mathbf{M}_{\text{grp}}^{(k)H} \mathbf{T} \mathbf{T}^H \mathbf{M}_{\text{grp}}^{(k)} + \sigma^2 \mathbf{M}_{\text{grp}}^{(k)H} \mathbf{M}_{\text{grp}}^{(k)})^{-1} \bar{\mathbf{z}}^{(k)} \quad (3.63)$$

by the matrix term $\mathbf{T}^{(k)H} \mathbf{M}_{\text{grp}}^{(k)}$, as described by the right-most elements of (3.45). For the remaining of this section, it is assumed, without loss of generality, that user k is shared by groups $j \in \{1, \dots, N_k\}$. To simplify the discussion, it is also assumed that all the groups have the same size so that $K_j = K_{j'}, \forall j, j'$.

The summary of the cost associated to each step in computing the combined MMSE symbol estimate for a shared user is given in Table 3.5.

Adding all the terms in Table 3.5, the total cost for each shared user can be expressed as

$$\mathcal{C}_{\text{comb}} = \mathcal{C}_{\text{icalc-comb}} + \mathcal{C}_{\text{chol-comb}} + \mathcal{C}_{\text{bs-comb}} + \mathcal{C}_{\text{post-comb}}, \quad (3.64)$$

Category	Operation	Label	Approximate cost (in CFLOPS)
Intermediate calculations	$\mathbf{M}_{\text{grp},j}$, for $j = (1, \dots, N_k)$	$\mathcal{C}_{\mathbf{M}_{\text{grp},j}}$	$10N^2 K_j^3 N_k$
	$\mathbf{M}_{\text{grp}}^{(k)H} \mathbf{T}$	$\mathcal{C}_{\mathbf{M}_{\text{grp}}^{(k)H} \mathbf{T}}$	$6N^2 K N_k K_j$
	$\mathbf{M}_{\text{grp}}^{(k)H} \mathbf{T} \mathbf{T}^H \mathbf{M}_{\text{grp}}^{(k)}$	$\mathcal{C}_{\mathbf{M}_{\text{grp}}^{(k)H} \mathbf{T} \mathbf{T}^H \mathbf{M}_{\text{grp}}^{(k)}}$	$2N^3 N_k^3 K$
	$\mathbf{M}_{\text{grp}}^{(k)H} \mathbf{M}_{\text{grp}}^{(k)}$	$\mathcal{C}_{\mathbf{M}_{\text{grp}}^{(k)H} \mathbf{M}_{\text{grp}}^{(k)}}$	$(N_k^2 + N_k) N^3 K_j$
	$(\mathbf{M}_{\text{grp}}^{(k)H} \mathbf{T} \mathbf{T}^H \mathbf{M}_{\text{grp}}^{(k)} + \sigma^2 \mathbf{M}_{\text{grp}}^{(k)H} \mathbf{M}_{\text{grp}}^{(k)})$	$\mathcal{C}_{\text{add-comb}}$	$N^2 N_k^2$
Linear system solution	Cholesky factorization	$\mathcal{C}_{\text{chol-comb}}$	$\frac{(NN_k)^3}{3}$
	Backsubstitutions	$\mathcal{C}_{\text{bs-comb}}$	$2(NN_k)^2$
Post-processing	$\mathbf{T}^{(k)H} \mathbf{M}_{\text{grp}}^{(k)} \bar{\mathbf{z}}^{(k) \prime}$	$\mathcal{C}_{\text{post-comb}}$	$2N^2 N_k$

Table 3.5 Approximate complexity (in CFLOPS) for the different steps of MMSE combining.

where $\mathcal{C}_{\text{calc-comb}}$ is the total overhead cost. Notice that additional saving may be obtained when several users are shared; indeed, the actual weights matrices $\mathbf{M}_{\text{grp},j}$ only need to be calculated once. Finally, it can be observed from Table 3.5 that for large N and K , the cost is dominated by the third overhead term ($\mathcal{C}_{\mathbf{M}_{\text{grp}}^{(k)H} \mathbf{T} \mathbf{T}^H \mathbf{M}_{\text{grp}}^{(k)}}$), and the total cost can thus be approximated as

$$\mathcal{C}_{\text{comb}} \approx 2N^3 N_k^3 K. \quad (3.65)$$

For the total complexity of a GRP-STMUD receiver with user sharing and MMSE combining, the cost in (3.65) must be added to the complexity associated to the GRP-STMUD receiver in (3.62). Note that for GRP-STMUD with user sharing and selection combining the cost is the same as the cost for the GRP-STMUD receiver expressed in (3.62) since there is no extra cost involved in combining the GRP-STMUD filter output

3.4.5 Summary

Table 3.6 summarizes the approximate cost of each receiver structure considered. To simplify, the maximum group size and maximum number of groups is assumed, so that $G = G_{\max}$ and $K_j = K_{\text{grp}}$, and the maximum number of users is given by $K_{\max} = G_{\max}K_{\text{grp}}$. As such, the complexity indicated in the table represents the cost for a practical system implementation, taking into consideration the worst case scenario.

Receiver structure	Approximate cost (CFLOPS)
Full STMUD	$2NK_{\max}MQ + \frac{10}{3}NK_{\max}^3$
GRP-STMUD-BF	$2NK_{\max}MQ + \frac{19}{3}NK_{\max}K_{\text{grp}}^2 + 2NQK_{\max}K_{\text{grp}}$
GRP-STMUD	$2NK_{\max}MQ + \frac{19}{3}NK_{\max}K_{\text{grp}}^2 + 16NK_{\max}K_{\text{grp}}$
MMSE Combining (per user)	$2N^3N_k^3K_{\max}$

Table 3.6 Summary of the complexity for the receiver structures.

It can be observed that for group-based approaches, the complexity savings occur essentially due to the cost of the Cholesky factorization, which is a cubic power of the number of user in the group. Also note that the cost associated to MMSE combining for each user is very high. Since the selective combining approach in practice requires no additional complexity when compared to the GRP-STMUD receiver with no user sharing, it may represent a more practical approach than MMSE combining.

Chapter 4

Group-based multistage receiver structures

4.1 Motivation

The GRP-STMUD receiver structure proposed in Chapter 3 takes into consideration the IGI via the term $\mathbf{C}_j \mathbf{C}_j^H$ in the MMSE MUD linear filter in (3.39). While this approach reduces the impact of inter-group interference, it may not provide sufficient attenuation when the IGI is strong. This situation may occur for example when the group size is too small to include additional interfering users.

In this Chapter, two new group-based iterative receiver structures are proposed to reduce the problematic IGI. The new structures are based on multistage interference cancellation, where the estimated interference for each group is removed from the signal at each stage to improve symbol detection. The two proposed receiver structures are based on successive interference cancellation (SIC) and parallel interference cancellation (PIC) approaches, respectively. The symbols are processed by blocks so that the ISI is also taken

into consideration. Because of the large dimension of the observation space, most of the processing is performed in the matched filter domain.

In Section 4.2, the single-stage group-based SIC (GRP-SIC) and the multistage group-SIC (MS-GRP-SIC) receivers are described. The MS-GRP-SIC receiver is shown to converge, as the number of stages increases, to the full decorrelator (or ZF) receiver. The new multistage group-based PIC (MS-GRP-PIC) receiver is then derived in Section 4.3 and is shown to converge, as the number of stages increases, to the full STMUD receiver. For this reason, and since the MS-GRP-PIC receiver is also a natural extension to the GRP-STMUD receiver, it is derived in the general context of user sharing with selective combining. The complexity of the receiver structures studied is then derived and analyzed in Section 4.4.

4.2 Group-based successive interference cancellation

4.2.1 Single-stage group-based SIC

The proposed GRP-SIC receiver consists of a series of G linear filters each followed by a non-linear decision device $\mathcal{Q}(\cdot)$, where G is the number of groups. The symbol estimates for each group are obtained from filtering the interference-reduced *error signal* coming from the previous group. The signal contribution from the detected symbol estimates is then subtracted from the error signal and fed to the next group, as illustrated in the block diagram of Fig. 4.1.

The groups are processed in succession. Let the MUD linear filter for group $j \in \{1, \dots, G\}$ of the GRP-SIC receiver be denoted by $\mathbf{M}_{\text{sic},j}$. The linear detection filter is applied to the error signal elements of the group of interest. Thus for group j , the soft and

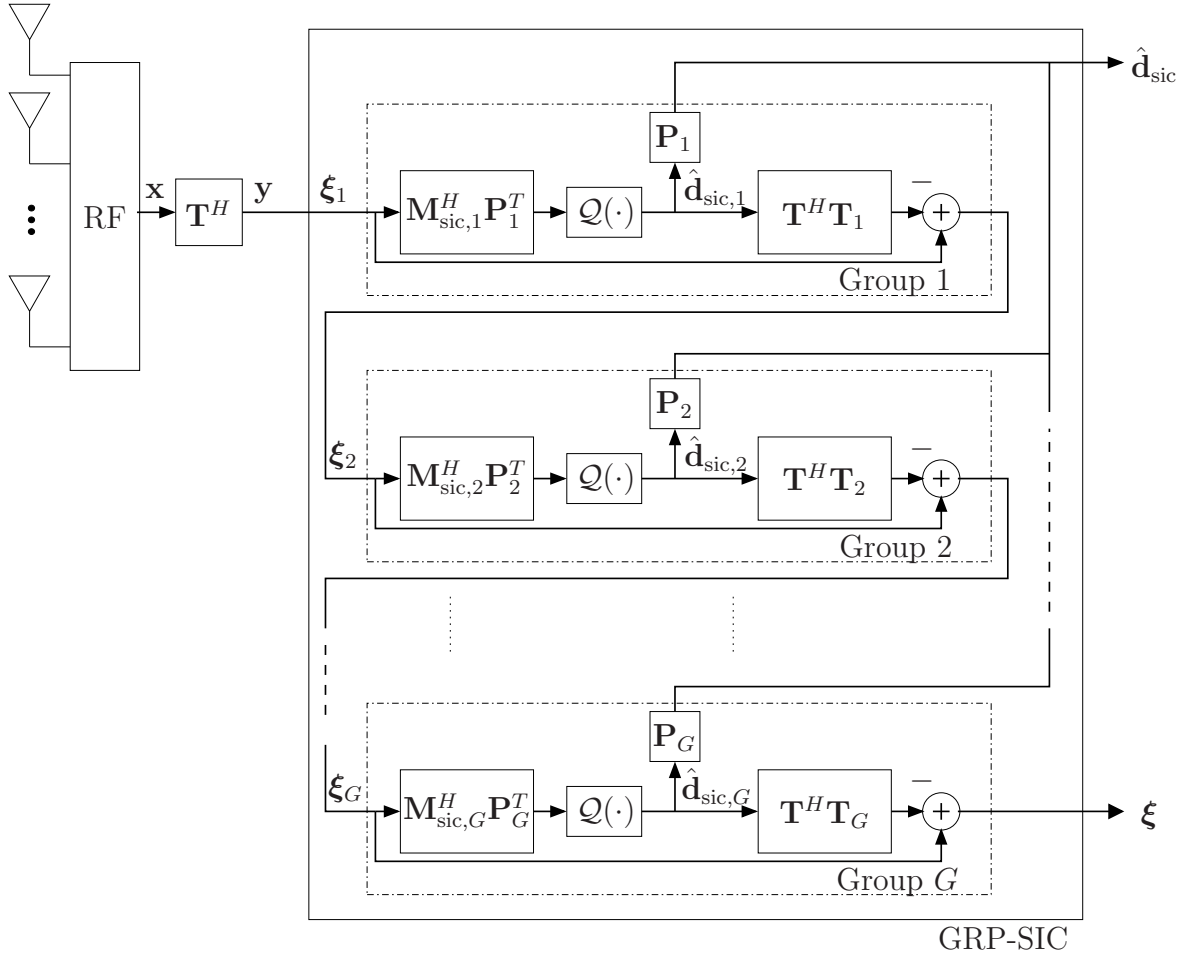


Fig. 4.1 Block diagram for the GRP-SIC receiver.

hard symbol estimates are given respectively by

$$\mathbf{z}_{\text{sic},j} = \mathbf{M}_{\text{sic},j}^H \mathbf{P}_j^T \boldsymbol{\xi}_j, \quad (4.1)$$

$$\hat{\mathbf{d}}_{\text{sic},j} = Q(\mathbf{z}_{\text{sic},j}), \quad (4.2)$$

where \mathbf{P}_j is the $NK \times NK_j$ selection matrix for the symbols associated to group j as defined in (3.6) and $\boldsymbol{\xi}_j$ is the input “error” signal vector of dimension $NK \times 1$ for group j . The error signal vector is obtained by removing the estimated signal contribution of the

previously detected groups from the input error signal. Thus the input error signal vector $\boldsymbol{\xi}_j \in \mathbb{C}^{NK \times 1}$ for group j can be expressed as

$$\boldsymbol{\xi}_j = \begin{cases} \mathbf{y} \triangleq \mathbf{T}^H \mathbf{x}, & j = 1 \\ \boldsymbol{\xi}_{j-1} - \mathbf{T}^H \mathbf{T}_{j-1} \hat{\mathbf{d}}_{\text{sic},j-1}, & j = 2, \dots, G, \end{cases} \quad (4.3)$$

where \mathbf{T}_{j-1} is the matrix containing the columns of \mathbf{T} corresponding to users of group $j-1$ (see definition in (3.11)). Since the error signal input for the first group ($j = 1$) has no prior signal contribution cancelled, it is given by the matched filter output.

The filter matrix $\mathbf{M}_{\text{sic},j}$ can be designed using several different criteria. To maintain uniformity with previous development, the minimum mean square error criterion is used in this work; the MMSE cost function for group $j \in \{1, \dots, G\}$ can be expressed as

$$J_{\text{sic},j}(\mathbf{M}) = E \|\mathbf{d}_j - \mathbf{M}^H \mathbf{P}_j^T \boldsymbol{\xi}_j\|^2. \quad (4.4)$$

For group j , the MMSE filter input $\boldsymbol{\xi}_j$ consists of the matched filter output \mathbf{y} , from which the signal contribution estimates from the previously detected groups have been removed. Using (4.3), $\boldsymbol{\xi}_j$ can be expressed as

$$\boldsymbol{\xi}_j = \mathbf{y} - \mathbf{T}^H \sum_{l=1}^{j-1} \mathbf{T}_l \hat{\mathbf{d}}_{\text{sic},l}. \quad (4.5)$$

The optimal matrix filter is the solution to the following optimization problem:

$$\mathbf{M}_{\text{sic},j} = \arg \min_{\mathbf{M}} J_{\text{sic},j}(\mathbf{M}). \quad (4.6)$$

To minimize the cost in (4.4) and solve (4.6), it is assumed for each group that the symbols

from the previous groups have been detected without error, a common assumption in the design of decision feedback detectors (see e.g.: [WRHR02]).

Proposition 4. *The solution to (4.6), giving the optimal MMSE weights for the group-based SIC receiver is given by the $NK_j \times NK_j$ matrix*

$$\mathbf{M}_{\text{sic},j} = (\mathbf{R}_j \mathbf{R}_j^H + \tilde{\mathbf{C}}_j \tilde{\mathbf{C}}_j^H + \sigma^2 \mathbf{R}_j)^{-1} \mathbf{R}_j^H, \quad (4.7)$$

where $\mathbf{R}_j = \mathbf{T}_j^H \mathbf{T}_j$ was previously defined in (3.28), and $\tilde{\mathbf{C}}_j$ is given by

$$\tilde{\mathbf{C}}_j \triangleq \mathbf{T}_j^H \tilde{\mathbf{T}}_j, \quad (4.8)$$

where $\tilde{\mathbf{T}}_j$ denotes the columns of \mathbf{T} associated to the users of the groups that have not been detected yet, i.e.:

$$\tilde{\mathbf{T}}_j \triangleq [\mathbf{T}_{j+1}, \dots, \mathbf{T}_G]. \quad (4.9)$$

Proof. The proof is in Appendix A.4. □

It can be observed that the filter in (4.7) takes into consideration the inter-group interference via the term $\tilde{\mathbf{C}}_j \tilde{\mathbf{C}}_j^H$. Note that as opposed to the group-based receiver described in Chapter 3, the IGI in the group-based SIC receiver consists of only the signal contribution from the groups that have not been detected yet, as reflected by (4.8) and (4.9). Indeed, in the group-based SIC receiver, the estimated signal contribution from the detected groups is removed after detection.

As in the group-based receiver structures derived in the previous chapter, the dimension of the new filter in (4.7) is reduced to $NK_j \times NK_j$, compared to the full STMUD filter of

dimension $NK \times NK$. Finally, note that the residual error

$$\boldsymbol{\xi} \triangleq \mathbf{y} - \sum_{j=1}^G \mathbf{T}^H \mathbf{T}_j \hat{\mathbf{d}}_{\text{sic},j} \quad (4.10)$$

in Fig. 4.1 can provide additional information on the background noise.

In a successive interference cancellation receiver, the detection order is important. Indeed, there is a risk of actually increasing the interference in case of a detection error, potentially leading to error propagation. In a group-based SIC receiver the concept is the same; groups must also be ordered so that those with the most reliable symbols are detected first. The ordering can be determined by using the grouping algorithm cost criterion, as discussed in the next chapter in Section 5.4.

4.2.2 Multistage group-based SIC

A logical extension to the proposed GRP-SIC receiver consists of using multiple stages to improve the detection [JR98]. In the proposed MS-GRP-SIC receiver, several GRP-SIC blocks are used in succession with the hard decisions delayed until the last stage, as illustrated in Fig. 4.2. The group detection blocks, labeled Stage i , $i = 1, \dots, S$ in the figure, are similar to the GRP-SIC block illustrated in Fig. 4.1, with the difference that the non-linear decision devices are *removed* to allow soft outputs to be passed on to subsequent stages. This technique is advantageous because it reduces the impact of decision errors propagation on interference cancellation [ZB03].

In the context of multistage GRP-SIC, it is expected that the inter-group interference decreases at each stage. Under this assumption, the linear filter design can be simplified to reduce the complexity of (4.7). To this end, it is assumed in the weight design that the IGI can be neglected for *all stages*. In essence this implies that for group j the match filter

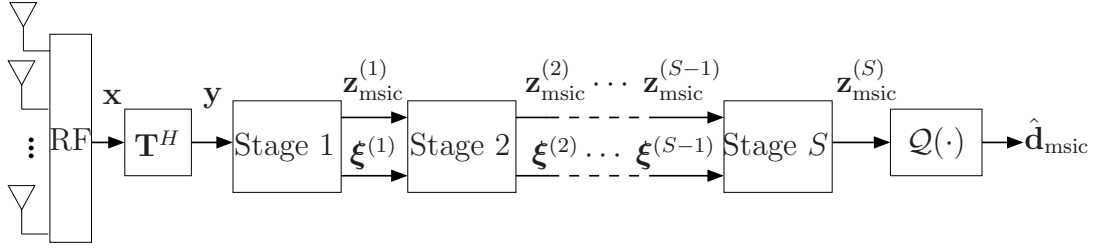


Fig. 4.2 Block diagram for the Multistage GRP-SIC receiver.

output can be approximated as follows

$$\mathbf{y}_j = \mathbf{T}_j^H \mathbf{x} \quad (4.11)$$

$$= \mathbf{T}_j^H (\mathbf{T}_j \mathbf{d}_j + \bar{\mathbf{T}}_j \bar{\mathbf{d}}_j + \mathbf{n}) \quad (4.12)$$

$$\approx \mathbf{T}_j^H (\mathbf{T}_j \mathbf{d}_j + \mathbf{n}), \quad (4.13)$$

where $\bar{\mathbf{T}}_j$ and $\bar{\mathbf{d}}_j$ are the columns of \mathbf{T} and the elements of \mathbf{d} related to the users *outside* of group j , as previously defined in (3.12) and (3.10), respectively, and (4.12) is obtained from (3.34). The approximation in (4.13) leads to the new sub-optimal cost function

$$J_{\text{msic},j}(\mathbf{M}) \triangleq E \|\mathbf{d}_j - \mathbf{M}^H \mathbf{T}_j^H (\mathbf{T}_j \mathbf{d}_j + \mathbf{n})\|^2, \quad (4.14)$$

where it can be observed that the contribution from the users outside of group j has effectively been neglected.

Notice that (4.14) has essentially the same form as the cost function for the “full STMUD MUD MMSE” filter in (2.28). It follows that the matrix filter minimizing (4.14) also takes the same form as the matrix filter in (2.30), and can be expressed as

$$\mathbf{M}_j = (\mathbf{T}_j^H \mathbf{T}_j + \sigma^2 \mathbf{I})^{-1}, \quad (4.15)$$

where \mathbf{M}_j is Hermitian and has dimension $NK_j \times NK_j$. Note that the filter in (4.15) is independent of the stage index, which is a consequence of neglecting the IGI in (4.14). In the proposed MS-GRP-SIC receiver, the filter matrix in (4.15) replaces the filter matrix $\mathbf{M}_{\text{sic},j}$ in the GRP-SIC of Fig. 4.1 for all the stages.

Let $\mathbf{z}_{\text{out},j}^{(s)}$ be the filter matrix output for group j at stage s , expressed as

$$\mathbf{z}_{\text{out},j}^{(s)} \triangleq \mathbf{M}_j^H \mathbf{P}_j^T \boldsymbol{\xi}_j^{(s)}, \quad (4.16)$$

where $\boldsymbol{\xi}_j^{(s)}$ is the error signal vector of dimension $NK \times 1$ at the input of group j at stage s . Also, let $\mathbf{z}_{\text{msic},j}^{(s)}$ denote the soft estimate vector of dimension $NK_j \times 1$ for symbols of group j at the output stage $s \in \{1, \dots, S\}$, after linear filtering. Following the work in [JR98] and the structures shown in Figures 4.1 and 4.2, $\mathbf{z}_{\text{msic},j}^{(s)}$ is updated at each stage and takes the form

$$\mathbf{z}_{\text{msic},j}^{(s)} = \begin{cases} \mathbf{0}, & s = 0 \\ \mathbf{z}_{\text{msic},j}^{(s-1)} + \mathbf{z}_{\text{out},j}^{(s)}, & s > 0, \end{cases} \quad (4.17)$$

where $\mathbf{z}_{\text{msic},j}^{(s-1)}$ can be interpreted as a state variable containing the soft symbol estimates at the previous stage and $\mathbf{z}_{\text{out},j}^{(s)}$ as the soft symbol estimates update for the current stage $s > 0$. Note that this form of successive interference cancellation is similar to Gauss-Seidel iterations for solving linear systems [RLJ00].

Using the formulation in (4.3) this time with soft symbol estimates, the error signal vector can be expressed as

$$\boldsymbol{\xi}_j^{(s)} = \begin{cases} \boldsymbol{\xi}_j^{(s-1)}, & j = 1 \\ \boldsymbol{\xi}_{j-1}^{(s)} - \mathbf{T}^H \mathbf{T}_{j-1} \mathbf{z}_{\text{out},j-1}^{(s)}, & j = 2, \dots, G, \end{cases} \quad (4.18)$$

where $\boldsymbol{\xi}^{(0)} = \mathbf{y}$ and the error signal vector at the output of stage s can be expressed as

$$\boldsymbol{\xi}^{(s)} = \boldsymbol{\xi}^{(s-1)} - \sum_{j=1}^G \mathbf{T}^H \mathbf{T}_j \mathbf{z}_{\text{out},j}^{(s)}, \quad s \geq 1. \quad (4.19)$$

Using these definitions and substituting the matrix filter output by its expression in (4.16), it can be shown (see [JR98]) that the recursion for the error signal vector after stage s in (4.18) can also be expressed as

$$\boldsymbol{\xi}_j^{(s)} = \prod_{l=1}^{j-1} (\mathbf{I} - \mathbf{T}^H \mathbf{T}_l \mathbf{M}_l^H \mathbf{P}_l^T) \boldsymbol{\Phi}^{s-1} \mathbf{y}, \quad (4.20)$$

where

$$\boldsymbol{\Phi} \triangleq \prod_{j=1}^G (\mathbf{I} - \mathbf{T}^H \mathbf{T}_j \mathbf{M}_j^H \mathbf{P}_j^T). \quad (4.21)$$

The error signal vector at the output of stage s can thus be expressed as

$$\boldsymbol{\xi}^{(s)} = \boldsymbol{\Phi}^s \mathbf{y}. \quad (4.22)$$

Using (4.16) to (4.21), it can be shown that the recursion equation in (4.17) for the soft symbol estimate vector for group j at stage s can be expressed as

$$\mathbf{z}_{\text{msic},j}^{(s)} = \mathbf{M}_j^H \mathbf{P}_j^T \prod_{l=1}^{j-1} (\mathbf{I} - \mathbf{T}^H \mathbf{T}_l \mathbf{M}_l^H \mathbf{P}_l^T) \left(\sum_{p=0}^{s-1} \boldsymbol{\Phi}^p \right) \mathbf{y}. \quad (4.23)$$

At each stage s , the vectors of soft symbol estimates for each group are combined into a single vector $\mathbf{z}_{\text{msic}}^{(s)}$ such that

$$\mathbf{z}_{\text{msic}}^{(s)} \triangleq \sum_{j=1}^G \mathbf{z}_{\text{msic},j}^{(s)} \mathbf{P}_j. \quad (4.24)$$

Then, as illustrated in Fig. 4.2, the hard symbol estimates are obtained at the output of

the non-linear device after the last stage S :

$$\hat{\mathbf{d}}_{\text{msic}} = \mathcal{Q}(\mathbf{z}_{\text{msic}}^{(S)}). \quad (4.25)$$

Finally, note that user sharing can also be used in the context of MS-GRP-SIC receiver.

4.2.3 Convergence analysis

It is essential to establish the convergence conditions of the MS-GRP-SIC receiver as the number of stages increases, and in particular for $S \rightarrow \infty$. It is shown in [JR98] that the group-wise successive interference canceller converges to the decorrelator, provided that the group-linear filter is invertible, which is usually the case.

To demonstrate that this conclusion can be applied to the proposed MS-GRP-SIC receiver, the recursion for the error signal vector in (4.19) is first expanded to obtain

$$\boldsymbol{\xi}^{(s)} = \mathbf{y} - \sum_{j=1}^G \mathbf{T}^H \mathbf{T}_j \mathbf{z}_{\text{out},j}^{(1)} - \sum_{j=1}^G \mathbf{T}^H \mathbf{T}_j \mathbf{z}_{\text{out},j}^{(2)} - \dots - \sum_{j=1}^G \mathbf{T}^H \mathbf{T}_j \mathbf{z}_{\text{out},j}^{(s)}, \quad (4.26)$$

where the fact that $\boldsymbol{\xi}^{(0)} = \mathbf{y}$ has been used. Noting that by definition (see (4.17))

$$\mathbf{z}_{\text{msic},j}^{(s)} = \sum_{l=1}^s \mathbf{z}_{\text{out},j}^{(l)}, \quad (4.27)$$

the error signal vector in (4.26) can be expressed compactly as

$$\boldsymbol{\xi}^{(s)} = \mathbf{y} - \sum_{j=1}^G \mathbf{T}^H \mathbf{T}_j \mathbf{z}_{\text{msic},j}^{(s)}. \quad (4.28)$$

Then, substituting (4.28) in (4.18), the error signal vector at the input of group j at stage

s can be expressed as

$$\boldsymbol{\xi}_j^{(s)} \equiv \mathbf{y} - \sum_{l=1}^{j-1} \mathbf{T}^H \mathbf{T}_l \mathbf{z}_{\text{msic},l}^{(s)} - \sum_{m=j}^G \mathbf{T}^H \mathbf{T}_m \mathbf{z}_{\text{msic},m}^{(s-1)}. \quad (4.29)$$

Notice that the interference terms in (4.29) are computed with the most current vector of soft symbol estimates for each group. It is convenient to express the vector of soft symbol estimate in (4.24) using a matrix formulation. To do so, it is first necessary to define the following three matrices:

$$\mathbf{M} \triangleq \text{diag}(\mathbf{M}_1, \dots, \mathbf{M}_G) \in \mathbb{C}^{NK \times NK}, \quad (4.30)$$

$$\mathbf{L} \triangleq \begin{bmatrix} \mathbf{0} & \cdots & & & \mathbf{0} \\ \mathbf{T}_2^H \mathbf{T}_1 & \mathbf{0} & \cdots & & \\ \mathbf{T}_3^H \mathbf{T}_1 & \mathbf{T}_3^H \mathbf{T}_2 & \mathbf{0} & \cdots & \vdots \\ \vdots & \vdots & \ddots & \ddots & \vdots \\ \mathbf{T}_G^H \mathbf{T}_1 & \mathbf{T}_G^H \mathbf{T}_2 & \cdots & \mathbf{T}_G^H \mathbf{T}_{G-1} & \mathbf{0} \end{bmatrix} \in \mathbb{C}^{NK \times NK}, \quad (4.31)$$

$$\mathbf{U} \triangleq \begin{bmatrix} \mathbf{T}_1^H \mathbf{T}_1 & \mathbf{T}_1^H \mathbf{T}_2 & \cdots & \mathbf{T}_1^H \mathbf{T}_G \\ \mathbf{0} & \mathbf{T}_2^H \mathbf{T}_2 & \cdots & \mathbf{T}_2^H \mathbf{T}_G \\ \vdots & & \ddots & \vdots \\ \mathbf{0} & \cdots & & \mathbf{0} \mathbf{T}_G^H \mathbf{T}_G \end{bmatrix} \in \mathbb{C}^{NK \times NK}. \quad (4.32)$$

Because of the above formulation, it is essential that the data vectors be ordered such that elements belonging to the same groups are adjacent. Thus let the permutation matrix \mathbf{P} be defined as

$$\mathbf{P} = [\mathbf{P}_1, \dots, \mathbf{P}_G], \quad (4.33)$$

and let the re-ordered matched filter vector and the re-ordered soft symbol estimate vector be expressed respectively as

$$\mathbf{z}_{\mathbf{P},\text{msic}}^{(s)} \triangleq \mathbf{P}^T \mathbf{z}_{\text{msic}}^{(s)} = [\mathbf{z}_{\text{msic},1}^{(s)T}, \dots, \mathbf{z}_{\text{msic},G}^{(s)T}]^T \quad (4.34)$$

$$\mathbf{y}_{\mathbf{P}} \triangleq \mathbf{P}^T \mathbf{y} = [\mathbf{y}_1^T, \dots, \mathbf{y}_G^T]^T, \quad (4.35)$$

where the “ \mathbf{P} ” subscript indicates the new ordering by group through matrix \mathbf{P} . Using the definitions above, substituting (4.29) in (4.16) and using (4.17), it can be shown that

$$\mathbf{z}_{\mathbf{P},\text{msic}}^{(s)} = \mathbf{z}_{\mathbf{P},\text{msic}}^{(s-1)} + \mathbf{M}^H (\mathbf{y}_{\mathbf{P}} - \mathbf{L} \mathbf{z}_{\mathbf{P},\text{msic}}^{(s)} - \mathbf{U} \mathbf{z}_{\mathbf{P},\text{msic}}^{(s-1)}). \quad (4.36)$$

If the proposed MS-GRP-SIC receiver converges as the number of stages increases, $\mathbf{z}_{\mathbf{P},\text{msic}}^{(s)}$ and $\mathbf{z}_{\mathbf{P},\text{msic}}^{(s-1)}$ will converge to the same value so that $\mathbf{z}_{\mathbf{P},\text{msic}}^{(s)} = \mathbf{z}_{\mathbf{P},\text{msic}}^{(s-1)}$. Since \mathbf{M} is invertible by definition, (4.36) can then be re-expressed as

$$\mathbf{z}_{\mathbf{P},\text{msic}}^{(s)} = (\mathbf{L} + \mathbf{U})^{-1} \mathbf{y}_{\mathbf{P}}, \quad (4.37)$$

$$= (\mathbf{T}_{\mathbf{P}}^H \mathbf{T}_{\mathbf{P}})^{-1} \mathbf{T}_{\mathbf{P}}^H \mathbf{x}, \quad (4.38)$$

where $\mathbf{T}_{\mathbf{P}} \triangleq \mathbf{T}\mathbf{P}$. It can be observed that the linear filter in (4.38) corresponds to the decorrelator. Thus if the MS-GRP-SIC receiver converges it will converge to the decorrelator.

When the system converges, $\mathbf{z}_{\text{out},j}^{(s)} \rightarrow \mathbf{0}$ as a consequence of (4.17), which in turn from (4.16) implies that the error vector $\boldsymbol{\xi}_j^{(s)}$ converges to zero. If Φ_j is defined as

$$\Phi_j \triangleq \prod_{l=1}^{j-1} (\mathbf{I} - \mathbf{T}^H \mathbf{T}_l \mathbf{M}_l^H \mathbf{P}_l^T) \prod_{l'=j}^G (\mathbf{I} - \mathbf{T}^H \mathbf{T}_{l'} \mathbf{M}_{l'}^H \mathbf{P}_{l'}^T), \quad (4.39)$$

then the expression for the error signal vector in (4.20) takes the convenient form

$$\boldsymbol{\xi}_j^{(s)} \equiv \boldsymbol{\Phi}_j^s \mathbf{y}. \quad (4.40)$$

It is shown in [JR98] that if the eigenvalues of $\boldsymbol{\Phi}_j$ are constrained by

$$|\lambda_n(\boldsymbol{\Phi}_j)| \leq 1, \quad \forall n \in \{1, \dots, NK\}, \quad (4.41)$$

where $\lambda_n(\boldsymbol{\Phi}_j)$ is the n^{th} eigenvalue of $\boldsymbol{\Phi}_j$, then the proposed MS-GRP-SIC receiver structure is guaranteed to converge to the full decorrelator receiver of (4.38).

As discussed in [JR98], it is difficult to show analytically that this convergence condition is always satisfied. However, experiments have shown that this is the case in practical scenarios.

Note that a group-based SIC receiver structure guaranteed to converge to the MMSE receiver has been proposed recently in [BZSB07]. As opposed to the MS-GRP-SIC structure proposed in this work, which uses the residual error as a state variable, the approach in [BZSB07] uses the interference estimate as a state variable.

4.3 Group-based parallel interference cancellation

4.3.1 Multistage group-based PIC

In the group-based generic receiver structure presented in Section 3.2 and shown in Fig. 3.1, all the groups are detected independently in parallel. In this section, the GRP-STMUD receiver discussed in Section 3.2.2 is extended to a multistage receiver structure supporting user sharing with selective combining.

In the context of multistage PIC, as was the case for the multistage SIC, it is reasonable

to expect that the IGI will be reduced after each stage. As such, the cost function in (4.14) can also be used to obtain the suboptimal MUD filter in (4.15), repeated here for convenience:

$$\mathbf{M}_j = (\mathbf{T}_j^H \mathbf{T}_j + \sigma^2 \mathbf{I})^{-1}. \quad (4.42)$$

Because of its simpler structure, this filter is computationally advantageous when compared to the group MMSE filter in (3.39). In the following, (4.42) is referred to as the *simplified* GRP-STMUD filter.

To derive the MS-GRP-PIC receiver with user sharing, it is necessary to define some terminology related to user sharing with selective combining. With user sharing, the groups are no longer mutually exclusive. Define an *extended* group as a group containing a set of *conventional* users with an optional set of *shared* users. Each user is a conventional user of only one group, but may be a shared user of up to $G_{\max} - 1$ groups. Table 4.1 provides an example of a grouping with user sharing. As it can be observed, extended group #1 is comprised of 3 conventional users (users #1,2, and 3) and of 1 shared user (user #7); user #7 is also a conventional user of extended group #3. Also note that extended group #4 does not actually contain any shared user, and that all extended groups have the maximum number of users.

Extended group #	Conventional users	Shared users
1	1,2,3	7
2	4,5	8,10
3	6,7,8	9
4	9,10,11,12	–

Table 4.1 Typical grouping example with conventional and shared users, for $K = 12$, $K_{\text{grp}} = 4$, $G_{\max} = 4$.

For each extended group, the filter output corresponding to the set of conventional users

is selected for detection; the filter output corresponding to the set of shared users is used to improve signal detection for the conventional users.

Let K'_j be the dimension of extended group j , of which K_j are conventional users and $(K'_j - K_j)$ are shared users, and let \mathbf{P}'_j be the $NK \times NK'_j$ selection matrix for extended group j so that

$$\mathbf{T}'_j \triangleq \mathbf{T}\mathbf{P}'_j, \quad \mathbf{T}'_j \in \mathbb{C}^{M(NQ+W-1) \times NK'_j} \quad (4.43)$$

contains the columns of \mathbf{T} corresponding to the users of extended group j . In this Chapter, the “prime” superscript designates variables associated to extended groups. Assume, without loss of generality, that the list of users for each extended group is arranged such that the shared users are located at the end of the list, and let $g_{j,l}^s$ be the index of the l^{th} *shared* user of extended group j . The selection matrix for the extended group then takes the form:

$$\mathbf{P}'_j = \left[\begin{array}{c} \mathbf{P}_j \\ \vdots \\ \mathbf{I}_N \otimes [\mathbf{e}_{g_{j,1}^s}, \dots, \mathbf{e}_{g_{j,(K'_j-K_j)}^s}] \end{array} \right], \quad (4.44)$$

where \mathbf{P}_j is the selection matrix for the conventional users only as defined in (3.6), and $\mathbf{e}_{g_{j,l}^s}$ is the elementary vector of dimension $K \times 1$ with value 1 at position $g_{j,l}^s$. It follows that:

$$\mathbf{M}'_j \triangleq (\mathbf{T}'_j{}^H \mathbf{T}'_j + \sigma^2 \mathbf{I})^{-1} \in \mathbb{C}^{NK'_j \times NK'_j} \quad (4.45)$$

$$\mathbf{y}'_j \triangleq \mathbf{T}'_j{}^H \mathbf{x} \in \mathbb{C}^{NK'_j \times 1} \quad (4.46)$$

$$\mathbf{z}'_{\text{pic},j} \triangleq \mathbf{M}'_j{}^H \mathbf{y}'_j \in \mathbb{C}^{NK'_j \times 1}, \quad (4.47)$$

where \mathbf{M}'_j , \mathbf{y}'_j , and $\mathbf{z}'_{\text{pic},j}$ are the extended simplified GRP-STMUD filter, matched filter and soft output for the extended group j , respectively. Thus the input of the extended simplified GRP-STMUD filter consists of the matched filter output not only of the conventional users, but also of the shared users, which in effect increases the observation space dimension of

the linear filter.

Let $\bar{\mathbf{P}}'_j$ be the selection matrix complement for the users *not* in extended group j so that

$$\bar{\mathbf{T}}'_j \triangleq \mathbf{T}\bar{\mathbf{P}}'_j, \quad \bar{\mathbf{T}}'_j \in \mathbb{C}^{M(NQ+W-1) \times N(K-K'_j)} \quad (4.48)$$

contains the columns of \mathbf{T} corresponding to the users that do not belong to extended group j . The selection matrix complement $\bar{\mathbf{P}}'_j$ of dimension $NK \times N(K - K'_j)$ takes the form

$$\bar{\mathbf{P}}'_j = \mathbf{I}_N \otimes [\mathbf{e}_{\bar{g}'_{j,1}}, \dots, \mathbf{e}_{\bar{g}'_{j,(K-K'_j)}}], \quad (4.49)$$

where $\bar{g}'_{j,l}$ is the index of the l^{th} user not in extended group j . Finally, let

$$\mathbf{z}_{\text{pic},j} \triangleq \bar{\mathbf{P}}_j^T \mathbf{z}'_{\text{pic},j} \quad (4.50)$$

be the vector of dimension $NK_j \times 1$ containing only the soft symbol estimates of the conventional users of extended group j . Based on the extended user list arrangement assumption in (4.44), $\tilde{\mathbf{P}}_j$ can be seen to take the form

$$\tilde{\mathbf{P}}_j = \begin{bmatrix} \mathbf{I}_{NK_j} \\ \mathbf{0}_{N(K'_j-K_j) \times NK_j} \end{bmatrix}. \quad (4.51)$$

In the proposed MS-GRP-PIC receiver, the parallel interference cancellation is based on the matrix algebraic approach without grouping presented in [GRSL00]. Specifically, let s represent the PIC stage index and let $\mathbf{z}_{\text{pic}}^{(s)} \in \mathbb{C}^{NK \times 1}$ be the soft symbol estimate vector at stage s and $\mathbf{z}_{\text{pic},j}^{(s)} \triangleq \mathbf{P}_j^T \mathbf{z}_{\text{pic}}^{(s)} \in \mathbb{C}^{NK_j \times 1}$ be the soft symbol estimate vector for the conventional users of group j . The reconstructed interference at stage s , $s \geq 1$, for the

conventional users of extended group j can be expressed as

$$\hat{\mathbf{z}}_j^{(s)} = \begin{cases} \mathbf{0}_{NK_j}, & s = 1 \\ \tilde{\mathbf{P}}_j^T \mathbf{M}_j'^H \mathbf{T}_j'^H \bar{\mathbf{T}}_j' \bar{\mathbf{z}}_{\text{pic},j}^{(s-1)'}, & s > 1 \end{cases} \quad (4.52)$$

where $\bar{\mathbf{z}}_{\text{pic},j}^{(s-1)'}$ is the soft symbol estimate vector from the previous stage for the users outside of extended group j . After interference cancellation, the soft symbol estimate vector can be expressed as

$$\mathbf{z}_{\text{pic},j}^{(s)} = \tilde{\mathbf{P}}_j^T \mathbf{M}_j'^H \mathbf{T}_j'^H \mathbf{x} - \hat{\mathbf{z}}_j^{(s)}, \quad 1 \leq s \leq S, \quad (4.53)$$

where S is the maximum number of stages in the PIC.

Figure 4.3 on page 88 illustrates the proposed MS-GRP-PIC receiver in block diagram form. The S -stages MS-GRP-PIC receiver can be summarized by the following two equations: first, the soft symbol estimation update equation, given here for $1 \leq s \leq S$ by

$$\mathbf{z}_{\text{pic}}^{(s)} = \mathbf{F}' \mathbf{y} - \mathbf{G}' \mathbf{z}_{\text{pic}}^{(s-1)}, \quad (4.54)$$

where

$$\mathbf{F}' \triangleq \begin{bmatrix} \tilde{\mathbf{P}}_1^T \mathbf{M}_1'^H \mathbf{P}_1'^T \\ \vdots \\ \tilde{\mathbf{P}}_G^T \mathbf{M}_G'^H \mathbf{P}_G'^T \end{bmatrix}, \quad (4.55)$$

$$\mathbf{G}' \triangleq \begin{bmatrix} \tilde{\mathbf{P}}_1^T \mathbf{M}_1'^H \mathbf{T}_1'^H \bar{\mathbf{T}}_1' \bar{\mathbf{P}}_1'^T \\ \vdots \\ \tilde{\mathbf{P}}_G^T \mathbf{M}_G'^H \mathbf{T}_G'^H \bar{\mathbf{T}}_G' \bar{\mathbf{P}}_G'^T \end{bmatrix}, \quad (4.56)$$

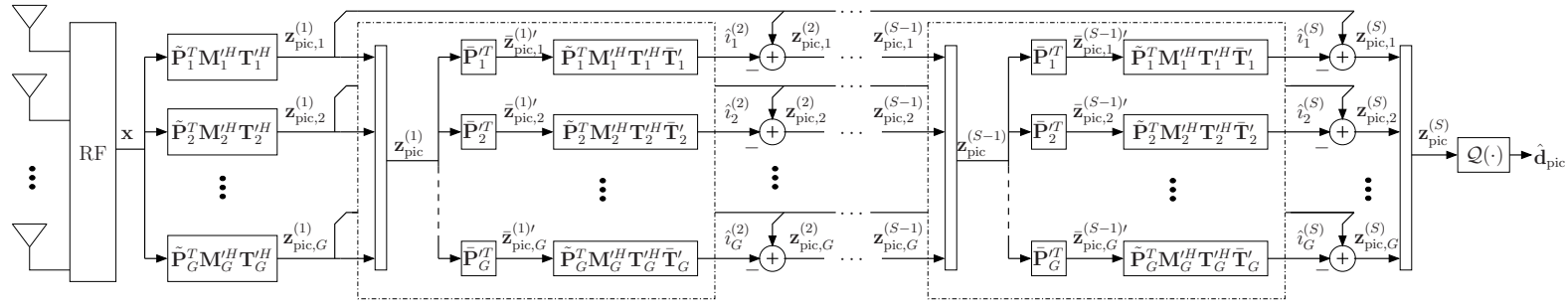


Fig. 4.3 Block diagram for the MS-GRP-PIC receiver.

\mathbf{y} is the MF output defined in (2.26) and $\mathbf{z}_{\text{pic}}^{(0)} = \mathbf{0}$, and second, the decision equation which can be expressed as

$$\hat{\mathbf{d}}_{\text{pic}} = \mathcal{Q}(\mathbf{z}_{\text{pic}}^{(S)}). \quad (4.57)$$

The number of stages S can be determined in real-time for instance by some metric based on convergence, but in practice it is usually constrained by the hardware to a small value. It should be noted that any matrix multiplication by a selection matrix do not actually add complexity to the receiver.

Notice that the term $\tilde{\mathbf{P}}_j^T \mathbf{M}_j'^H \mathbf{T}_j'^H \bar{\mathbf{T}}_j' \bar{\mathbf{z}}_{\text{pic},j}^{(s-1)}$ in (4.52) consists of the extended simplified GRP-STMUD filter output response for the conventional users of extended group j to the excitation caused by the users outside of the group. Thus the term $\tilde{\mathbf{P}}_j^T \mathbf{M}_j'^H \mathbf{T}_j'^H \bar{\mathbf{T}}_j'$ in each block row of (4.56) integrates the corresponding effects of the channel, matched filter and MUD linear filter into a single matrix. The right matrix product by $\bar{\mathbf{P}}_j'^T$ in (4.56) causes columns of zeros to be inserted at the location associated to the symbols of the users of extended group j . It effectively transforms the $NK_j \times N(K - K'_j)$ matrix into a $NK_j \times NK$ matrix. Assume, for illustration purposes and without loss of generality, that the user indices are arranged according to their respective grouping so that users $k \in \{1, \dots, K_1\}$ belong to conventional group #1, users $k \in \{K_1 + 1, \dots, K_1 + K_2\}$ belong to conventional group #2, and so on. Then the structure of the matrix \mathbf{G}' used in (4.54)

and defined in (4.56) can be shown to take the form:

$$\mathbf{G}' = \begin{array}{c} \begin{array}{ccc} \xrightarrow{NK_1} & \dots & \xrightarrow{NK_G} \\ \begin{array}{|c|c|c|} \hline \text{0} & \text{ } & \begin{array}{|c|c|} \hline \text{0} & \text{0} \\ \hline \end{array} \\ \hline \begin{array}{|c|c|} \hline \text{0} & \text{0} \\ \hline \end{array} & \text{0} & \begin{array}{|c|c|} \hline \text{0} & \text{0} \\ \hline \end{array} \\ \hline \begin{array}{|c|c|} \hline \text{0} & \text{0} \\ \hline \end{array} & \text{ } & \text{0} \\ \hline \end{array} \\ \end{array} \end{array}, \quad (4.58)$$

where for each block row the white areas and the dashed areas correspond to the columns of conventional and shared users, respectively. These columns are filled with zeros since they correspond to symbols that do not interfere with the detection for that group.

The system equations in (4.52)-(4.56) represent the general case where groups may contain shared users. In the traditional group-based PIC receiver, there is no user sharing among groups. In that case, the system equations can be obtained by removing the “prime” superscript in (4.52)-(4.54) and noting that since $K'_j = K_j$, it follows that $\tilde{\mathbf{P}}_j = \mathbf{I}_{NK_j}$ (see (4.51)). Also, the structure of \mathbf{G} is similar to the structure illustrated in (4.58) but with no off-diagonal blocks of zeros [PC06b].

4.3.2 Convergence analysis

Using the matrix-based model in (4.54) to (4.56), it can be shown that at the final stage S , the group-based soft symbol estimate vector in (4.54) can be expressed as

$$\mathbf{z}_{\text{pic}}^{(S)} = \sum_{s=1}^S (-\mathbf{G}')^{s-1} \mathbf{F}' \mathbf{y} \quad (4.59)$$

$$= (\mathbf{I} - (-\mathbf{G}')^S)(\mathbf{I} + \mathbf{G}')^{-1} \mathbf{F}' \mathbf{y}, \quad (4.60)$$

where (4.60) is obtained by using the expression for the convergence of the geometric matrix sum in (4.59) (see e.g.: [Ber05]). Assuming for now that the inverse in (4.60) exists, it can be observed that the convergence properties of the soft symbol estimate are essentially determined by the eigenvalues of \mathbf{G}' . The necessary and sufficient condition for convergence as $S \rightarrow \infty$ is therefore $\lambda'_{\max} < 1$ with

$$\lambda'_{\max} = \arg \max_{\forall n} |\lambda'_n|, \quad (4.61)$$

where λ'_n is the n^{th} eigenvalue of \mathbf{G}' , $n = 1, \dots, NK$. Note that since \mathbf{G}' is not Hermitian, its eigenvalues are not necessarily real-valued. According to the Geršgorin disc theorem (see e.g.: [HJ90]), each eigenvalue of \mathbf{G}' satisfies at least one of the inequalities

$$|\lambda'_n - g'_{pp}| \leq r'_p, \quad \text{where } r'_p = \sum_{\substack{q=1 \\ q \neq p}}^{NK} |g'_{pq}|, \quad (4.62)$$

where g'_{pq} is the element at position (p, q) of \mathbf{G}' for $p, q = 1, \dots, NK$. Because of the structure of \mathbf{G}' in (4.58), $g'_{pp} = 0, \forall p$. Thus to guarantee the convergence of (4.59), the

following must be satisfied:

$$r'_{\max} < 1, \quad \text{where } r'_{\max} \triangleq \max_{\forall p} r'_p. \quad (4.63)$$

It is possible to interpret r'_p as the sum of the absolute values of the residual inter-group interference after filtering, as can be observed from (4.56) and (4.62). The actual value taken by each r'_p therefore depends on the MAI, on the grouping and on how much IGI reduction is provided by the extended simplified GRP-STMUD linear filters.

In general it is difficult to guarantee convergence, but in practical interference scenarios, the conditions for convergence can be satisfied by using a combination of effective grouping algorithms and resource allocation mechanisms. Thus when compared to the traditional linear parallel interference cancellation receiver, which has been shown to diverge for relatively small system loads [GS01], the group-based approach provides an additional tool to improve convergence. For example by grouping users with strong mutual interference together, their contribution to r'_p may be reduced. Alternatively, in a typical cellular system, problematic users can be re-allocated to a different time-slot/frequency. Also note that larger groups are in general preferable over (more numerous) smaller groups. Finally, user sharing is advantageous because it effectively increases the number of users in each group, thus reducing the number of contributing terms to r'_p in (4.62).

Provided the conditions for convergence are met, it can be seen that the sum in (4.59) converges as $S \rightarrow \infty$ to

$$\mathbf{z}_{\text{pic}}^{(\infty)} = \underbrace{(\mathbf{I} + \mathbf{G}')^{-1} \mathbf{F}' \mathbf{y}}_{\mathbf{M}_{(\infty)}^H}, \quad (4.64)$$

where $\mathbf{M}_{(\infty)}$ is defined here as the *total* linear filter.

Proposition 5. *The total linear filter $\mathbf{M}_{(\infty)}$ in (4.64) minimizes the MMSE cost function*

in (2.28) and is thus equivalent to the full STMUD filter in (2.30).

Proof. Define

$$\mathbf{M}' \triangleq \text{diag}(\mathbf{M}'_1, \dots, \mathbf{M}'_G) \quad (4.65)$$

$$\mathbf{D}' \triangleq \text{diag}(\mathbf{T}'_1{}^H \mathbf{T}'_1, \dots, \mathbf{T}'_G{}^H \mathbf{T}'_G) \quad (4.66)$$

$$\tilde{\mathbf{P}}' \triangleq \text{diag}(\tilde{\mathbf{P}}'_1, \dots, \tilde{\mathbf{P}}'_G) \quad (4.67)$$

$$\mathbf{P}' \triangleq [\mathbf{P}'_1, \dots, \mathbf{P}'_G]. \quad (4.68)$$

Using these definitions, and observing that $\mathbf{F}' = \tilde{\mathbf{P}}'^T \mathbf{M}'^H \mathbf{P}'^T$, the matrix $(\mathbf{I} + \mathbf{G}')$ to be inverted in (4.64) can then be expressed in the form

$$(\mathbf{I} + \mathbf{G}') = \mathbf{I} + \tilde{\mathbf{P}}'^T \mathbf{M}'^H (\mathbf{P}'^T \mathbf{T}^H \mathbf{T} - \mathbf{D}' \mathbf{P}'^T) \quad (4.69)$$

$$= \mathbf{I} + \tilde{\mathbf{P}}'^T \mathbf{M}'^H \mathbf{P}'^T (\mathbf{T}^H \mathbf{T} + \sigma^2 \mathbf{I}) - \tilde{\mathbf{P}}'^T \mathbf{M}'^H (\mathbf{D}' + \sigma^2 \mathbf{I}) \mathbf{P}'^T \quad (4.70)$$

$$= \mathbf{F}' (\mathbf{T}^H \mathbf{T} + \sigma^2 \mathbf{I}), \quad (4.71)$$

where the fact that $\tilde{\mathbf{P}}'^T \mathbf{P}'^T = \mathbf{I}$ has been used in (4.71). If there are no identical extended groups, which is always the case in a practical system, it can be shown that \mathbf{F}' is full rank and thus its inverse exists.

Let the estimation error vector for the soft symbol estimate in (4.64) be given by

$$\boldsymbol{\xi}_{\text{pic}} = \mathbf{d} - (\mathbf{I} + \mathbf{G}')^{-1} \mathbf{F}' \mathbf{y} \quad (4.72)$$

According to the principle of orthogonality (e.g.: [Hay02]), the necessary and sufficient

condition to minimize the mean-squared error is given by

$$E[\mathbf{y}\boldsymbol{\xi}_{\text{pic}}^H] = \mathbf{0}. \quad (4.73)$$

Substituting (4.71) for $(\mathbf{I} + \mathbf{G}')$ in the expression of the estimation error vector, it follows that

$$\begin{aligned} E[\mathbf{y}\boldsymbol{\xi}_{\text{pic}}^H] &= E[(\mathbf{T}^H\mathbf{T}\mathbf{d} + \mathbf{T}^H\mathbf{n})(\mathbf{d}^H - (\mathbf{T}^H\mathbf{T}\mathbf{d} + \mathbf{T}^H\mathbf{n})^H\mathbf{F}'^H(\mathbf{I} + \mathbf{G}')^{-H})] \\ &= \mathbf{T}^H\mathbf{T}(\mathbf{I} - (\mathbf{T}^H\mathbf{T} + \sigma^2\mathbf{I})\mathbf{F}'^H(\mathbf{I} + \mathbf{G}')^{-H}) \\ &= \mathbf{T}^H\mathbf{T}\left(\mathbf{I} - (\mathbf{T}^H\mathbf{T} + \sigma^2\mathbf{I})(\mathbf{F}'^H) \cdot (\mathbf{F}')^{-H}(\mathbf{T}^H\mathbf{T} + \sigma^2\mathbf{I})^{-H}\right) \\ &= \mathbf{0}, \end{aligned} \quad (4.74)$$

where the fact that the inverse of \mathbf{F}' exists is used resulting in the cancellation of the inner terms. It can be concluded that $\mathbf{z}_{\text{pic}}^{(\infty)}$ is the MMSE soft symbol estimate, and consequently $\mathbf{z}_{\text{pic}}^{(\infty)} \equiv \mathbf{z}_o$, where \mathbf{z}_o is the full STMUD MMSE soft symbol estimate in (2.27). \square

It can be observed from (4.71), that $(\mathbf{I} + \mathbf{G}')$ is full rank and the inverse in (4.64) exists; therefore (4.60) is a valid expression for the corresponding geometric sum.

The error between the soft estimate after S stages in (4.60) and the MMSE soft estimate given by the full STMUD receiver of Section 2.5 can be expressed as

$$\mathbf{z}_{\text{pic}}^{(S)} - \mathbf{z}_o = (\mathbf{I} - (-\mathbf{G}')^S)(\mathbf{I} + \mathbf{G}')^{-1}\mathbf{F}'\mathbf{y} - \mathbf{M}_o^H\mathbf{y} \quad (4.75)$$

$$= (\mathbf{I} - (-\mathbf{G}')^S)\mathbf{M}_o^H\mathbf{y} - \mathbf{M}_o^H\mathbf{y} \quad (4.76)$$

$$= (-\mathbf{G}')^S\mathbf{z}_o. \quad (4.77)$$

The normalized norm error can thus be bounded by

$$\frac{\|\mathbf{z}^{(S)} - \mathbf{z}_o\|}{\|\mathbf{z}_o\|} \leq \|(-\mathbf{G}')^S\|_2 \leq (\lambda'_{\max})^S, \quad (4.78)$$

where the inequalities come from properties of the matrix norm [HJ90]. Since from (4.62) it follows that $\lambda'_{\max} \leq r'_{\max}$, the convergence rate depends essentially on the residual inter-group interference after filtering. This information can be used together with the observations of Section 4.3.1 to improve the speed of convergence via better grouping.

Finally, it can be concluded that as the number of stages increases, the soft symbol estimate provided by the proposed receiver structure converges in norm to the MMSE symbol estimate provided by the full STMUD receiver. A similar conclusion has been recently obtained in [BZSB07] for a SIC group-based receiver structure.

4.3.3 Multistage group-based PIC with weighting

It is shown in [GS01] that the convergence of linear PIC for CDMA systems can be guaranteed by using well-known generalizations of the Jacobi iteration method. As with traditional PIC, weighting is also necessary to guarantee the convergence of the MS-GRP-PIC receiver. Incorporating the first-order iterative method in [Axe94] to the MS-GRP-PIC receiver, the weighted iterative equation can be shown to take the form:

$$\mathbf{z}_{\text{pic},\tau}^{(s)} = \begin{cases} \mathbf{0}, & s = 0 \\ \tau_s \mathbf{F}' \mathbf{y} + ((1 - \tau_s) \mathbf{I} - \tau_s \mathbf{G}') \mathbf{z}_{\tau}^{(s-1)}, & 1 \leq s \leq S \end{cases} \quad (4.79)$$

where $\mathbf{z}_{\text{pic},\tau}^{(s)}$ is the vector of soft symbol estimate at stage s for the weighted iterative method, and τ_s is the iterative weighting factor at stage s . Notice that when $\tau_s = 1, \forall s$,

the weighted equation in (4.79) is equivalent to (4.54).

Several approaches to selecting the set of weighting factors exist. In practice, since the maximum number of stages is likely to be known due to hardware limitations, it may be advantageous to choose the weighting factors to minimize the norm of the error after S stages, i.e. $\|\mathbf{z}_{\text{pic},\tau}^{(S)} - \mathbf{z}_o\|$. This can be achieved by using the Chebyshev iterative method, in which case the set of weighting factors can be expressed for $1 \leq s \leq S$ as [Axe94]:

$$\frac{1}{\tau_s} = \frac{\alpha'_{\max} - \alpha'_{\min}}{2} \cos \theta_s + \frac{\alpha'_{\max} + \alpha'_{\min}}{2}, \quad (4.80)$$

$$\theta_s \triangleq \frac{2(s-1)+1}{2S}\pi, \quad (4.81)$$

where α'_{\max} and α'_{\min} are parameters related to the maximum and minimum eigenvalues of \mathbf{G}' , respectively.

Estimation of the eigenvalues of \mathbf{G}' is a computationally intensive task. Fortunately, the Chebyshev iterative method is less sensitive to eigenvalue estimation errors than other iterative methods. As a result, in this work, a computationally simple set of approximations is proposed where the estimates for α'_{\max} and α'_{\min} are given respectively by

$$\hat{\alpha}'_{\max} = a + b\|\mathbf{G}'\|_F, \quad (4.82)$$

$$\hat{\alpha}'_{\min} = 1, \quad (4.83)$$

where $\|\cdot\|_F$ is the Frobenius norm [GVL96], and the values for a and b are obtained from empirical data. The computer simulation results obtained in Chapter 6 demonstrate that the convergence of the MS-GRP-PIC receiver with weighting does not suffer significantly from using these estimates, when compared to using the exact values of α'_{\max} and α'_{\min} .

4.4 Complexity analysis

In this section, the complexity of the receiver structures described in this Chapter is analyzed. As in the previous Chapter, the cost is expressed in terms of complex floating point operations (CFLOPS), for each part of the equations describing the receiver structures. All the computations involved in computing the vector of soft symbol estimates from the observation signal \mathbf{x} are taken into consideration. To simplify, the cost expressed in most cases is approximated by neglecting smaller order terms.

4.4.1 Single-stage GRP-SIC

As in Chapter 3, the cost for each receiver structure is divided in a number of categories. For the GRP-SIC receiver, the first category consists of the matched filter. The cost associated to the matched filter is the same as for the full STMUD receiver. The second category includes the intermediate calculations required to prepare the matrix for the linear system solution. The third category is the linear system solution (LSS), which essentially consists of solving the inverse system expressed by (4.1) and (4.7). The fourth category consists of the post-processing related to the linear system solution. The last category is unique to interference cancellation receiver structures, and consists of the actual interference cancellation step.

Table 4.2 summarizes the cost for each of the steps related to the GRP-SIC receiver. The total cost for the GRP-SIC receiver can be expressed as

$$\mathcal{C}_{\text{sic}} = \mathcal{C}_{\text{mf}} + \mathcal{C}_{\mathbf{T}^H \mathbf{T}} + \sum_{j=1}^G \left\{ \mathcal{C}_{\mathbf{R}_j(\mathbf{R}_j + \sigma^2 \mathbf{I})} + \mathcal{C}_{\tilde{\mathbf{C}}_j \tilde{\mathbf{C}}_j^H} + \mathcal{C}_{\text{chol},j} + \mathcal{C}_{\text{bs},j} + \mathcal{C}_{\mathbf{R}_j \mathbf{z}} \right\} + \sum_{j'=1}^{G-1} \mathcal{C}_{\text{sic},j'}, \quad (4.84)$$

where it can be noted that for single stage SIC the interference cancellation does not need

Category	Operation	Label	Approximate cost (in CFLOPS)
Matched filter	$\mathbf{T}^H \mathbf{x}$	\mathcal{C}_{mf}	$2NKM(Q + W - 1)$
Intermediate calculations	$\mathbf{T}^H \mathbf{T}$	$\mathcal{C}_{\mathbf{T}^H \mathbf{T}}$	$MK^2(Q + 3W)$
	$\mathbf{R}_j(\mathbf{R}_j + \sigma^2 \mathbf{I})$	$\mathcal{C}_{\mathbf{R}_j(\mathbf{R}_j + \sigma^2 \mathbf{I})}$	$12K_j^3 + 4K_j^2 + K_j$
	$\tilde{\mathbf{C}}_j \tilde{\mathbf{C}}_j^H$	$\mathcal{C}_{\tilde{\mathbf{C}}_j \tilde{\mathbf{C}}_j^H}$	$12K_j^2 \tilde{K}_j + 4K_j^2$
Linear system solution	Cholesky factorization	$\mathcal{C}_{\text{chol},j}$	$\frac{19NK_j^3}{3}$
	Backsubstitutions	$\mathcal{C}_{\text{bs},j}$	$10NK_j^2$
Post processing	$\mathbf{R}_j(\cdot)$ (see (4.7))	$\mathcal{C}_{\mathbf{R}_j \mathbf{z}}$	$6NK_j^2$
Interference cancellation	$\boldsymbol{\xi}_j^{(s)} - \mathbf{T}^H \mathbf{T}_j \mathbf{z}_{\text{out},j}^{(s)}$	$\mathcal{C}_{\text{sic},j}$	$6NKK_j$

Table 4.2 Approximate complexity (in CFLOPS) for the different steps of the GRP-SIC receiver.

to be performed after the last group.

The total cost for the GRP-SIC receiver in (4.84) can be approximated as

$$\mathcal{C}_{\text{sic}} \approx 2NKMQ + \sum_{j=1}^G \left\{ \frac{19NK_j^3}{3} + 16NK_j^2 \right\} + \sum_{j'=1}^{G-1} 6NKK_{j'}, \quad (4.85)$$

where it is assumed that N and K are large compared to K_j , and that Q is large compared to W . The smaller order terms in Table 4.2 have been neglected.

4.4.2 MS-GRP-SIC

The complexity associated to the MS-GRP-SIC receiver structure described in Section 4.2.2 is very similar to the complexity of the GRP-SIC receiver. The main difference here is that the multistage receiver repeats the filtering and interference cancellation several times.

Table 4.3 shows the cost associated to the different steps involved in the MS-GRP-SIC receiver. It can be observed that because of the simplified GRP-STMUD filter in (4.42),

Category	Operation	Label	Approximate cost (in CFLOPS)
Matched filter	$\mathbf{T}^H \mathbf{x}$	\mathcal{C}_{mf}	$2NKM(Q + W - 1)$
Intermediate calculations	$\mathbf{T}^H \mathbf{T}$	$\mathcal{C}_{\mathbf{T}^H \mathbf{T}}$	$MK^2(Q + 3W)$
	$\mathbf{T}^H \mathbf{T} + \sigma^2 \mathbf{I}$	$\mathcal{C}_{\mathbf{T}^H \mathbf{T} + \sigma^2 \mathbf{I}}$	K
Linear system solution	Cholesky factorization	$\mathcal{C}_{\text{chol}^*,j}$	$\frac{10NK_j^3}{3}$
	Backsubstitutions	$\mathcal{C}_{\text{bs}^*,j}$	$6NK_j^2$
Interference cancellation	$\boldsymbol{\xi}_j^{(s)} - \mathbf{T}^H \mathbf{T}_j \mathbf{z}_{\text{out},j}^{(s)}$	$\mathcal{C}_{\text{msic},j}$	$6NKK_j$

Table 4.3 Approximate complexity (in CFLOPS) for the different steps of the MS-GRP-SIC receiver.

the intermediate calculations and the linear system solution costs are smaller for the MS-GRP-SIC receiver than for the GRP-SIC receiver. For the simplified GRP-STMUD filter, the costs for Cholesky factorization and backsubstitutions are denoted in the table by $\mathcal{C}_{\text{chol}^*,j}$ and $\mathcal{C}_{\text{bs}^*,j}$, respectively. If the maximum number of stages in the receiver is S , then the total cost for the MS-GRP-SIC receiver can be expressed as

$$\mathcal{C}_{\text{msic}} = \mathcal{C}_{\text{mf}} + \mathcal{C}_{\mathbf{T}^H \mathbf{T}} + \mathcal{C}_{\mathbf{T}^H \mathbf{T} + \sigma^2 \mathbf{I}} + \sum_{j=1}^G \{ \mathcal{C}_{\text{chol}^*,j} + S(\mathcal{C}_{\text{bs}^*,j} + \mathcal{C}_{\text{msic},j}) \}. \quad (4.86)$$

Neglecting the smaller order terms in Table 4.3, the total cost for the MS-GRP-SIC receiver in (4.86) can be approximated as

$$\mathcal{C}_{\text{msic}} \approx 2NKMQ + \sum_{j=1}^G \frac{10NK_j^3}{3} + 6SNKK_j. \quad (4.87)$$

4.4.3 MS-GRP-PIC

The complexity associated to the MS-GRP-PIC receiver structure described in Section 4.2.2 is also very similar to the complexity of the MS-GRP-SIC receivers above, which also uses

the simplified GRP-STMUD filter structure. The actual cost for each step associated to the MS-GRP-PIC receiver is shown in Table 4.4.

Category	Operation	Label	Approximate cost (in CFLOPS)
Matched filter	$\mathbf{T}^H \mathbf{x}$	\mathcal{C}_{mf}	$2NKM(Q + W - 1)$
Intermediate calculations	$\mathbf{T}^H \mathbf{T}$	$\mathcal{C}_{\mathbf{T}^H \mathbf{T}}$	$MK^2(Q + 3W)$
	$\mathbf{T}^H \mathbf{T} + \sigma^2 \mathbf{I}$	$\mathcal{C}_{\mathbf{T}^H \mathbf{T} + \sigma^2 \mathbf{I}}$	K
Linear system solution	Cholesky factorization	$\mathcal{C}_{\text{chol}^*,j}$	$\frac{10NK_j'^3}{3}$
	Backsubstitutions	$\mathcal{C}_{\text{bs}^*,j}$	$6NK_j'^2$
Interference cancellation	$\mathbf{T}_j'^H \bar{\mathbf{T}}_j' \mathbf{z}$	$\mathcal{C}_{\mathbf{T}_j'^H \bar{\mathbf{T}}_j' \mathbf{z}}$	$6NK_j'(K - K_j')$
	$\mathbf{M}_j'^H (\mathbf{T}_j'^H \bar{\mathbf{T}}_j' \mathbf{z})$	$\mathcal{C}_{\mathbf{M}_j'^H (\mathbf{T}_j'^H \bar{\mathbf{T}}_j' \mathbf{z})}$	$6NK_j'^2$
	$\tilde{\mathbf{P}}_j^H \mathbf{M}_j'^H \mathbf{T}_j'^H \mathbf{x} - \hat{v}_j^{(s)}$	$\mathcal{C}_{\text{pic},j}$	K_j'

Table 4.4 Approximate complexity (in CFLOPS) for the different steps of the MS-GRP-PIC receiver.

Using the steps listed in Table 4.4, and using the same assumptions as in Section 4.4.1, the total cost for the MS-GRP-PIC receiver can be expressed as follows:

$$\begin{aligned} \mathcal{C}_{\text{pic}} &= \mathcal{C}_{\text{mf}} + \mathcal{C}_{\mathbf{T}^H \mathbf{T}} + \mathcal{C}_{\mathbf{T}^H \mathbf{T} + \sigma^2 \mathbf{I}} \\ &+ \sum_{j=1}^G \left\{ \mathcal{C}_{\text{chol}^*,j} + \mathcal{C}_{\text{bs}^*,j} + (S-1) \left(\mathcal{C}_{\mathbf{T}_j'^H \bar{\mathbf{T}}_j' \mathbf{z}} + \mathcal{C}_{\mathbf{M}_j'^H (\mathbf{T}_j'^H \bar{\mathbf{T}}_j' \mathbf{z})} + \mathcal{C}_{\text{pic},j} \right) \right\}. \end{aligned} \quad (4.88)$$

Neglecting the smaller order terms in Table 4.4, the total cost for the MS-GRP-PIC receiver can be approximated as

$$\mathcal{C}_{\text{pic}} \approx 2NKMQ + \sum_{j=1}^G \left\{ \frac{10NK_j'^3}{3} + 6NK_j'^2 + (S-1)(6NKK_j) \right\}. \quad (4.89)$$

Note that the $(S-1)$ factor in (4.89) is a consequence of the MS-GRP-PIC structure shown in Fig. 4.3, where no interference cancellation is necessary at the first stage.

Finally, the complexity associated to computing the weighting factors in the MS-GRP-PIC receiver with weighting described in Section 4.3.3 can be shown to be negligible when compared to the total cost in (4.89). Indeed, the bulk of the cost associated to computing the weighting factors originates from the Frobenius norm of \mathbf{G}' in (4.82), which in practice can be shown to require approximately K^2 CFLOPS.

4.4.4 Summary

Table 4.5 summarizes the approximate cost of each receiver structure considered. As in Table 3.6, the maximum group size and maximum number of groups is assumed so that $G = G_{\max}$ and $K_j = K_{\text{grp}}$, and the maximum number of users is given by $K_{\max} = G_{\max}K_{\text{grp}}$. As such, the complexity indicated in the table represents the cost for a practical system implementation, taking into consideration the worst case scenario.

Receiver structure	Approximate cost (CFLOPS)
GRP-SIC	$2NMK_{\max}^2 + \frac{19}{3}NK_{\max}K_{\text{grp}}^2 + 2NK_{\max}(8K_{\text{grp}} + 3K_{\max})$
MS-GRP-SIC	$2NMK_{\max}^2 + \frac{10}{3}NK_{\max}K_{\text{grp}}^2 + 6NSK_{\max}(K_{\max} + K_{\text{grp}})$
MS-GRP-PIC	$2NMK_{\max}^2 + \frac{10}{3}NK_{\max}K_{\text{grp}}^2 + 6N(S - 1)K_{\max}^2$

Table 4.5 Summary of the approximate cost for the multistage receiver structures.

As expected, the MF cost is the same for each structure and represents a large portion of the total cost. For structures employing the simplified GRP-STMUD filter, the cost for the linear system solution is smaller. It can also be observed that the total cost for the MS-GRP-SIC and MS-GRP-PIC structures is of the same order of magnitude. Note that by nature, the MS-GRP-SIC receiver introduces more latency than the MS-GRP-PIC receiver. For both receiver structures, and if latency is not an issue, the group-based MUD filtering hardware can be shared among groups, further reducing the overall implementation cost.

Chapter 5

Grouping algorithms

5.1 Motivation

In the previous Chapters, the group-based receiver structures were developed assuming a pre-existing and fixed grouping. This assumption was introduced to avoid the difficulty of providing a joint-optimal set of filter coefficients and grouping. Grouping is an important operation as it can significantly affect the BER performance of the structures studied in Chapter 3 and 4. The grouping also influences the convergence properties of multistage receivers such as the MS-GRP-SIC and MS-GRP-PIC receivers proposed in Chapter 4.

In a practical receiver, the maximum number of groups G_{\max} and maximum number of users per groups K_{grp} are usually limited by the hardware resources. The existing threshold-based grouping algorithms in [HSMTG00, LLC05] do not take this important aspect into account and cannot be applied in this context. Moreover, these algorithms do not consider the possible extra computing resources available for user sharing. In this Chapter, a practical algorithm for mutually exclusive grouping respecting hardware limitations is proposed along with an extension providing non-mutually exclusive grouping for user sharing.

As discussed in Chapter 3, grouping problems are in general NP-hard: there is no known polynomial time complexity algorithm that is guaranteed to provide an optimal solution [Fal98]. Thus to find the optimal grouping, it is necessary to resort to an exhaustive search. Unfortunately, the number of possible groupings is extremely high even for a moderate number of users.

To illustrate this point, consider the case $K = 12$, $G_{\max} = 4$ and $K_{\text{grp}} = 4$. In this scenario, the group-based receiver is designed to support a maximum of $K_{\max} = G_{\max}K_{\text{grp}} = 16$ users. Define *computing resource* as the computational load required to support a single user. Since $K < K_{\max}$, the receiver here has $K_{\max} - K = 4$ extra computing resources. This results in essentially 5 different grouping configurations, each with a different number of users per group. Table 5.1 lists the different grouping configuration with the associated number of different grouping for each, obtained using combinatorial analysis (see e.g. [LG94]). The total number of different groupings, indicated in the last row of Table 5.1, is close to 300,000 for the case considered. Moreover, due to the combinatorial nature of the problem, the number of possibilities increases very rapidly with increasing number of users.

To find the optimal grouping for a given receiver structure using an exhaustive search, a cost function must be evaluated for each of the possible grouping. In general, this operation requires to actually design the filter weights for each possible grouping.

In the following Section, a grouping cost function based on the normalized cross-correlation between the effective signatures of users is derived. This simplified cost function does not require the computation of the actual MUD linear filters and is therefore more practical to use in an exhaustive search. In Section 5.3, new sub-optimal grouping algorithms that do not require an exhaustive search are proposed. The special case of grouping for group-based SIC receivers is discussed in Section 5.4, and finally the complexity of the

Nb. users/group				Nb. of possibilities
K_1	K_2	K_3	K_4	
3	3	3	3	$\frac{\binom{12}{3}\binom{9}{3}\binom{6}{3}}{4!} = 15,400$
4	3	3	2	$\frac{\binom{12}{4}\binom{8}{3}\binom{5}{3}}{2!} = 138,600$
4	4	3	1	$\frac{\binom{12}{4}\binom{8}{4}\binom{4}{3}}{2!} = 69,300$
4	4	2	2	$\frac{\binom{12}{4}\binom{8}{4}\binom{4}{2}}{2!2!} = 51,975$
4	4	4	0	$\frac{\binom{12}{4}\binom{8}{4}}{3!} = 5,775$
Total:				281,050

Table 5.1 Number of possibilities for each possible grouping configuration, for the case $G_{\max} = 4$, $K_{\text{grp}} = 4$, $K = 12$.

proposed algorithms is studied in Section 5.5.

5.2 Grouping cost function

To objectively compare different groupings, it is necessary to use a cost function. The cost function may be based on a variety of *cost criteria* such as the BER, MSE, SNR, or other. Since the cost may also depend on the MUD filter weights, it is assumed here that the GRP-STMUD filter weights in (3.39) are used.

To simplify the development, and for the purpose of group selection only, the inter-symbol interference is neglected. This is equivalent to setting the off-diagonal blocks of matrix $\mathbf{R} \equiv \mathbf{T}^H \mathbf{T}$ in (2.32) to zero, resulting in a block diagonal matrix with N blocks $\mathbf{V}^H \mathbf{V}$. Since the interference perceived at each symbol interval has the same statistics within a block, the same grouping can be used for the N symbol intervals. Also, since there is no inter-symbol interference, the grouping can be based on the effective signature matrix \mathbf{V} in (2.23), instead of the entire system matrix \mathbf{T} . Thus, for the purpose of simplifying the

notation for the development of the grouping algorithm, a system with $N = 1$ is considered. This is equivalent to the general system with block size $N > 1$ with no ISI.

5.2.1 Grouping notation

It is essential here to recall some important notations regarding the grouping. The system grouping \mathcal{G} is defined as a set of G groups, and can be expressed as

$$\mathcal{G} = \{\mathcal{G}_1, \dots, \mathcal{G}_G\}, \quad (5.1)$$

where each \mathcal{G}_j contains a set of user indices, as defined in (3.1) and rewritten here for convenience:

$$\mathcal{G}_j = \{g_{j,1}, \dots, g_{j,K_j}\}, \quad (5.2)$$

where $g_{j,l} \in \mathcal{S}$ is the index of the l^{th} user of group j , and $\mathcal{S} = \{1, \dots, K\}$. Each user typically belongs to at least one group; thus $\bigcup_{j=1}^G \mathcal{G}_j = \mathcal{S}$. If the groups are mutually exclusive, then $\mathcal{G}_j \cap \mathcal{G}_i = \emptyset$, for any $j \neq i$, and $K = \sum_j K_j$.

5.2.2 MSE-based cost function

In the context of MMSE MUD filtering, it is natural to use the MSE as a cost criterion. As such, the MSE-based cost function for a given grouping \mathcal{G} takes the form

$$J_{\text{MSE}}(\mathcal{G}) = \sum_{j=1}^G J_{\text{grp},j}(\mathbf{M}_{\text{grp},j}), \quad (5.3)$$

where $J_{\text{grp},j}(\mathbf{M}_{\text{grp},j})$ is defined in (A.15) in Appendix A and corresponds to the MSE for group j when the GRP-STMUD filter matrix $\mathbf{M}_{\text{grp},j}$ is used. Note that the dependence on the grouping \mathcal{G} in (5.3) is implied in the filter matrix $\mathbf{M}_{\text{grp},j}$ and on the number of groups

\mathcal{G} .

Using (5.3), the optimal grouping with respect to the MSE can be expressed as

$$\mathcal{G}^{(o)} = \arg \min_{\forall \mathcal{G}} J_{\text{MSE}}(\mathcal{G}), \quad (5.4)$$

which can be solved using an exhaustive search over all possible groupings satisfying the conditions in Section 5.2.1.

5.2.3 Simplified cost function

Computing the MSE for each grouping as in (5.3) is computationally intensive; for a real-time system it is preferable to use a simpler and efficient cost criterion. In the following, a new simplified cost function based on the MSE criterion is derived.

As shown in (A.15), the MSE at the output of the group optimal filter in (3.39) is given by

$$J_{\text{grp},j} \equiv J_{\text{grp},j}(\mathbf{M}_{\text{grp},j}) = \text{tr}[\mathbf{I} - \mathbf{R}_j(\mathbf{R}_j\mathbf{R}_j^H + \mathbf{C}_j\mathbf{C}_j^H + \sigma^2\mathbf{R}_j)^{-1}\mathbf{R}_j^H], \quad (5.5)$$

where the dimension of $\mathbf{M}_{\text{grp},j}$ is $K_j \times K_j$ due to the no inter-symbol interference assumption. Matrices \mathbf{R}_j and \mathbf{C}_j refer to the group signature auto-correlation and cross-correlation matrices as defined in (3.37) and (3.38), respectively.

Since matrix $\mathbf{C}_j\mathbf{C}_j^H$ is Hermitian and non-negative definite, there exists a unitary transformation $\mathbf{\Gamma}$ such that

$$\mathbf{C}_j\mathbf{C}_j^H = \mathbf{\Gamma}\mathbf{\Lambda}\mathbf{\Gamma}^H, \quad (5.6)$$

where $\mathbf{\Lambda} = \text{diag}(\lambda_1, \dots, \lambda_{K_j})$ with $\lambda_k \geq 0, \forall k$ [HJ90]. Using this formulation, the group

MSE in (5.5) may be expressed as

$$J_{\text{grp},j} = K_j - \text{tr}[[\mathbf{I} + \mathbf{S}_{\mathbf{R}}^{-2}(\boldsymbol{\Lambda} + \sigma^2 \mathbf{S}_R)]^{-1}], \quad (5.7)$$

where $\mathbf{S}_{\mathbf{R}} \triangleq \boldsymbol{\Gamma}^H \mathbf{R}_j \boldsymbol{\Gamma}$. For large signal-to-interference plus noise ratio (SINR) *after matched filtering*, σ^2 and $\text{tr}(\boldsymbol{\Lambda})$ can be assumed small enough so that $\|\mathbf{S}_{\mathbf{R}}^{-2}(\boldsymbol{\Lambda} + \sigma^2 \mathbf{S}_R)\|_2 \ll 1$ where $\|\cdot\|_2$ denotes the matrix 2-norm. Then the term $[\mathbf{I} + \mathbf{S}_{\mathbf{R}}^{-2}(\boldsymbol{\Lambda} + \sigma^2 \mathbf{S}_R)]^{-1}$ in $J_{\text{grp},j}$ above may be expanded in a series [HJ90] such that

$$J_{\text{grp},j} = K_j - \text{tr} \left[\sum_{l=0}^{\infty} (-\mathbf{S}_{\mathbf{R}}^{-2}(\boldsymbol{\Lambda} + \sigma^2 \mathbf{S}_R))^l \right]. \quad (5.8)$$

Neglecting the higher order terms in (5.8) and taking the limit as $\sigma^2 \rightarrow 0$, the MSE becomes

$$J_{\text{grp},j} \simeq \text{tr}(\boldsymbol{\Lambda} \mathbf{S}_{\mathbf{R}}^{-2}) = \sum_{l=1}^{K_j} \lambda_l [\mathbf{S}_{\mathbf{R}}^{-2}]_{l,l} \quad (5.9)$$

where $[\mathbf{S}_{\mathbf{R}}^{-2}]_{l,l}$ denotes the l^{th} diagonal element of matrix $\mathbf{S}_{\mathbf{R}}^{-2}$. By employing the Cauchy-Schwartz inequality, the MSE in (5.9) can be upper-bounded by

$$J_{\text{grp},j} \leq \sqrt{\sum_{l=1}^{K_j} \lambda_l^2} \sqrt{\sum_{l=1}^{K_j} [\mathbf{S}_{\mathbf{R}}^{-2}]_{l,l}^2}. \quad (5.10)$$

Using (5.6) and the fact that matrix $(\mathbf{C}_j \mathbf{C}_j^H)$ is normal¹, it can be shown that

$$\begin{aligned} \sum_{l=1}^{K_j} \lambda_l^2 &= \sum_{l=1}^{K_j} [\mathbf{C}_j \mathbf{C}_j^H]_{l,l}^2 \\ &= \sum_{l=1}^{K_j} (\|\mathbf{c}_{j,l}\|^2)^2, \end{aligned} \quad (5.11)$$

where $\mathbf{c}_{j,l}$ is a vector containing the elements of the l^{th} row of \mathbf{C}_j , i.e.:

$$\mathbf{c}_{j,l} \triangleq \mathbf{e}_{j,l}^T \mathbf{C}_j, \quad (5.12)$$

and where $\mathbf{e}_{j,l}$ is an elementary vector of dimension $K_j \times 1$ with a 1 at position l . Also, by definition, $\mathbf{S}_{\mathbf{R}}^2$ is similar² to $\mathbf{R}_j \mathbf{R}_j^H$, and they consequently share the same eigenvalues.

Hence

$$\sum_{l=1}^{K_j} [\mathbf{S}_{\mathbf{R}}^{-2}]_{l,l}^2 = \sum_{l=1}^{K_j} [(\mathbf{R}_j \mathbf{R}_j^H)^{-1}]_{l,l}^2. \quad (5.13)$$

Using (5.11) and (5.13) in (5.10), it can finally be shown that

$$J_{\text{grp},j} \leq \sqrt{\sum_{l=1}^{K_j} (\|\mathbf{c}_{j,l}\|^2)^2} \sqrt{\sum_{l=1}^{K_j} [(\mathbf{R}_j \mathbf{R}_j^H)^{-1}]_{l,l}^2}. \quad (5.14)$$

Notice that $\mathbf{R}_j \mathbf{R}_j^H$ in (5.14) is positive definite by assumption. Also, in a practical system with effective power control, the diagonal entries of matrix $\mathbf{R}_j \mathbf{R}_j^H$ can be assumed to be much larger than the off-diagonal ones. Thus for a relatively low cross-correlation power and a fixed group size, the second product term in (5.14) remains approximately constant regardless of the actual group membership. It can therefore be argued that the MSE upper

¹A matrix $\mathbf{A} \in \mathbb{C}^{n \times n}$ is said to be *normal* if $\mathbf{A}^H \mathbf{A} = \mathbf{A} \mathbf{A}^H$ [HJ90].

²A matrix $\mathbf{B} \in \mathbb{C}^{n \times n}$ is said to be *similar* to matrix $\mathbf{A} \in \mathbb{C}^{n \times n}$ if there exists a non-singular matrix $\mathbf{S} \in \mathbb{C}^{n \times n}$ such that $\mathbf{B} = \mathbf{S}^{-1} \mathbf{A} \mathbf{S}$ [HJ90].

bound can be reduced by choosing \mathcal{G} such that the first multiplicative term in (5.14) is minimized for all groups. This can be achieved in particular by minimizing $\|\mathbf{c}_{j,l}\|^2$ for all users in the group, where

$$\|\mathbf{c}_{j,l}\|^2 = \sum_{l'=1}^{K-K_j} |\mathbf{v}_{g_{j,l}}^H \mathbf{v}_{\bar{g}_{j,l'}}|^2, \quad (5.15)$$

$g_{j,l}$ is the index of the l^{th} user in group j and $\bar{g}_{j,l'}$ is the index of the l'^{th} user *not* in group j .

Based on these observations and in particular on (5.14) and (5.15), the new simplified cost function is defined as

$$J_{\text{sc}}(\mathcal{G}) \triangleq \sum_{j=1}^G \sqrt{\sum_{l=1}^{K_j} \left(\sum_{l'=1}^{K-K_j} |\mathbf{v}_{g_{j,l}}^H \mathbf{v}_{\bar{g}_{j,l'}}|^2 \right)^2}. \quad (5.16)$$

The cost $J_{\text{sc}}(\mathcal{G})$ has a computational advantage over the MSE cost function in (5.3) because it only requires the correlation matrix $\mathbf{V}^H \mathbf{V}$, which can be recycled towards the calculation of the optimal MMSE filter in (3.39) once the grouping is determined. The optimal grouping with respect to this new cost function is then given by

$$\mathcal{G}^{(\text{sc})} = \arg \min_{\forall \mathcal{G}} J_{\text{sc}}(\mathcal{G}). \quad (5.17)$$

As for the optimal grouping in (5.4), obtained with the MSE cost function, solving for (5.17) requires an exhaustive search over all possible grouping. Even with the reduced-complexity cost function in (5.16), finding $\mathcal{G}^{(\text{sc})}$ represents a significant challenge because of the large search space dimension.

5.3 Proposed grouping algorithms

5.3.1 Grouping criterion

In the current literature, the normalized cross-correlation between the effective signatures is commonly used as a criterion for grouping users (see e.g. [HSMTG00, LLC05]). Not only it is simple to calculate, it is also intuitive; users with strong cross-correlation should be in the same group because they benefit the most from joint detection. The normalized cross-correlation between the effective signature of users k' and k can be expressed as

$$\rho_{k',k} = \frac{\mathbf{v}_{k'}^H \mathbf{v}_k}{\|\mathbf{v}_{k'}\| \|\mathbf{v}_k\|}, \quad (5.18)$$

where it can be noted that as opposed to $\varphi_{k',k}$ in (2.10), $\rho_{k',k}$ includes the effects of channel distortion in addition to the DS-CDMA code sequence and pulse shaping. Notice that (5.18) can also be interpreted as a form of normalized proximity metric between the two users. Since $\rho_{k',k} \in \mathbb{C}$, it is more appropriate to use the following real-valued *grouping criterion*:

$$\varrho_{k',k} \triangleq |\rho_{k',k}|^2 = \frac{|\mathbf{v}_{k'}^H \mathbf{v}_k|^2}{\|\mathbf{v}_{k'}\|^2 \|\mathbf{v}_k\|^2}, \quad (5.19)$$

when comparing different pairs of users.

While the use of (5.19) for grouping users is intuitive, it has not been appropriately justified in the literature. It now becomes possible to do so with the derivation of the simplified cost function in Section 5.2.3 above. Indeed, it can be observed that the cross-correlation between effective signature vectors plays a fundamental part in the MSE. This can be seen directly from (5.14) and (5.15) above. In effect, these two equations justify the use of the effective signature waveform cross-correlation as a basis for choosing the grouping.

The normalization in (5.19) becomes important when the power between users vary significantly. To demonstrate, consider the following illustrative scenario: let $K = 3$, and let the effective signature cross-correlation matrix be given by:

$$\mathbf{V}^H \mathbf{V} = \begin{bmatrix} 1 & 0.6 & 0.5 \\ 0.6 & 100 & 0 \\ 0.5 & 0 & 1 \end{bmatrix}, \quad (5.20)$$

where it can be observed that user #2 has 20dB of excess power over the other two users. Table 5.2 lists the values taken by the grouping criterion in (5.19) and for $|\mathbf{v}_{k'}^H \mathbf{v}_k|^2$, which is essentially the same as the grouping criterion but with no normalization, for the scenario described by (5.20). Clearly, the high power of user #2 has a significant impact on the

(k', k)	$ \mathbf{v}_{k'}^H \mathbf{v}_k ^2$	$\varrho_{k',k}$
(1, 2)	0.36	0.0036
(1, 3)	0.25	0.25
(2, 3)	0	0

Table 5.2 Comparison of normalized and non-normalized grouping criteria.

grouping criterion, as indicated by the values in the first row.

Consider the following two grouping scenarios: in scenario A, the grouping is determined by pairing users with the largest $|\mathbf{v}_{k'}^H \mathbf{v}_k|^2$, and in scenario B, the grouping is obtained by pairing users with the largest grouping criterion $\varrho_{k',k}$. Using the values in Table 5.2 it follows that for scenario A, users 1 and 2 will be grouped together first, while for scenario B, users 1 and 3 will be grouped together first.

Those two different groupings lead to different inter-group-interference characteristics. Specifically, consider the ratio of IGI power over signal power, as measured after matched

filtering for the user of interest. For user k in group j , this ratio can be expressed as

$$\Gamma_{\text{IGI},k} \triangleq \frac{\sum_{l \notin \mathcal{G}_j} |\mathbf{v}_k^H \mathbf{v}_l|^2}{\|\mathbf{v}_k\|^2}, \quad (5.21)$$

where it is assumed that users belonging to the same group do not interfere due to ideal MUD. Table 5.3 indicates the ratio of IGI power over signal power for each user for the two scenarios considered using the values in (5.20). As it can be seen from the Table, choosing

Scenario	$\Gamma_{\text{IGI},1}$	$\Gamma_{\text{IGI},2}$	$\Gamma_{\text{IGI},3}$
A: $\mathcal{G}_A = \{\{1, 2\}, \{3\}\}$	0.25	0.0	0.25
B: $\mathcal{G}_B = \{\{1, 3\}, \{2\}\}$	0.36	0.0036	0.0

Table 5.3 IGI power for each grouping scenario.

the grouping based on the normalized cross-correlation in (5.19) reduces the number of users suffering from IGI; in scenario A, two users suffer from significant IGI whereas in scenario B, only one user does.

This simple but informative example can be generalized to more complex cases. While this example does not show the effect of normalization on the performance directly, it can nevertheless be argued from this discussion that the normalization in (5.19) is advantageous when compared to using $|\mathbf{v}_k^H \mathbf{v}_k|^2$ alone. This observation has also been confirmed by experimental results.

5.3.2 Mutually exclusive grouping

The proposed algorithm carries out pairwise grouping of users or groups successively until it is no longer possible to do so. Starting with an initial grouping where all the users are in separate groups, the grouping is refined at each iteration. At each iteration, the elements to merge are selected from the ordering of all pairs of users or groups according to the

so-called *proximity metric* defined below.

Let the proximity metric between groups $\mathcal{G}_{l'}, \mathcal{G}_l \in \mathcal{G}$ be defined as the largest grouping criterion between all possible pairs of corresponding users:

$$\delta_{\mathcal{G}_{l'}, \mathcal{G}_l} = \arg \max_{\substack{\forall p \in \mathcal{G}_{l'} \\ \forall q \in \mathcal{G}_l}} \varrho_{p,q}, \quad (5.22)$$

where $\varrho_{p,q}$ is defined in (5.19). Note that for groups with single users, (5.22) is equivalent to the grouping criterion in (5.19). Using the maximum in (5.22) can be justified by observing that the cost is dominated by the users suffering from the strongest interference, as (5.16) indicates.

The flow diagram for the proposed grouping algorithm is illustrated in Fig. 5.1. The algorithm starts with $\mathcal{G} = \{\{1\}, \dots, \{K\}\}$ and thus $G = K$. The subsets (or groups) composing \mathcal{G} are “refined” at each iteration until no more grouping can be done, at which point $\mathcal{G}^{(\text{ga})} = \mathcal{G}$. At each iteration, the proximity metric is computed for all $N_p = \binom{G}{2}$ possible pairs of subsets in \mathcal{G} , where G is the number of subsets in \mathcal{G} at any point in time. Grouping is then attempted in decreasing order of proximity metric (close pairs first), an approach also used in [BSZ06]. Merging a pair of groups $\mathcal{G}_{l'}$ and \mathcal{G}_l may result in four possible outcomes:

1. A new group is formed ($|\mathcal{G}_{l'}| = 1$ and $|\mathcal{G}_l| = 1$);
2. Two existing groups are combined ($|\mathcal{G}_{l'}| > 1$ and $|\mathcal{G}_l| > 1$);
3. A user is added to an existing group ($|\mathcal{G}_{l'}| = 1$ and $|\mathcal{G}_l| > 1$, or $|\mathcal{G}_{l'}| > 1$ and $|\mathcal{G}_l| = 1$);
4. No merging is possible ($|\mathcal{G}_{l'}| + |\mathcal{G}_l| > K_{\text{grp}}$, or $|\mathcal{G}_{l'}| = 1$, $|\mathcal{G}_l| = 1$ and $G = G_{\text{max}}$).

If the elements cannot be merged because of the hardware constraints, the algorithm tries

with the next pair. The algorithm stops when attempts for grouping have failed for all of the N_p pairs, at which point $\mathcal{G}^{(\text{ga})} = \mathcal{G}$. If $K \leq K_{\max}$, the algorithm will allocate all the users successfully.

5.3.3 Grouping with user sharing

According to the hardware considerations discussed above, a practical receiver for GRP-STMUD would provide a total of K_{\max} “computing resources”. If $K < K_{\max}$ there are $K_{\text{extra}} = K_{\max} - K$ extra computing resources available for sharing, that are essentially free of extra computational cost because the hardware is already designed to support K_{\max} simultaneous users.

The proposed algorithm for grouping with user sharing starts with the mutually exclusive grouping $\mathcal{G}^{(\text{ga})}$ obtained using the algorithm described in the previous Section. Since adding users to an existing group does not deteriorate the performance [Var95], the new algorithm “fills” the unused computing resources in each group with shared users, and provides a new “shared” grouping, $\mathcal{G}^{(\text{ga-sh})} \triangleq \{\mathcal{G}_1^{(\text{ga-sh})}, \dots, \mathcal{G}_G^{(\text{ga-sh})}\}$.

The flow diagram in Fig. 5.2, illustrates the grouping procedure for user sharing. The algorithm proceeds group by group; for the j^{th} group, the $K_{\text{grp}} - K_j$ empty computing resources, if any, are filled with a user $k \notin \mathcal{G}_j^{(\text{ga})}$. The users are selected in order of decreasing proximity metric with the group of interest. To simplify the presentation, assume that the users outside group j are already in the desired order, such that

$$\delta_{\mathcal{G}_j^{(\text{ga})}, \{\bar{g}_{j,1}\}} \geq \delta_{\mathcal{G}_j^{(\text{ga})}, \{\bar{g}_{j,2}\}} \geq \dots \geq \delta_{\mathcal{G}_j^{(\text{ga})}, \{\bar{g}_{j,K-K_j}\}}, \quad (5.23)$$

where $\bar{g}_{j,l}$ is the index of the l^{th} user *not* in group j . Then, assuming that there are enough remaining users to fill the group (i.e.: $K - K_j \geq K_{\text{grp}}$), the set of $K_{\text{grp}} - K_j$ “shared” users

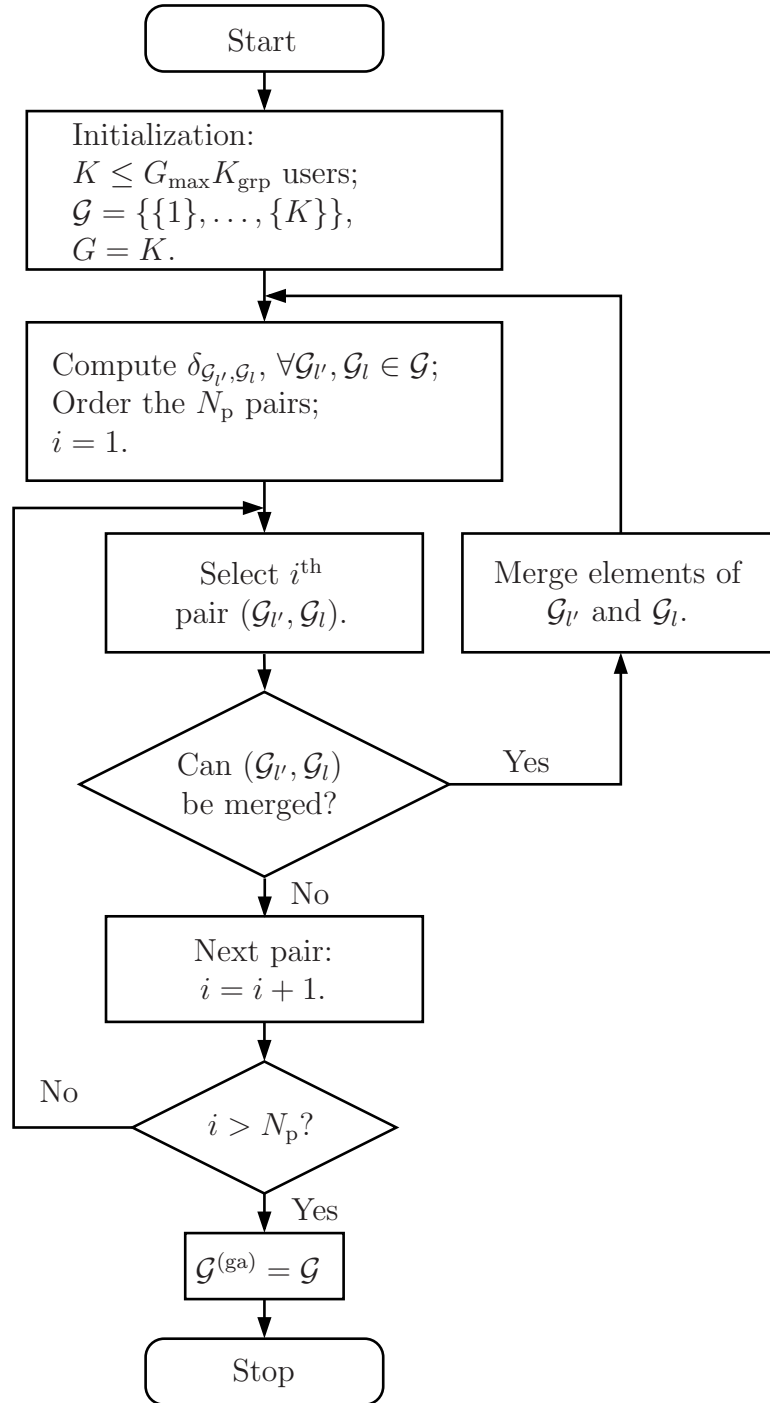


Fig. 5.1 Flow diagram for the grouping algorithm without sharing.

for group j are given by

$$\mathcal{U}_j \triangleq \{\bar{g}_{j,1}, \dots, \bar{g}_{j,K_{\text{grp}}-K_j}\}, \quad (5.24)$$

and the new, shared group becomes

$$\mathcal{G}_j^{(\text{ga-sh})} = \mathcal{G}_j^{(\text{ga})} \cup \mathcal{U}_j. \quad (5.25)$$

Note that the algorithm does not create new groups; in the case where $G < G_{\text{max}}$, the extra computing resources provided by the empty groups will not be used.

5.4 Group ordering for SIC

The group ordering can have an important impact on the performance of successive interference cancellation receivers, such as the GRP-SIC and MS-GRP-SIC receiver structures described in Section 4.2. In traditional SIC receivers, the most reliable symbols are in general detected first. There are several approaches to determine the order of symbol reliability; while some approaches are based on received power only (see e.g.: [SB00a]), other approaches use the information in the de-spread signal [PVBB03, PH94, Vit90].

In group-based SIC, the concept of group ordering is similar; groups with the most reliable symbols are detected first so that it is less likely that the interference is increased by a bad decision [BSZ06, CP05]. In MS-GRP-SIC the group ordering also affects the convergence rate. To determine which group has the most reliable estimates, a new metric for both mutually and non-mutually exclusive grouping and based on the simplified cost

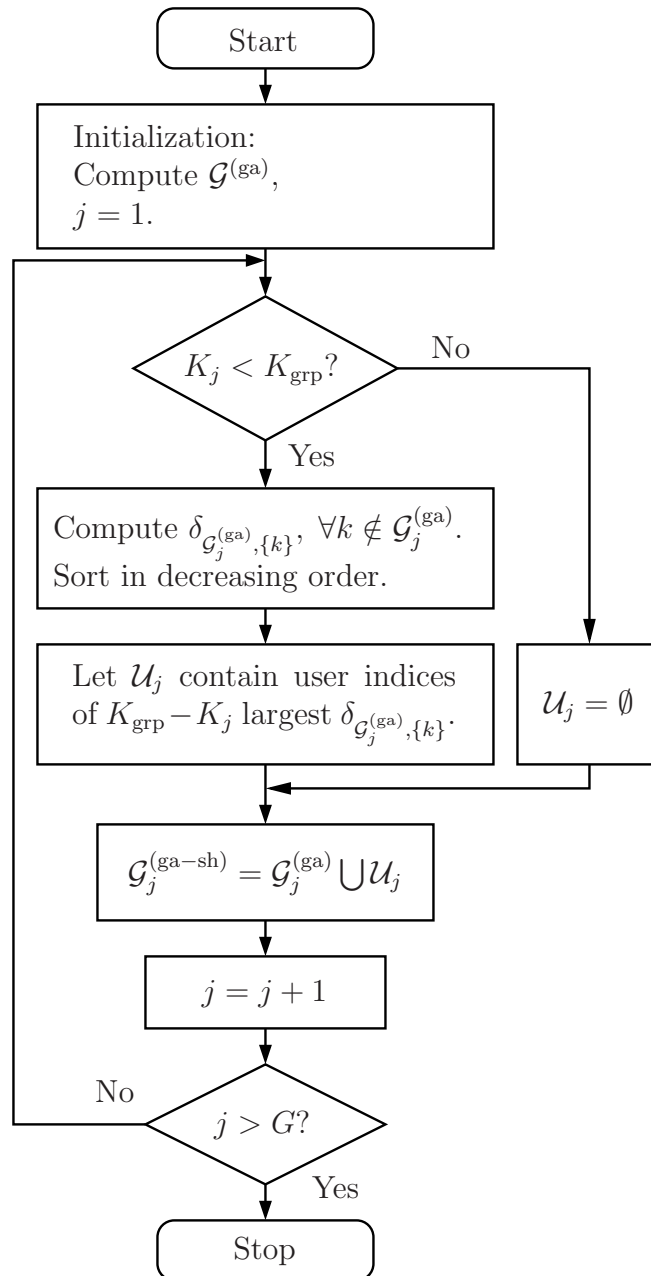


Fig. 5.2 Flow diagram for the grouping algorithm extension for user sharing.

function in (5.16) is used. The proposed metric is given by

$$J_{\text{sc},j}(\mathcal{G}_j) \triangleq \sum_{l=1}^{K_j} \left(\sum_{l'=1}^{K-K_j} |\mathbf{v}_{g_j,l}^H \mathbf{v}_{\bar{g}_j,l'}|^2 \right)^2, \quad (5.26)$$

where it can be observed from the definition in (5.16) that $J_{\text{sc}}(\mathcal{G}) = \sum_{j=1}^G \sqrt{J_{\text{sc},j}(\mathcal{G}_j)}$. Thus for the GRP-SIC and MS-GRP-SIC receivers, the group order metric in (5.26) is computed for each \mathcal{G}_j , $j = 1, \dots, G$, and the groups are re-ordered such that

$$J_{\text{sc},1}(\mathcal{G}_1) \leq J_{\text{sc},2}(\mathcal{G}_2) \leq \dots \leq J_{\text{sc},G}(\mathcal{G}_G), \quad (5.27)$$

so that the groups suffering the less with inter-group interference are detected first.

5.5 Complexity analysis

In this Section, the grouping algorithm complexity is analyzed in terms of number of operations (OPS) and number of complex floating points operations (CFLOPS). To do so, the number of operations and calculations is counted for each step of the algorithm using the same approach as in the previous two Chapters.

5.5.1 Mutually exclusive grouping

The mutually exclusive grouping algorithm of Section 5.3.2 consists essentially of three categories of operations; computation of the grouping criterion in (5.19) used in the proximity metric in (5.22), sorting of the proximity metrics, and the iterations. By using proper data structures, it is possible to compute the grouping criterion for all pairs of users and perform the sorting only once, which results in a substantial complexity reduction.

Notice that the cost for computing $\mathbf{v}_{k'}^H \mathbf{v}_k$, $\forall k', k$, is already taken into account in the computation of the GRP-STMUD matrix filter through the calculation of $\mathbf{V}^H \mathbf{V}$. Thus computing each criterion in (5.19) only requires 3 CFLOPS (2 multiplications and 1 division). The total cost in terms of CFLOPS for all $\binom{K_{\max}}{2} \approx K_{\max}^2/2$ pairs is therefore

$$C_{|\varrho_{k',k}|^2} \approx \frac{3K_{\max}^2}{2}. \quad (5.28)$$

Sorting an array of numbers is a computationally intensive task, with complexity varying between $\mathcal{O}(N_a \log N_a)$ to $\mathcal{O}(N_a^2)$ depending on the algorithm and the array to sort, where $\mathcal{O}(\cdot)$ denotes the *order* of complexity and N_a is the array dimension [Sed88,PTVF92]. For small N_a , it is preferable to use straight insertion and Shell's method, while for larger N_a it is preferable to use a quicksort [PTVF92]; the choice of the algorithm is therefore very application-specific. Assuming the worst-case scenario for sorting the array, the complexity in terms of CFLOPS is of the order of

$$C_{\text{sort}} \approx \mathcal{O}\left(\frac{K_{\max}^4}{4}\right), \quad (5.29)$$

where it is assumed that each comparison between the values in the array to sort requires a complex subtraction.

As illustrated by the flow diagram in Fig. 5.1, the grouping algorithm iteratively merges groups together at each iteration until it is no longer possible. The algorithm starts with K_{\max} groups and ends with G_{\max} groups for a total of $K_{\max} - G_{\max} + 1$ iterations. The main operation at each iteration consists of selecting from the sorted list the pair with the largest metric that can be merged. Combining the two groups then requires a single pass through the sorted list to remove the duplicate items resulting from the merge. Therefore,

no actual computations are needed at each iteration; only a single pass through the sorted list is required.

At iteration i , the number of groups is $K_{\max} - i + 1$, and the number of possible pair is $N_p(i) = \binom{K_{\max} - i + 1}{2}$. It can be shown that the total cost in terms of number of operations (OPS) can be expressed as

$$\mathcal{C}_{\text{iter}} = \sum_{i=1}^{K_{\max} - G_{\max} + 1} \mathcal{O}(N_p(i)) \quad (5.30)$$

$$\approx \sum_{i=1}^{K_{\max} - G_{\max} + 1} \mathcal{O}\left(\frac{(K_{\max} - i)^2}{2}\right) \quad (5.31)$$

$$\approx \mathcal{O}\left(\frac{K_{\max}^3}{6} - \frac{G_{\max}^3}{6}\right), \quad (5.32)$$

where the first and second approximations follow from the assumption that $K_{\max} \gg 1$ and $G_{\max} \gg 1$.

5.5.2 Non-mutually exclusive grouping

The non-mutually exclusive grouping algorithm, described in Section 5.3.3, proceeds group by group and fills the empty computing resources with shared users. For group j , there are K_j users in the group and $(K_{\max} - K_j)$ users outside of the group, resulting in a total of $K_j(K_{\max} - K_j)$ possible pairs of users to consider. The out-of-group users corresponding to the $K_{\text{grp}} - K_j$ largest metrics will be selected as shared users.

The proximity metric between users is already available from the mutually exclusive grouping algorithm and do not need to be re-computed. The core of the algorithm therefore resides in finding the $K_{\text{grp}} - K_j$ largest elements of a list of $K_j(K_{\max} - K_j)$ elements.

Notice that for the i^{th} shared user to choose, $i = 1, \dots, K_{\text{grp}} - K_j$, the list has dimension $(K_j + i - 1)(K_{\max} - (K_j + i - 1))$. Since the number of operation for each shared user consists

of comparing elements in the list to find the largest, the cost in CFLOPS for finding the i^{th} shared user in group j can be expressed as

$$\mathcal{C}_{\text{largest},j}(i) \approx (K_j + i - 1)(K_{\text{max}} - (K_j + i - 1)). \quad (5.33)$$

Thus the total cost for group j is given by

$$\mathcal{C}_{\text{sharing},j} = \sum_{i=1}^{K_{\text{grp}}-K_j} \mathcal{C}_{\text{largest},j}(i) \quad (5.34)$$

$$\begin{aligned} &\approx (K_{\text{grp}} - K_j) \left(K_j(K_{\text{max}} - K_j) \right. \\ &\quad \left. + \frac{(K_{\text{max}} - 2K_j)(K_{\text{grp}} - K_j)}{2} - \frac{(K_{\text{grp}} - K_j)^2}{3} \right) \end{aligned} \quad (5.35)$$

$$\approx (K_{\text{grp}} - K_j)K_jK_{\text{max}}, \quad (5.36)$$

where in the first approximation it is assumed that $(K_{\text{grp}} - K_j)(K_{\text{grp}} - K_j - 1) \approx (K_{\text{grp}} - K_j)^2$. For the second approximation, it is assumed that $(K_{\text{grp}} - K_j)$ is small compared to the other terms and that $K_{\text{max}} \gg K_j$.

5.5.3 Summary

The complexity of the mutually exclusive grouping algorithm and the additional cost for user sharing is summarized in Table 5.4. As it can be observed from the table, the com-

Operation	Label	Approximate cost
Computing $q_{k',k}, \forall k', k$	$\mathcal{C}_{ q_{k',k} ^2}$	$\frac{3K_{\text{max}}^2}{2}$ CFLOPS
Sorting $\frac{K_{\text{max}}^2}{2}$ elements	$\mathcal{C}_{\text{sort}}$	$\mathcal{O}\left(\frac{K_{\text{max}}^4}{4}\right)$ CFLOPS
Iterations $(K_{\text{max}} - G_{\text{max}} + 1)$	$\mathcal{C}_{\text{iter}}$	$\mathcal{O}\left(\frac{K_{\text{max}}^3}{6} - \frac{G_{\text{max}}^3}{6}\right)$ OPS
Sharing user (per shared group)	$\mathcal{C}_{\text{sharing},j}$	$(K_{\text{grp}} - K_j)K_jK_{\text{max}}$ CFLOPS

Table 5.4 Grouping algorithm complexity.

plexity of the algorithm is essentially dominated by the sorting operation. Fortunately, depending on the block size N , the cost associated to grouping may represent only a fraction of the total cost associated to the group-based receiver.

To demonstrate, consider the GRP-STMUD receiver. Assuming $G_{\max} = K_{\text{grp}} = \sqrt{K_{\max}}$, it can be shown using Table 3.6 and Table 5.4 that the ratio of the complexity associated to the grouping over the complexity of the GRP-STMUD receiver can be approximated as

$$\Gamma_{\text{complexity}} \approx \frac{\mathcal{O}(K_{\max}^2)}{8NM}. \quad (5.37)$$

In practice this ratio can be very small. For example for $K_{\max} = 16$, $N = 100$, and $M = 4$, the ratio in (5.37) takes value $\Gamma_{\text{complexity}} \approx \alpha 0.08$, where α is a sorting algorithm specific constant. In essence, α is the ratio of the actual complexity of the sorting algorithm over $K_{\max}^4/4$, the argument of the $\mathcal{O}(\cdot)$ operator in the expression for $\mathcal{C}_{\text{sort}}$ in Table 5.4. For relatively small α , this represent a small portion of the total complexity.

For small values of N , the portion of the complexity dedicated to the grouping algorithm may become very large. To simplify the sorting, it may become practical to perform a *pre-grouping* based on thresholding of the normalized cross-correlation in (5.19) first. This approach deserves to be studied further as it has the potential to significantly reduce the number of elements to sort in the algorithm resulting in a much smaller cost.

Chapter 6

Results

In this Chapter, computer simulation results showing the performance of the different receiver structures studied and the grouping algorithms developed in this work are shown. The experimental data is obtained through computer simulations under the MATLAB environment. The simulation parameters specific to the cellular system are chosen to follow in part the uplink of the TDD mode of UTRA, as specified by the 3rd Generation Partnership Project (3GPP) [3GPb, HKK⁺00].

The methodology used for the experiments is discussed next in Section 6.1. In Section 6.2, the BER performance of the new receiver structures proposed is compared to the full STMUD and traditional matched filter receivers. Results concerning the performance of the proposed grouping algorithm are shown in Section 6.3, and finally the complexity of the different receiver structures studied is compared in Section 6.4.

6.1 Methodology

As discussed above, the experimental scenarios are based on the UTRA/TDD specifications. The focus is on the uplink, however the proposed receiver structures can also be employed on the downlink at the mobile terminal. The UTRA/TDD mode uses WCDMA with short repeating channelization codes as basic transmission technology. The channelization codes are chosen from a set of orthogonal variable spreading factor (OVSF) codes of length $Q \in \{1, 2, 4, 8, 16\}$. The codes are then multiplied by a cell-specific spreading code to minimize the inter-cell interference. Within a cell, the OVSF codes lose their orthogonality due to the inevitable channel dispersion, resulting in MAI. Since the WCDMA codes are fixed for the duration of a data block, it becomes practical to use multiuser detection, because the filter coefficients can be re-used across several symbol intervals. Also, because of the relatively large MAI, MUD becomes essential for proper interference mitigation.

For most of the experiments, the spreading factor is fixed at $Q = 16$, however the receiver structures and grouping algorithms can also be used in multirate systems as well. This can be achieved by considering each symbol transmitted as originating from a different “virtual user” (see e.g.: [HL00]).

6.1.1 Space-time channel model

In the space-time model used in this work, each user has up to W time-differentiable paths arriving at the base station multi-antennas receiver. Each path arrives with a given direction-of-arrival (DOA), delay, amplitude and phase, which have to be specified. There exists several models for determining these parameters, including ray-tracing methods and statistical approaches [ECS⁺98, LR99]. Ray-tracing approaches provide a propagation model for a given environment with a specific geometry and well-defined obstacles, whereas

statistical models provide the propagation model statistics for a generalized environment, often parametrized by a small number of variables.

The proposed method for determining each differentiable path spatial parameters in this work is based on a statistical approach. For each channel realization and for each user, the DOA of the different paths are selected randomly. For user k , the main path has DOA $\theta_{k,1}$ uniformly distributed within the sector width of 120° , and the DOAs for the other $W - 1$ paths are uniformly distributed within $[\theta_{k,1} - \Delta\theta, \theta_{k,1} + \Delta\theta]$, with $\Delta\theta = 15^\circ$, thus

$$\theta_{k,l} \sim \begin{cases} U(0, 120^\circ) & l = 1 \\ U(\theta_{k,1} - \Delta\theta, \theta_{k,1} + \Delta\theta) & l = 2, \dots, W. \end{cases} \quad (6.1)$$

This approach is very similar to the geometrically based single bounce circular model (GBSBCM) [LR99], except that the delays here are assigned independently of the DOA. The time-delay, amplitude and phase of each path in the proposed model are assigned using one of the two following approaches:

Channel-1. Normalized power

In this approach, the *average* power of each path is normalized to 1. Except for the main path which has unit gain and zero phase, the complex amplitude of the other paths is random with a circular Gaussian distribution resulting in a Rayleigh distributed amplitude and a uniformly distributed phase over $[-\pi, \pi]$. The discrete time-delays are assigned linearly; the main path has no relative delay (synchronous), the second path has a relative delay of T_c , the third path has delay $2 T_c$, and so on up to the last path which has relative delay $(W - 1)T_c$.

Channel-2. Vehicular channel A

In this approach, the frequency selective channel consists of six paths with power-delay profile following the vehicular channel type A specifications [ETS98]. In the case of interest, the transmission rate is $1/T_c = 3.84$ MHz so that the total channel length in terms of T_c is $W = 11$. Table 6.1 shows the resulting channel relative delays and their relative power. For each of the

Relative delay (in units of T_c)	Relative power (in dB)
0	0.0
1	-1.0
3	-9.0
4	-10.0
7	-15.0
10	-20.0

Table 6.1 Vehicular channel A power-delay profile.

6 paths, the amplitude is chosen so that the power in Table 6.1 is respected, and the phase is random, uniformly distributed over $[-\pi, \pi]$.

Unless otherwise stated, the antenna array at the receiver has $M = 6$ elements. The geometry of the array consists of a standard linear array, i.e.: the elements form a straight line and are separated by half a carrier frequency wavelength [VT02]. Thus the channel realization consists of the set of DOAs, path delays, amplitudes and phases for each user.

For both approaches, ideal power control is assumed so that $P_k \triangleq \|\mathbf{v}_k\|^2 = 1, \forall k$, and the signal-to-noise ratio for each user becomes $\text{SNR} \equiv \text{SNR}_k = 1/\sigma^2, \forall k$. Finally, the channel coefficients are assumed to be known perfectly at the receiver.

6.1.2 Group-based receiver parameters

There are several hardware configurations possible for the group-based receiver structures proposed. Table 6.2 lists the two main receiver configurations used in the simulations.

Configuration	G_{\max}	K_{grp}	K_{\max}
Config-1	4	4	16
Config-2	16	1	16

Table 6.2 Receiver structure hardware configurations.

Notice that the two configurations provide the same number of computing resources as the maximum number of users allowed by the spreading factor, i.e.: $K_{\max} \equiv Q$. It is also possible to consider configurations with more computing resources than the maximum number of users (see [PC06c]); the extra computing resources available can be used for user sharing. Also note that configuration Config-2 is a degenerate case essentially corresponding to the matched filter and is used for comparison purposes.

6.1.3 BER measurements

To obtain the bit error rate measurement, the proposed receiver structures are implemented and simulated using the MATLAB software environment. The information symbols are transmitted using BPSK without channel coding. To maintain an acceptable simulation time, one of two approaches is used for each experiment:

BER-1. Fixed channel

In this approach, the channel realization is fixed for the duration of the simulation. The BER is obtained through Monte-Carlo simulations, by counting the number of errors at the output of the decision device. To obtain accurate measurements,

a large number of information symbols for each user is processed (from 10^6 to 10^8 depending on the experiment).

Using this approach, it is possible to use larger block sizes (in all cases $N = 50$), which allows to take into account the ISI in the measurements.

BER-2. Exact BER

In this approach, the *exact* BER is measured for a number of different channel realizations. This method allows to obtain an *ensemble* average of the receiver performance over different channel realization.

Since the exact BER measurement requires an averaging over all possible information symbol vector (see equation C.2 in Appendix C), it is computationally difficult to include large block sizes and thus ideal ISI cancellation is assumed.

6.2 BER performance comparison

6.2.1 GRP-STMUD-BF

The GRP-STMUD-BF receiver, introduced in Section 3.2.1, consists of a set of beamformers (one per user) followed by a matched filter and a linear MMSE MUD filter. Figure 6.1 shows the BER performance of the GRP-STMUD-BF receiver and compares it to the full STMUD receiver and the GRP-STMUD receiver. For the GRP-STMUD-BF, two different beamforming weight design strategies are considered, namely the conventional beamforming (Conv. BF) and the maximum power distortionless response (MPDR) [VT02]. In this particular experiment, the number of antenna elements is $M = 12$ resulting in a relatively small beamwidth, $K = 8$, $W = 1$ and $N = 1$. The CDMA code sequences in this experiment are random, but fixed for the length of the experiment. Similarly, the DOAs for each user

are fixed for the entire simulation time; Table 6.3 lists the DOA for each user along with the associated grouping. The BER is measured using the BER-1 approach.

User #	1	2	3	4	5	6	7	8
Group #	1	1	2	2	3	3	4	4
DOA (in deg.)	0	10	45	55	-25	-20	-45	-50

Table 6.3 User DOA and grouping

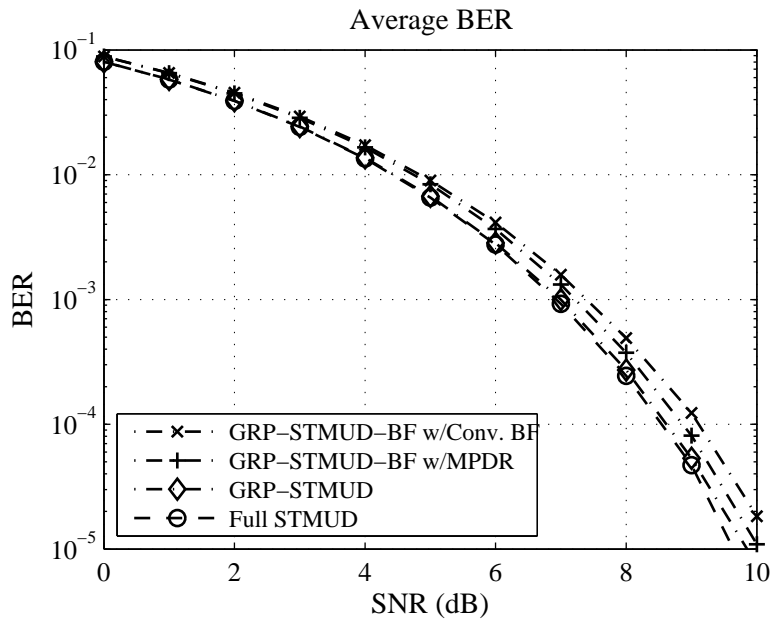


Fig. 6.1 GRP-STMUD-BF receiver average BER performance, with parameters $K = 8$, $M = 12$, $W = 1$, $N = 1$, and BER-1.

It can be easily observed from Fig. 6.1 that the BER difference between the receiver structures studied is small. Indeed, at BER of 10^{-4} , the corresponding differences in terms of input SNR between the full STMUD and GRP-STMUD-BF with MPDR and Conv. BF are approximately 0.2dB and 0.5dB, respectively and only 0.05dB with GRP-STMUD.

The GRP-STMUD and GRP-STMUD-BF receiver have essentially the same complexity (see Table 3.6), but the GRP-STMUD-BF receiver needs additional hardware to compute

the beamforming weights. In addition, the performance of the GRP-STMUD-BF is reduced by the beamforming operation, which in essence is a redundant non-invertible linear filtering operation. There is therefore no practical advantage of using the GRP-STMUD-BF receiver structure when compared to the GRP-STMUD receiver structure. These results have been published in [PC05].

6.2.2 GRP-STMUD with user sharing

In this experiment, the BER performance of the GRP-STMUD receiver structure with and without user sharing, as proposed in Chapter 3, is compared to the BER performance of the matched filter and the full STMUD receiver structures.

Figure 6.2 shows the BER averaged over the BER of all users in the system, for the different algorithms, with $K = 12$, $N = 50$, group-based hardware receiver structure Config-1, Channel-1 approach, and the BER is evaluated using the BER-1 technique with 10^8 symbols transmitted per user.

As expected, the full STMUD receiver of Section 2.5 performs better than the group-based techniques. Nonetheless, for this particular experiment, the GRP-STMUD receiver with sharing at a BER of 10^{-3} has a difference in SNR of approximately 0.85dB with the full STMUD. The different grouping approaches perform similarly well on average; indeed, at BER of 10^{-3} sharing (with selective of MMSE combining) reduces the difference in SNR with the full STMUD receiver to approximately 0.6dB.

The results shown in Fig. 6.2 indicate a marginal gain when sharing users. In general, only a handful of users will benefit significantly from sharing, an information lost in the averaging. Table 6.4 shows the grouping obtained using the proposed algorithms of Chapter 5 for this specific experiment. The difference (shown in boldface) between the mutually exclusive grouping and the non-mutually exclusive grouping is small; only 4 users in total

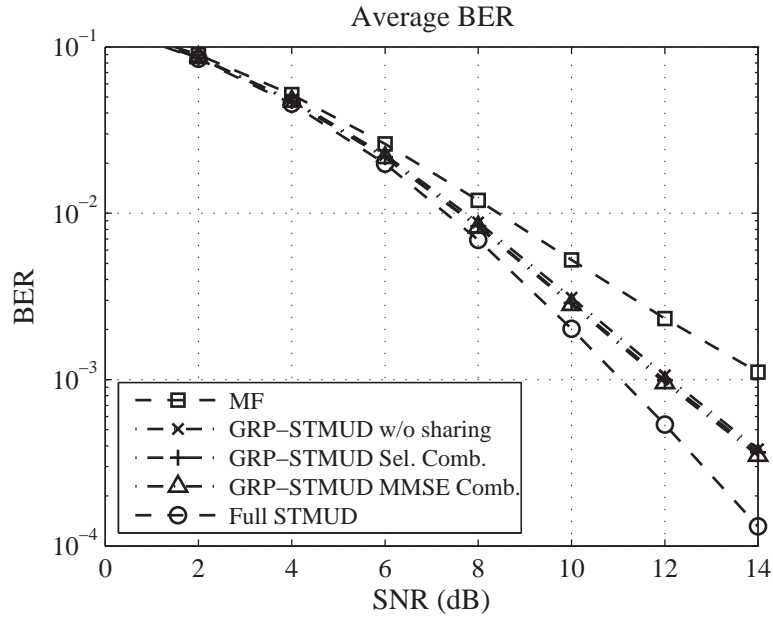


Fig. 6.2 GRP-STMUD receiver average BER performance for $K = 12$, $N = 50$, Config-1, Channel-1, and BER-1.

are shared. Two groups obtain one shared user, while one group obtains 2 shared users. This small difference in grouping as seen for most users explains the small impact of user sharing on the average BER.

Group #	Grouping	
	w/o sharing	with sharing
1	3,5,7,9	3,5,7,9
2	1,2,4	1,2,4, 11
3	10,11,12	8 ,10,11,12
4	6,8	5 ,6,8, 12

Table 6.4 Grouping obtained from experimental data.

The choice of shared users is essentially based on cross-correlation power. Figure 6.3 illustrates the cross-correlation power among the users for this specific experiment, in different shades of gray. As can be observed from Fig. 6.3 and Table 6.4, user #8, belonging

to group #4, is correlated with users # 5, 6, and 12. Group #4 is the smallest group and increases in size the most; it gets two shared users. Naturally, since user #6 is not strongly correlated with any other user than user #8, group #4 will benefit the most from sharing users #5 and 12.

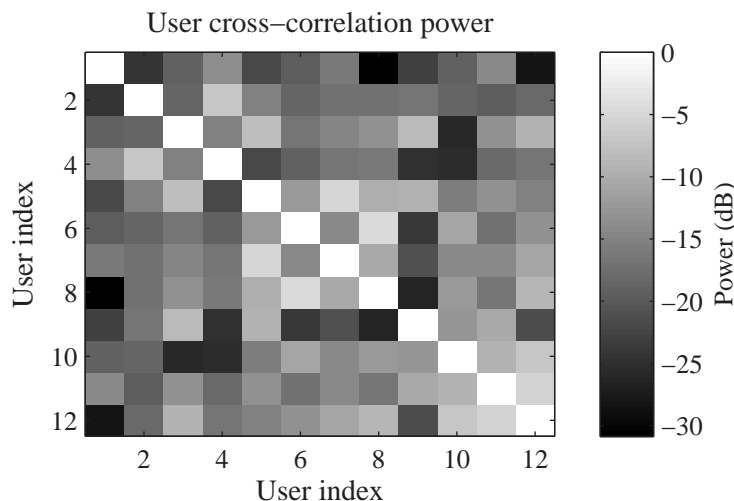


Fig. 6.3 User cross-correlation power.

Figure 6.4 shows the BER performance for user #8 alone. The gain obtained from user sharing is significant in this case; it can be measured at BER of 10^{-3} to be approximately 1.5dB for MMSE and selective combining; the two combining approaches perform similarly in this case. Note that similar behavior can be observed for user # 12 as well because it benefits from sharing user #8 in group #3; the results are not shown here for conciseness.

It can also be observed from Fig. 6.4 that for user #8, the BER performance of the GRP-STMUD receiver without sharing approaches the BER performance of the matched filter. This is a consequence of the mutually exclusive grouping; indeed, without sharing group #4 contains only 2 users and suffers from the IGI originating from the other 10 users.

Dominant users may have a significant effect on the performance of the different algo-

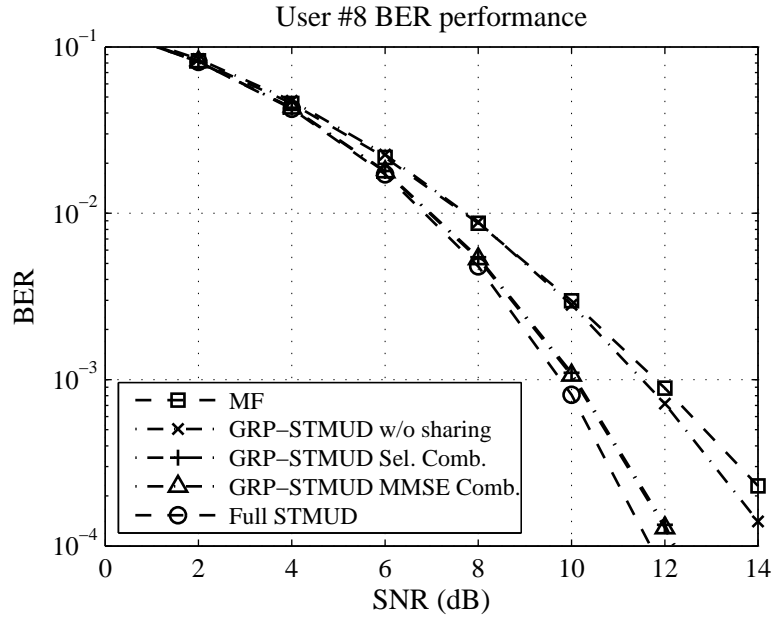


Fig. 6.4 GRP-STMUD receiver BER performance for user # 8, $N = 50$, Config-1, Channel-1, and BER-1.

rithms. To demonstrate, the received signal for one user is increased from 0dB to 20dB of excess power. The SNR for the other, non-dominant users is fixed to 10dB.

The average BER for the non-dominant users is shown in Fig. 6.5, where the BER-2 approach is used to obtain the results. It can be observed that the BER performance of the GRP-STMUD without user sharing suffers considerably from the IGI caused by the presence of a dominant user. Since in this particular case $K_{\text{extra}} \geq G_{\text{max}} - 1$, the dominant user can be shared essentially by all the other groups, resulting in a much improved performance for the GRP-STMUD with MMSE and selective combining. Sharing thus provides additional robustness to imperfect power control in group-based receivers. Note that in this context, the users with excess power are most likely to be shared. Since those shared users already have a strong signal, MMSE combining does not improve the performance further; selective combining is sufficient.

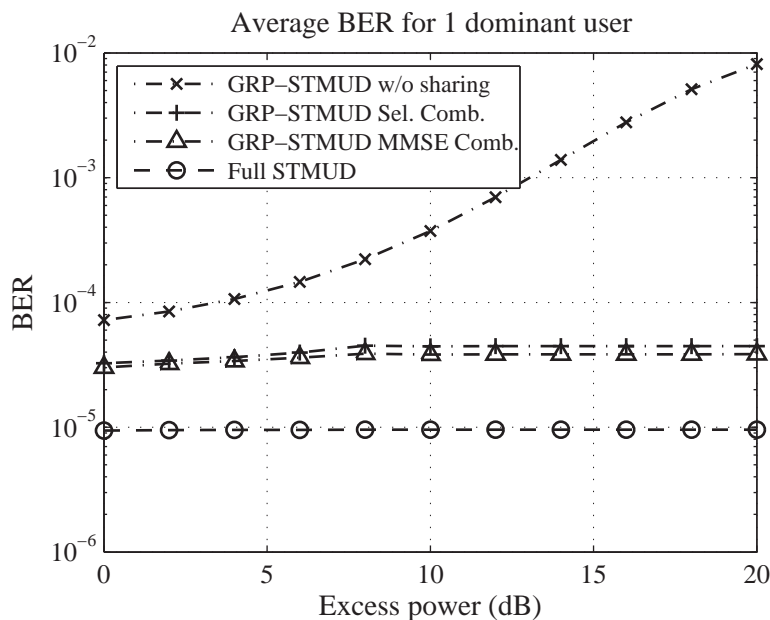


Fig. 6.5 GRP-STMUD receiver average BER performance for the non-dominant users at SNR=10dB versus excess power for the single dominant user.

These results have been published in [PC07], and additional results on the GRP-STMUD comparing different hardware configurations have also been published in [PC06c].

6.2.3 Iterative and multistage receiver structures

MS-GRP-SIC

In this experiment, the GRP-SIC and MS-GRP-SIC receiver structures described in Section 4.2 are studied. The BER is measured using the BER-1 approach with $N = 50$ and over 10^6 symbols transmitted using the Channel-2 approach. The receiver structure has configuration Config-1, and the *loading factor* ($LF \triangleq K/K_{\max}$) is $LF = 80\%$ (i.e.: for a spreading factor of $Q = 16$, this corresponds to $K = 13$).

Figure 6.6 shows the BER for the different receiver structures, averaged over the BER of all $K = 13$ users. In this experiment, the GRP-STMUD w/o IGI receiver structure

corresponds to the GRP-STMUD receiver structure of Section 3.2.2 but using the simplified linear filters in (4.15) instead of the optimal filters in (3.39). The simplified filters are essentially designed assuming no IGI. An improvement of approximately 1.8dB at BER of 10^{-3} over the MF can be observed when using the GRP-STMUD w/o IGI receiver.

It can also be observed that the GRP-SIC receiver, which uses hard decision for interference cancellation, and MS-GRP-SIC receiver with a single stage (MS-GRP-SIC 1) provide essentially the same BER performance, which is slightly better than the BER performance of the GRP-STMUD receiver structure without IGI. When using 2 stages (MS-GRP-SIC 2), the difference at BER of 10^{-3} between MS-GRP-SIC and the full STMUD reduces to a negligible 0.2dB.

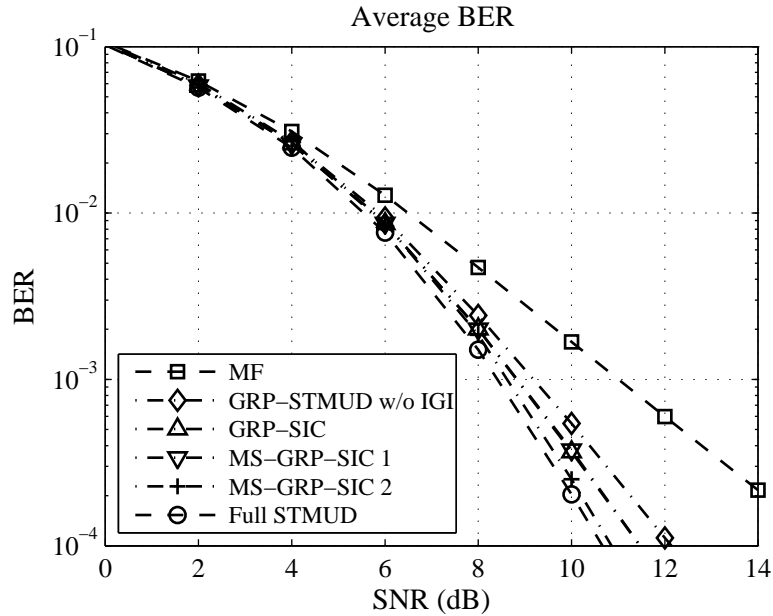


Fig. 6.6 GRP-SIC and MS-GRP-SIC BER performance.

Figure 6.7 shows the average BER for the MS-GRP-SIC receiver at SNR=10dB as the number of iterations or stages increases. As it can be observed, only a few SIC iterations are necessary for the receiver to converge, confirming what has already been observed

in Fig. 6.6. Also, as noted in [JR98], the BER converges slowly to the decorrelator but performs slightly better in the first few iterations after the first stage. The convergence rate depends on several parameters and in general, the grouping and order of cancellation can have a significant effect [JR98]. The above results on the MS-GRP-SIC receiver structures have been published in [PC06a].

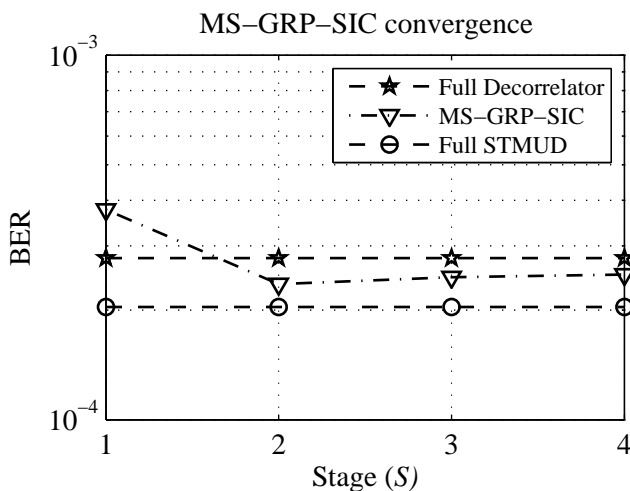


Fig. 6.7 MS-GRP-SIC BER convergence.

MS-GRP-PIC

In this experiment, the BER is measured using the BER-2 technique, averaged over 30 realizations of the channel, obtained using the Channel-2 approach. Using this methodology, the performance of the proposed receiver structure can be studied for an ensemble of channel realizations.

Figure 6.8 shows the BER performance averaged over the different channel realizations and over the BER of all users for the MF receiver, the proposed MS-GRP-PIC receiver with $S = 1, 2$ and 3, and the full STMUD receiver. The receiver hardware is assumed to have $M = 4$ antenna elements and grouping configuration Config-1. The loading factor in

this experiment is $LF = 75\%$ (i.e. $K = 12$ users).

As expected, the MF yields the poorest BER performance while the full STMUD provides the best BER performance. It can be observed that on average, the proposed receiver requires in this case only 2 stages to provide essentially the same BER performance as the full STMUD. Note that with only $S = 1$ the BER performance also is very close to the BER performance of the full STMUD, especially at lower SNR where the interference is no longer the dominant source of signal degradation.

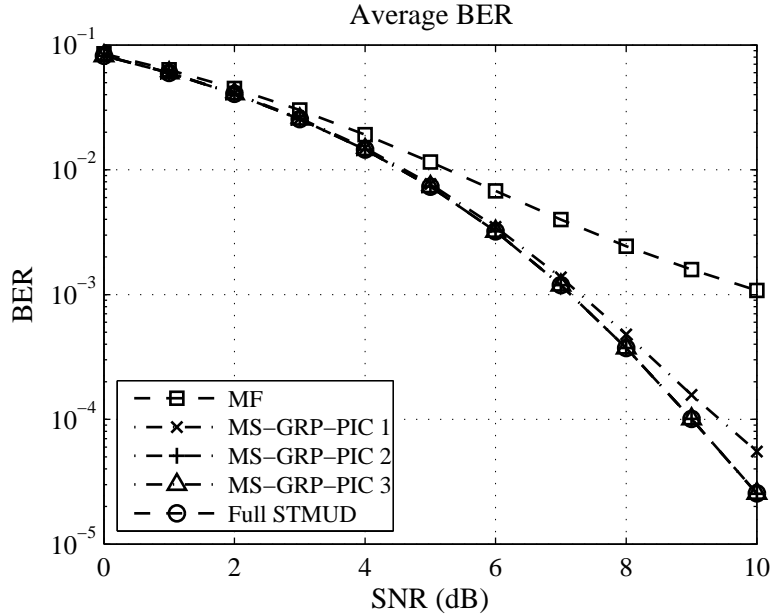


Fig. 6.8 MS-GRP-PIC BER performance comparison for moderate interference conditions averaged over 30 scenarios with $G_{\max} = 4$, $K_{\max} = 4$, $LF = 75\%$, $M = 4$, and grouping configuration Config-1.

For low SIR cases, which happens for instance when the loading factor is large or when the number of antenna elements is small (or a combination of the two) the MS-GRP-PIC may not converge and weighting is required, as discussed in Section 4.3.3. Figure 6.9 shows the BER convergence for the MS-GRP-PIC receiver with weighting as the number of stages increases, averaged over the different scenarios and over all users for different

weighting strategies. As it can be observed in this low SIR scenario ($M = 1$ and Grouping config. #2), the MS-GRP-PIC receiver with Chebyshev weighting converges to the full STMUD solution while the MS-GRP-PIC receiver with no weighting does not. It can also be noted that the estimated Chebyshev weights obtained using (4.82) and (4.83) perform very well when compared to the ideal case.

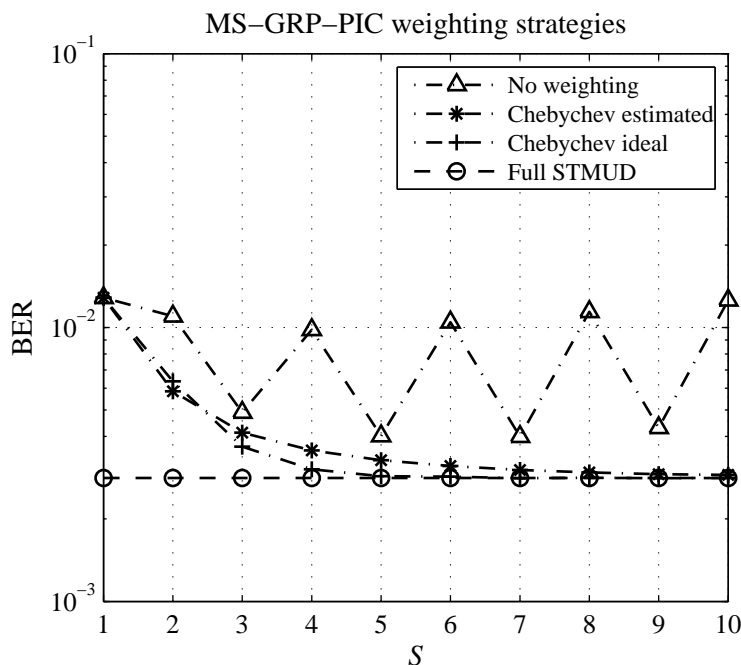


Fig. 6.9 MS-GRP-PIC weighting strategies for $M = 1$, $LF = 75\%$, $SNR=8dB$, and Grouping config. #2.

Figure 6.10 shows the convergence in BER as the number of stages S is increased for the MS-GRP-PIC receiver with Chebyshev weighting using estimated coefficients. The results are averaged over the different scenarios and over all users, for different grouping configurations for both $M = 1$ and $M = 4$ at a fixed SNR of 8dB. For $M = 4$, the convergence is relatively fast i.e.: approximately 2 stages for the proposed MS-GRP-PIC receiver with Chebyshev weighting for grouping configuration #1 and 5 stages for grouping configuration #2. Note that similar results have been obtained for $M = 8$, but for conciseness they are

not shown here. For the stronger interference case with $M = 1$, the proposed approach with grouping configuration #1 converges in 3 stages.

It is interesting to note in Figure 6.10 that for both $M = 1$ and $M = 4$, the convergence when using a random grouping (RG) is significantly slower than when using the grouping algorithm in [PC07]. In both cases the convergence of the grouping configuration #1 with random grouping approaches the convergence of the grouping configuration #2, which essentially does not benefit from grouping at all. The parameters for estimating the

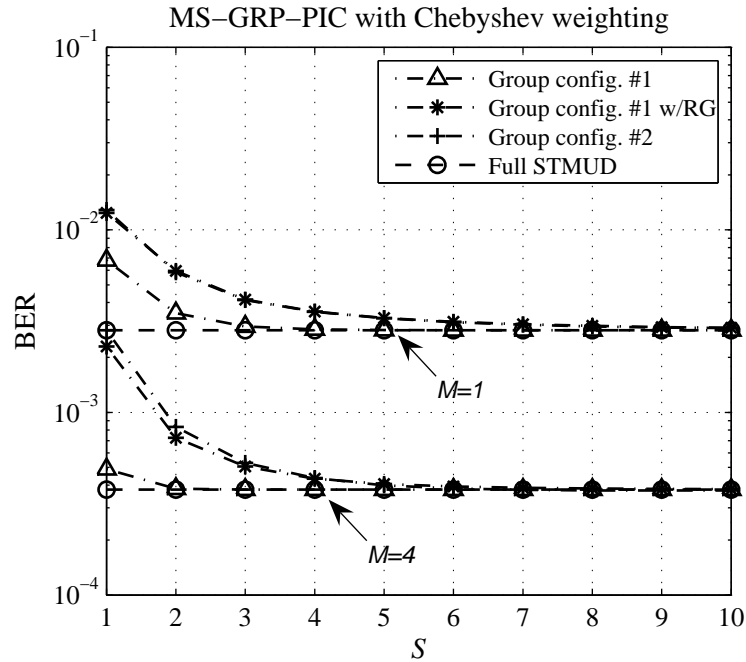


Fig. 6.10 BER convergence of the MS-GRP-PIC receiver with Chebyshev weighting using estimated coefficients for different grouping configuration at SNR=8dB with $LF = 75\%$.

Chebyshev weighting coefficients using (4.82) for the results shown in figures 6.9 and 6.10 are given in Table 6.5.

As discussed above, sharing usually benefits only a few users depending on the scenario, and this is mainly due to the low percentage of users actually being shared. To illustrate,

Group config.	Param.	M	
		1	4
#1	a	0.2130	0.0701
	b	0.6606	0.6327
#2	a	0.0305	0.0710
	b	0.6625	0.6412

Table 6.5 Chebyshev weighting coefficients estimation parameters for $LF = 75\%$ and $\text{SNR}=8\text{dB}$.

consider Config-1 with $LF = 70\%$ (corresponding to $K = 11$ users). Because there are 5 extra computing resources available here ($G_{\max}K_{\max} - K$) for sharing, and since the maximum group size is $K_{\max} = 4$, the conventional grouping algorithm (with no sharing) will usually assign 2 full groups and 1 group with 3 users. This leaves space to essentially 1 shared user in that group and none for the others. Therefore in general only a few users (e.g. 3 in this case) can actually benefit from user sharing.

Figure 6.11 shows the empirical cumulative distribution function (CDF) of the SNR gain, measured at $\text{BER} = 10^{-3}$, from exploiting user sharing under the presence of 20% of the users with excess power of 0dB, 10dB, and 20dB. Only the users that can benefit from sharing, i.e. the users belonging to an extended group, are considered in Fig. 6.11. To obtain a relatively smooth CDF, the data is accumulated this time over 100 different channel realizations, using the Channel-2 approach.

As it can be observed, a large number of those users benefit significantly from sharing at the first stage, particularly in the presence of strong interferers: at 20dB of excess power, approximately 25% of the users considered obtain an improvement over 0.5dB in SNR. The gain in SNR is less important at the following stages.

User sharing can also help the convergence of the users in extended groups. Figure 6.12 shows the BER convergence for the MS-GRP-PIC with and without user sharing. The av-

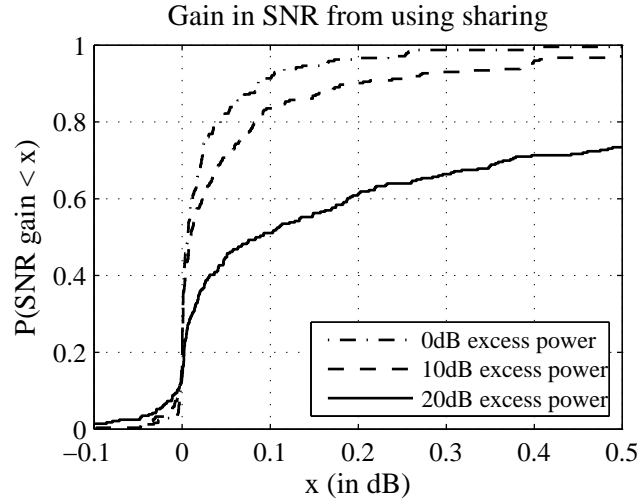


Fig. 6.11 CDF of SNR gain for the first stage of the MS-GRP-PIC receiver when using sharing at $\text{BER}=10^{-3}$, for $G_{\max} = 4$, $K_{\max} = 4$, $LF = 70\%$, $M = 4$.

erage here is performed over the BER corresponding to users belonging to extended groups only. The same experiment is repeated with no user sharing for comparison purposes. The case considered consists of a relatively strong interference scenario with $M = 1$, $LF = 75\%$, and using hardware configuration Config-1. The results show the advantage of using sharing when possible: it takes on average 4 stages to converge when user sharing is enabled, while it takes over 6 stages otherwise.

Part of these results on the MS-GRP-PIC receiver structure have been published in [PC06b]. In addition, the work on the MS-GRP-PIC receiver with user sharing and weighting will appear in the IEEE Transactions on Vehicular Technology in 2008.

6.3 Grouping algorithms

The purpose of this experiment is to validate the simplified cost function of Section 5.2, and at the same time show that the proposed grouping algorithms perform well. The experiment

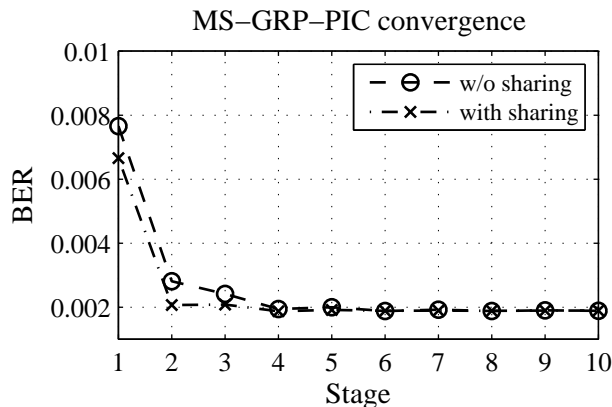


Fig. 6.12 BER convergence for MS-GRP-PIC for users in extended groups for $LF = 75\%$, $M = 1$, Config-1, and $\text{SNR} = 8\text{dB}$.

consists of comparing the MSE of the different optimal and sub-optimal groupings for a large number of channel realizations.

The experiment proceeds by finding the different groupings and measuring their respective MSE using $J_{\text{MSE}}(\mathcal{G})$ defined in (5.3). The optimal grouping with respect to the MSE found using an exhaustive search over all possible grouping is used as a reference. Recall that the optimal grouping with respect to the MSE is given by $\mathcal{G}^{(o)}$ in (5.4) and the corresponding MSE is given by

$$J_{\text{MSE}}^o \equiv J_{\text{MSE}}(\mathcal{G}^{(o)}). \quad (6.2)$$

Three grouping algorithms are considered in this experiment. The first algorithm consists of finding the optimal grouping with respect to the simplified cost function in (5.16) using an exhaustive search. The second algorithm consists of the proposed approach for mutually exclusive grouping, as described in Section 5.3.2. The third approach is the grouping algorithm with user sharing, as described in Section 5.3.3. Recall that the actual grouping for each of these approaches is given by $\mathcal{G}^{(\text{sc})}$, $\mathcal{G}^{(\text{ga})}$, and $\mathcal{G}^{(\text{ga-sh})}$, respectively,

and the corresponding MSE is given by

$$J_{\text{MSE}}^{(\text{sc})} \equiv J_{\text{MSE}}(\mathcal{G}^{(\text{sc})}) \quad (6.3)$$

$$J_{\text{MSE}}^{(\text{ga})} \equiv J_{\text{MSE}}(\mathcal{G}^{(\text{ga})}) \quad (6.4)$$

$$J_{\text{MSE}}^{(\text{ga-sh})} \equiv J_{\text{MSE}}(\mathcal{G}^{(\text{ga-sh})}), \quad (6.5)$$

respectively. Note that with user sharing, the MSE is also calculated using (5.3) by taking into considerations only the conventional users for each group.

This experiment is repeated 300 times for sampling different correlation matrices corresponding to different user positions and channel conditions. The normalized difference in MSE for the three different grouping is calculated for each channel realization and is given by

$$\Delta_{\text{sc}} \triangleq \frac{J_{\text{MSE}}^{(\text{sc})} - J_{\text{MSE}}^{\text{o}}}{J_{\text{MSE}}^{\text{o}}} \quad (6.6)$$

$$\Delta_{\text{ga}} \triangleq \frac{J_{\text{MSE}}^{(\text{ga})} - J_{\text{MSE}}^{\text{o}}}{J_{\text{MSE}}^{\text{o}}} \quad (6.7)$$

$$\Delta_{\text{ga-sh}} \triangleq \frac{J_{\text{MSE}}^{(\text{ga-sh})} - J_{\text{MSE}}^{\text{o}}}{J_{\text{MSE}}^{\text{o}}}, \quad (6.8)$$

respectively. In practice it is highly desirable to have a small Δ_{ga} and $\Delta_{\text{ga-sh}}$; this would indicate that the grouping obtained provides a MSE which is close to the minimum MSE achievable. Similarly, a small Δ_{sc} indicates that the choice of simplified cost function in (5.16) provides similar results to the more complex MSE criterion.

Columns in Table 6.6 show the proportion of grouping scenarios that resulted in a difference in normalized MSE, less than or equal to 1%, and 2%, respectively. For this particular experiment, the SNR is fixed at 10dB, the receiver has hardware configuration

Config-1, and the channel model is Channel-1. The results essentially indicate that a very

t	$P(\Delta_{sc} \leq t)$	$P(\Delta_{ga} \leq t)$	$P(\Delta_{ga-sh} \leq t)$
0.01	0.93	0.90	0.90
0.02	0.99	0.97	0.97

Table 6.6 Statistics on the grouping algorithm performance at SNR=10dB, for hardware configuration Config-1 and under channel model Channel-1.

large proportion of the grouping obtained using the simplified cost function lead to a MSE very close to the optimal one, therefore justifying the use of the simplified cost function and the associated cost criterion. Moreover, 97% of the grouping obtained using the proposed grouping algorithms of Section 5.3 result in a MSE no more than 2% away from the optimal one. Furthermore, by linearizing the MSE with respect to the noise power, it can be shown that such a difference in MSE is equivalent to a loss in SNR of approximately 0.1dB. This is a very good performance considering the computational complexity of the algorithm compared to the computational complexity of an exhaustive search.

Figure 6.13 shows the CDF for the 300 channel realizations for Δ_{sc} , Δ_{ga} , and Δ_{ga-sh} . It can be observed that the three grouping approaches have a very small normalized MSE difference (up to approximately 0.04) for most cases. In addition, for approximately 12% of the cases, the grouping algorithm with user sharing actually leads to a *smaller* MSE than the optimal grouping with respect to MSE. This is explained by the fact that only mutually exclusive groupings are considered in the search for the optimal grouping with respect to the MSE.

6.4 Complexity comparison

For any practical receiver structure, it is essential to determine the relative implementation complexity. Using the results of Sections 3.4 and 4.4, the complexity of the GRP-STMUD-

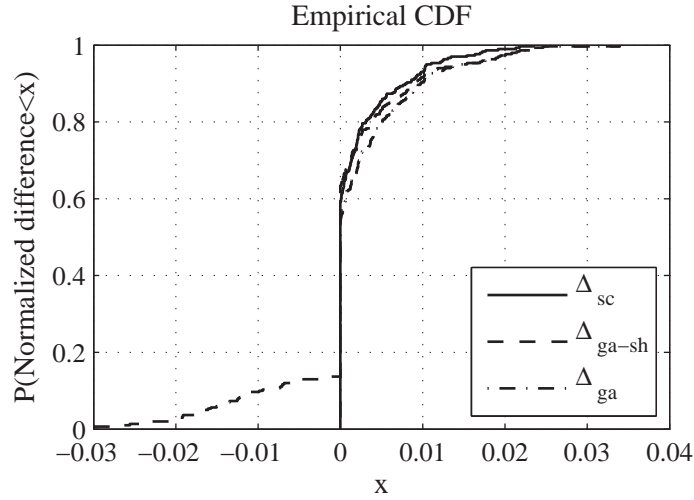


Fig. 6.13 Empirical CDF for the normalized MSE difference with respect to the optimal MSE.

BF, the GRP-STMUD and the MS-GRP-PIC receiver structures is compared to the complexity of the full STMUD receiver. Note that since the MS-GRP-SIC receiver is slightly more complex than the MS-GRP-PIC receiver (see e.g. Table 4.5), and since it converges to the decorrelator and not to the full STMUD, it is not considered in this Section.

Figure 6.14 shows the complexity in terms of CFLOPS for the GRP-STMUD, GRP-STMUD-BF and the full STMUD receivers. The complexity of each category (beamforming (BF), matched filter (MF), intermediate calculations (Icalc.), linear system solution (LSS), and post processing (Post)) is shown in a different shade of gray and the total length of each bar indicates the total complexity. To properly evaluate the hardware complexity, the worse-case scenario is considered so that all computing resources are assumed to be fully utilized ($K = Q$, $K_j = K_{\text{grp}} \forall j$, and $G = G_{\text{max}}$). In the scenario considered, $N = 50$, $Q = 16$, $W = 6$, $M = 6$, and the receiver configuration is Config-1.

It can be observed from Fig. 6.14 that it is computationally advantageous to use group-based approaches. As expected, most of the computational savings come from the LSS

category. It can also be observed that the GRP-STMUD-BF receiver is much more costly than the GRP-STMUD receiver, mainly due to the beamforming step and the higher overhead¹.

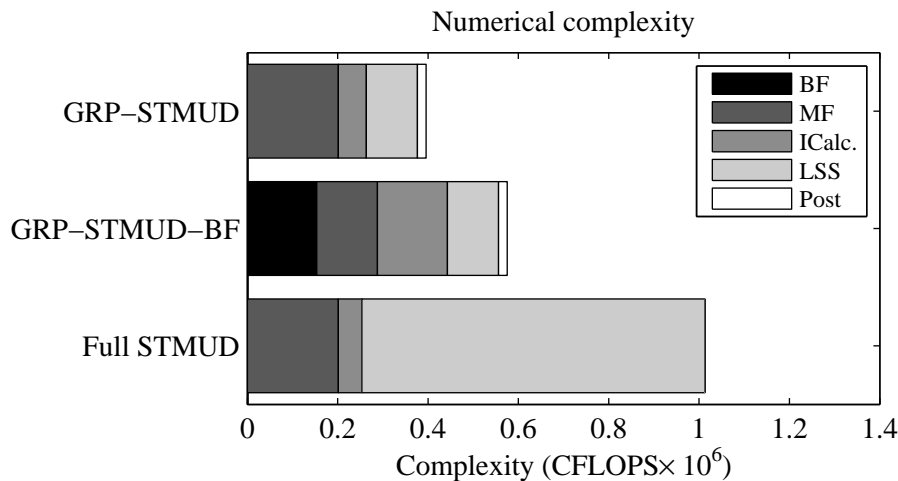


Fig. 6.14 Complexity comparison for group-based receivers for $N = 50$, $K = Q = 16$, $W = 6$, $M = 6$, and receiver configuration Config-1.

In Fig. 6.15 the complexity of the MS-GRP-PIC receiver with $S = 2$ is compared to the complexity of the GRP-STMUD and full STMUD receivers. The cost of matched filtering is the same for the three approaches, and it is not included in the Figure.

It can be observed that both the GRP-STMUD receiver and the MS-GRP-PIC receiver with $S = 2$ have approximately the same complexity. In particular for the MS-GRP-PIC receiver with $S = 2$, it was shown (see Fig. 6.10) that its BER performance is similar to the BER performance of the full STMUD. Yet according to Fig. 6.15, it only requires approximately one quarter of the full STMUD complexity.

Table 6.7 shows the complexity of the different parts of the computations of the solution for both full STMUD and MS-GRP-PIC receivers for different combinations of K_{\max} , G_{\max} and K_{grp} for $N = 1$. The common operations, such as matched filtering, are not listed in

¹The cost of computing the beamforming weights is not included in the calculations.

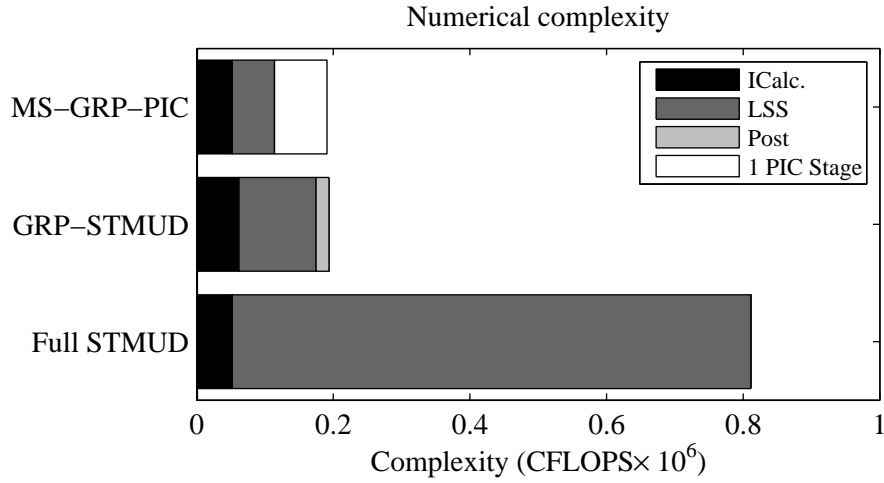


Fig. 6.15 Complexity comparison for multistage receivers for $N = 50$, $K = Q = 16$, $W = 6$, $M = 6$, and receiver configuration Config-1.

the table.

The complexity gain varies from one scenario to the next. Considering the case $G_{\max} = K_{\text{grp}} = \sqrt{K_{\max}}$, it can be shown that the ratio of the MS-GRP-PIC complexity over the full STMUD complexity approaches

$$\Gamma_{\text{complexity}} = \frac{1 + 9/5(S - 1)}{K_{\max}} \quad (6.9)$$

for large K_{\max} . The table shows that the reduction in complexity can be significant: for the smallest value of K_{\max} considered, the MS-GRP-PIC has approximately one fifth the complexity of the full STMUD. The complexity reduction is even more significant for larger values of K_{\max} .

If the channel is coherent for a longer period than the block size, then it is advantageous to re-use the Cholesky factors. Let N_c be the *re-use factor*, i.e. the number of consecutive blocks for which the channel and Cholesky factors remain constant. Using the results from

Receiver	Operation	Cost for $(K_{\max}, G_{\max}, K_{\text{grp}})$		
		(16,4,4)	(64,8,8)	(256,16,16)
Full STMUD	Cholesky	1.37×10^4	8.74×10^5	5.59×10^7
	Back sub.	1.54×10^3	2.46×10^4	3.93×10^5
	Total (C_A)	1.52×10^4	8.98×10^5	5.63×10^7
MS-GRP-PIC	Cholesky	8.53×10^2	1.37×10^4	2.18×10^5
	Back sub.	3.84×10^2	3.07×10^3	2.46×10^4
	PIC	1.54×10^3	2.46×10^4	3.93×10^5
	Total (C_B)	2.77×10^3	4.13×10^4	6.36×10^5
Ratio of complexity	$\Gamma = C_B/C_A$	0.18	0.05	0.01
Largest N_c	See eq. (6.12)	33	280	2267

Table 6.7 Complexity comparison of the MS-GRP-PIC receiver with $S = 2$ and the full STMUD, for $N = 1$.

Table 3.2, the cost for the linear system solution for the Full STMUD can be expressed as

$$C_A = \frac{10}{3}NK_{\max}^3 + 6N_cNK_{\max}^2, \quad (6.10)$$

where the first term is the cost associated to computing the Cholesky factorization, and the second term is the cost associated to computing the backsubstitution for the N_c blocks. Considering the case where $G = K_{\text{grp}} = \sqrt{K_{\max}}$, the cost for solving the linear system solution and executing the interference cancellation for the MS-GRP-PIC receiver can be expressed using the terms in (4.89) as

$$C_B = \frac{10}{3}NK_{\max}^2 + 6N_cNK_{\max} \left[\sqrt{K_{\max}} + (S-1)K_{\max} \right]. \quad (6.11)$$

Using (6.10) and (6.11), it can be shown that for large K , it is always computationally

advantageous to use the MS-GRP-PIC receiver when

$$N_c < \frac{5K_{\max}^2}{9(\sqrt{K_{\max}} + (S - 2)K_{\max})}, \quad S \geq 2. \quad (6.12)$$

The maximum N_c for which it is computationally advantageous to use the proposed MS-GRP-PIC receiver structure over the full STMUD receiver is shown in Table 6.7 for each scenario considered. As it can be seen, when the channel varies, the MS-GRP-PIC receiver is computationally advantageous, especially for systems with larger K_{\max} .

Chapter 7

Summary and conclusion

7.1 Summary of the work

The capacity of DS-CDMA systems is limited by multiple-access interference. To take advantage of the available spectrum, it is essential to mitigate this interference. Fortunately, there exists several approaches to interference reduction, including beamforming and multiuser detection. Beamforming requires an antenna array at the receiver and dedicated hardware for spatial filtering, and multiuser detection necessitates complex signal processing hardware for joint detection. Optimal multiuser detection is very complex for real-time processing. As a result, sub-optimal linear approaches such as MMSE MUD filtering become a practical alternative. Group-based approaches are also attractive since they provide a means for performance/complexity trade-off. In this work, reduced-complexity group-based receiver structures for space-time linear multiuser detection were studied in the context of Third Generation cellular systems based on short-code WCDMA technology.

Most existing space-time group-based MUD receiver use beamforming to separate the users in space so that the interference among groups is reduced. This concept lead to

the GRP-STMUD-BF receiver structure, that employs beamforming before linear MUD filtering. This approach requires one beamforming unit per user, where each unit not only carries out spatial filtering but also computes the actual beamforming weights. Moreover, since beamforming actually reduces the observation space dimension independently of the MUD unit, the beamforming unit output may not provide the best samples to the MUD filter.

By analyzing the structure of the GRP-STMUD-BF receiver, it was found that beamforming is redundant in this context. This observation motivated the development of the proposed GRP-STMUD receiver, that does not require a set of independent beamforming units. Rather, space-time matched filtering provides the set of sufficient statistics to the linear group-based multiuser detection filters.

A practical receiver is limited by hardware restrictions; it is reasonable to assume that a practical group-based receiver would contain a limited number of groups, each supporting a maximum number of users. In this context, when the number of users in a group is smaller than the maximum, there are unused computing resources available. Thus by introducing non-mutually exclusive grouping, it was shown that it is possible to improve the group-based receiver performance while exploiting the hardware resources to its full potential. This new and innovative concept is referred to as user sharing. With user sharing, a soft estimate for the shared user is available at the output of each group-based MUD unit that share the user. While it is possible to optimally combine the different outputs with a MMSE filter, the results have demonstrated that selective combining performs just as well at no additional cost in complexity. It was also shown that the user sharing approach reduces the impact of IGI, in particular in the presence of users with excess power causing the near-far effect.

To further reduce the IGI, and at the same time reduce the complexity of the filter

design, new multistage receiver structures were proposed. It was shown that the MS-GRP-SIC receiver converges as the number of stages increases to the decorrelator, whereas the new MS-GRP-PIC receiver with or without user sharing converges to the MMSE receiver. The multistage approaches in this case eliminate the IGI as the number of stages increases. Moreover, employing user sharing in the proposed group-based multistage receiver structures can not only make a system converge, but it can also improve the convergence rate.

The user grouping is a key factor in the performance of the group-based receiver structures. Most existing grouping algorithms for space-time group-based MUD are based on thresholding and cannot be applied to practical implementations with limited hardware resources. In this work, a mutually-exclusive grouping algorithm for practical system implementation was proposed. The new algorithm is based on a cost criterion that is justified both mathematically and experimentally. A new grouping algorithm for user sharing was also proposed. The results demonstrated that the proposed algorithms perform very close in terms of MSE to the optimal grouping MSE, at a fraction of the computational cost.

To complete the study, the complexity of the proposed receiver structures and the grouping algorithms were derived and analyzed; an essential aspect missing in the existing literature. The results clearly demonstrated the computational advantage of the group-based approaches. In particular, it is shown that the MS-GRP-PIC approach with two stages provides essentially the same BER performance as the full STMUD BER performance, for approximately one quarter of the computational cost.

7.2 Concluding remarks

This work is a thorough study of group-based approach to linear block multiuser detection. New ideas and concepts are introduced such as user sharing and group-based multiuser

detection in a limited resource hardware receiver. The research work was carried out in the general context of Third Generation cellular systems, yet the scope of application of the group-based approach and the innovative ideas presented is much larger and can encompass many non-orthogonal multiuser systems.

Of particular interest, future cellular systems are likely to be based on orthogonal frequency division multiple access (OFDMA). While on the downlink the orthogonality among sub-carriers is guaranteed, on the uplink the orthogonality is lost due to carrier frequency offsets (CFO) among the different mobiles. This creates multiple access interference that can be mitigated efficiently at a low cost using the new concepts presented in this work.

The grouping approach and sharing concept developed in this work can certainly be applied to other fields of engineering and sciences as well. The possibilities in this respect are endless.

7.3 Future work

Promising avenues for research have been identified during the development of this Thesis. The following deserve particular attention:

- i) *Reduced-complexity grouping algorithm.* To reduce the complexity of the grouping algorithm, it is essential to reduce the number of elements to sort. As discussed in Chapter 5, this can be achieved with a pre-grouping based on a simple thresholding.
- ii) *Adding groups.* It was noted in Chapter 5 that it is possible for the proposed grouping algorithm to leave some groups empty. The concept of user sharing could be pushed further by allowing new groups to be created to improve the detection.
- iii) *Performance/complexity trade-off function.* One of the main strengths of group-based

receiver structures is the ability to provide an efficient trade-off between performance and complexity. To further help hardware designers and system engineers in the decision making process, it would be highly desirable to derive the performance directly in terms of the complexity for a family of group-based receiver structures.

- iv) *Adaptive grouping and filtering.* Practical cellular systems are extremely dynamic by nature; mobile users move in and out of cells, communications are initiated and terminated. As such, it becomes of interest to research and develop low-complexity adaptive algorithms for both grouping and group-based filter design.
- v) *Hardware implementation.* To further validate the findings and the new concepts introduced in this work, a hardware implementation of the proposed algorithms could be developed and tested. This can be achieved at first using a generic digital signal processing development platform. Hardware implementation on a field programmable gate-array can then be developed to provide a prototype for the multiuser receiver.

Appendix A

Derivation of the various MMSE linear filters

In this appendix, proofs for the propositions involving MMSE linear filters are provided. For convenience, the text of the related propositions is also included in this Appendix.

A.1 Optimal MMSE linear filter for the GRP-STMUD-BF receiver

Proposition 1. *The solution to (3.26), giving the optimal MMSE weights for the group-based linear receiver after beamforming is given by the $NK_j \times NK_j$ matrix*

$$\mathbf{M}_{\text{bf},j} = (\mathbf{R}_{jj}\mathbf{R}_{jj}^H + \mathbf{C}_{jj}\mathbf{C}_{jj}^H + \mathbf{T}_{jj}^H\mathbf{R}_{\text{nn}}\mathbf{T}_{jj})^{-1}\mathbf{R}_{jj}^H, \quad (\text{A.1})$$

where

$$\mathbf{R}_{jj} \triangleq \mathbf{T}_{jj}^H \mathbf{T}_{jj}, \quad (\text{A.2})$$

$$\mathbf{C}_{jj} \triangleq \mathbf{T}_{jj}^H \bar{\mathbf{T}}_{jj}. \quad (\text{A.3})$$

Proof. Using the technique in [Ver98], the cost in (3.35) is expanded to give

$$J_{\text{bf},j}(\mathbf{M}) = E(\mathbf{d}_j - \mathbf{M}^H \mathbf{y}_{\text{bf},j})^H (\mathbf{d}_j - \mathbf{M}^H \mathbf{y}_{\text{bf},j}) \quad (\text{A.4})$$

$$= \text{tr}[E(\mathbf{d}_j - \mathbf{M}^H \mathbf{y}_{\text{bf},j})(\mathbf{d}_j - \mathbf{M}^H \mathbf{y}_{\text{bf},j})^H] \quad (\text{A.5})$$

$$= \text{tr}[\mathbf{I} - \mathbf{R}_{jj}^H \mathbf{M} - \mathbf{M}^H \mathbf{R}_{jj} + \mathbf{M}^H \mathbf{Q}_{jj} \mathbf{M}], \quad (\text{A.6})$$

where $\mathbf{Q}_{jj} \triangleq (\mathbf{R}_{jj} \mathbf{R}_{jj}^H + \mathbf{C}_{jj} \mathbf{C}_{jj}^H + \sigma^2 \mathbf{R}_{jj})$ and (A.6) follows from the statistical independence between the information symbols and the noise. Through algebraic manipulations, (A.6) becomes

$$J_{\text{bf},j}(\mathbf{M}) = \text{tr}[\mathbf{I} - \mathbf{R}_{jj} \mathbf{Q}_{jj}^{-1} \mathbf{R}_{jj}^H + (\mathbf{M} - \bar{\mathbf{M}})^H \mathbf{Q}_{jj} (\mathbf{M} - \bar{\mathbf{M}})], \quad (\text{A.7})$$

where $\bar{\mathbf{M}} \triangleq \mathbf{Q}_{jj}^{-1} \mathbf{R}_{jj}^H$. It can be seen from (A.7) that the cost function is minimized when $\mathbf{M} = \bar{\mathbf{M}}$. Therefore the MMSE linear filter matrix is given by

$$\begin{aligned} \mathbf{M}_{\text{bf},j} &= \mathbf{Q}_{jj}^{-1} \mathbf{R}_{jj}^H \\ &= (\mathbf{R}_{jj} \mathbf{R}_{jj}^H + \mathbf{C}_{jj} \mathbf{C}_{jj}^H + \mathbf{T}_{jj}^H \mathbf{R}_{\text{nm}} \mathbf{T}_{jj})^{-1} \mathbf{R}_{jj}^H, \end{aligned} \quad (\text{A.8})$$

as in (3.39). The minimum cost can be expressed by substituting (A.8) in (A.7), which essentially causes the last term of (A.7) to cancel and thus

$$J_{\text{bf},j}(\mathbf{M}_{\text{bf},j}) = \text{tr}[\mathbf{I} - \mathbf{R}_{jj} \mathbf{Q}_{jj}^{-1} \mathbf{R}_{jj}^H]. \quad (\text{A.9})$$

□

A.2 Optimal MMSE linear filter for the GRP STMUD receiver

Proposition 2. *The solution to the group MMSE linear weights optimality criterion of (3.36) is given by the $NK_j \times NK_j$ matrix*

$$\mathbf{M}_{\text{grp},j} = (\mathbf{R}_j \mathbf{R}_j^H + \mathbf{C}_j \mathbf{C}_j^H + \sigma^2 \mathbf{R}_j)^{-1} \mathbf{R}_j^H. \quad (\text{A.10})$$

Proof. Using the technique in [Ver98], and following the derivation for the GRP-STMUD-BF MMSE weights in above, the cost in (3.35) is expanded to give

$$J_{\text{grp},j}(\mathbf{M}) = E(\mathbf{d}_j - \mathbf{M}^H \mathbf{y}_j)^H (\mathbf{d}_j - \mathbf{M}^H \mathbf{y}_j) \quad (\text{A.11})$$

$$= \text{tr}[\mathbf{I} - \mathbf{R}_j^H \mathbf{M} - \mathbf{M}^H \mathbf{R}_j + \mathbf{M}^H \mathbf{Q}_j \mathbf{M}], \quad (\text{A.12})$$

where $\mathbf{Q}_j \triangleq (\mathbf{R}_j \mathbf{R}_j^H + \mathbf{C}_j \mathbf{C}_j^H + \sigma^2 \mathbf{R}_j)$ and (A.12) follows from the statistical independence between the information symbols and the noise. Through algebraic manipulations, (A.12) becomes

$$J_{\text{grp},j}(\mathbf{M}) = \text{tr}[\mathbf{I} - \mathbf{R}_j \mathbf{Q}_j^{-1} \mathbf{R}_j^H + (\mathbf{M} - \bar{\mathbf{M}})^H \mathbf{Q}_j (\mathbf{M} - \bar{\mathbf{M}})], \quad (\text{A.13})$$

where $\bar{\mathbf{M}} \triangleq \mathbf{Q}_j^{-1} \mathbf{R}_j^H$. It can also be seen that the cost function is minimized when $\mathbf{M} = \bar{\mathbf{M}}$. Therefore the linear filter minimizing the MMSE cost function in (A.12) can be expressed as in (A.10) and takes the form

$$\begin{aligned} \mathbf{M}_{\text{grp},j} &= \mathbf{Q}_j^{-1} \mathbf{R}_j^H \\ &= (\mathbf{R}_j \mathbf{R}_j^H + \mathbf{C}_j \mathbf{C}_j^H + \sigma^2 \mathbf{R}_j)^{-1} \mathbf{R}_j^H \end{aligned} \quad (\text{A.14})$$

and the minimum cost is given by

$$J_{\text{grp},j}(\mathbf{M}_{\text{grp},j}) = \text{tr}[\mathbf{I} - \mathbf{R}_j \mathbf{Q}_j^{-1} \mathbf{R}_j^H]. \quad (\text{A.15})$$

□

A.3 Optimal MMSE linear combining weights for user sharing

Proposition 3. *The optimal MMSE weight matrix that minimizes the cost in (3.43) is given by*

$$\begin{aligned} \mathbf{M}_{c,o}^{(k)} &= [\mathbf{M}_{\text{grp}}^{(k)H} (\mathbf{T}\mathbf{T}^H + \sigma^2 \mathbf{I}) \mathbf{M}_{\text{grp}}^{(k)}]^{-1} \mathbf{M}_{\text{grp}}^{(k)H} \mathbf{T}^{(k)} \\ &= [\mathbf{M}_{\text{grp}}^{(k)H} \mathbf{T}\mathbf{T}^H \mathbf{M}_{\text{grp}}^{(k)} + \sigma^2 \mathbf{M}_{\text{grp}}^{(k)H} \mathbf{M}_{\text{grp}}^{(k)}]^{-1} \mathbf{M}_{\text{grp}}^{(k)H} \mathbf{T}^{(k)}, \end{aligned} \quad (\text{A.16})$$

where $\mathbf{T}^{(k)} \triangleq \mathbf{T}(\mathbf{I}_N \otimes \mathbf{e}_k) \in \mathbb{C}^{M(NQ+W-1) \times N}$ contains the columns of \mathbf{T} corresponding to user k only, with \mathbf{e}_k being the elementary vector of dimension $K \times 1$ with value 1 at position k , and

$$\mathbf{M}_{\text{grp}}^{(k)H} \triangleq \begin{bmatrix} (\mathbf{I}_N \otimes \mathbf{e}_{u_{1,k}})^T \mathbf{M}_{\text{grp},1}^H \mathbf{T}_1^H \\ \vdots \\ (\mathbf{I}_N \otimes \mathbf{e}_{u_{N_k,k}})^T \mathbf{M}_{\text{grp},N_k}^H \mathbf{T}_{N_k}^H \end{bmatrix}, \quad \mathbf{M}_{\text{grp}}^{(k)H} \in \mathbb{C}^{NN_k \times M(NQ+W-1)}. \quad (\text{A.17})$$

Proof. Let $\mathbf{R}_{\mathbf{z}\mathbf{d}}^{(k)} \triangleq E[\tilde{\mathbf{z}}^{(k)} \mathbf{d}^{(k)H}]$ and $\mathbf{R}_{\mathbf{z}}^{(k)} \triangleq E[\tilde{\mathbf{z}}^{(k)} \tilde{\mathbf{z}}^{(k)H}]$ be the $NN_k \times N$ cross-correlation and $NN_k \times NN_k$ correlation matrices, respectively. The cost function (3.43) can then be

expanded to give

$$J_c^{(k)}(\mathbf{M}_c) = E [(\mathbf{d}^{(k)} - \mathbf{M}_c^H \tilde{\mathbf{z}}^{(k)})^H (\mathbf{d}^{(k)} - \mathbf{M}_c^H \tilde{\mathbf{z}}^{(k)})] \quad (\text{A.18})$$

$$= \text{tr}[\mathbf{I} - \mathbf{M}_c^H \mathbf{R}_{\mathbf{z}\mathbf{d}}^{(k)} - \mathbf{R}_{\mathbf{z}\mathbf{d}}^{(k)H} \mathbf{M}_c + \mathbf{M}_c^H \mathbf{R}_{\mathbf{z}}^{(k)} \mathbf{M}_c]. \quad (\text{A.19})$$

The cross-correlation matrix is obtained by considering its j^{th} $N \times N$ block:

$$E[\mathbf{z}_j^{(k)} \mathbf{d}^{(k)H}] = (\mathbf{I}_N \otimes \mathbf{e}_{u_{j,k}})^T E[\mathbf{z}_j \mathbf{d}^{(k)H}] \quad (\text{A.20})$$

$$= (\mathbf{I}_N \otimes \mathbf{e}_{u_{j,k}})^T \mathbf{M}_{\text{grp},j}^H \mathbf{T}_j^H \mathbf{T} E[\mathbf{d}\mathbf{d}^{(k)H}] \quad (\text{A.21})$$

$$= (\mathbf{I}_N \otimes \mathbf{e}_{u_{j,k}})^T \mathbf{M}_{\text{grp},j}^H \mathbf{T}_j^H \mathbf{T}^{(k)}, \quad (\text{A.22})$$

where in (A.21) the cross-term has been canceled, and (A.22) follows from $E[\mathbf{d}\mathbf{d}^{(k)H}] = (\mathbf{I}_N \otimes \mathbf{e}_k)$. The index $u_{j,k}$ is defined below equation (3.41). Stacking the N_k blocks together, the cross-correlation matrix then becomes

$$\mathbf{R}_{\mathbf{z}\mathbf{d}}^{(k)} = \mathbf{M}_{\text{grp}}^{(k)H} \mathbf{T}^{(k)}, \quad (\text{A.23})$$

where $\mathbf{M}_{\text{grp}}^{(k)} \in \mathbb{C}^{M(NQ+W-1) \times NN_k}$ is defined in (A.17). Note that the \mathbf{T}_j^H term in (A.22) has been absorbed in $\mathbf{M}_{\text{grp}}^{(k)}$ to simplify the presentation. It can be shown that the (p, q) , $p, q \in \{1, \dots, N_k\}$, $N \times N$ block of correlation matrix $\mathbf{R}_{\mathbf{z}}^{(k)}$ in (A.19) is given by

$$E[\mathbf{z}_p^{(k)} \mathbf{z}_q^{(k)}] = (\mathbf{I}_N \otimes \mathbf{e}_{u_{p,k}})^T \mathbf{M}_{\text{grp},p}^H \mathbf{T}_p^H \mathbf{R}_{\mathbf{x}} \mathbf{T}_q \mathbf{M}_{\text{grp},q} (\mathbf{I}_N \otimes \mathbf{e}_{u_{q,k}}), \quad (\text{A.24})$$

where $\mathbf{R}_{\mathbf{x}} \triangleq E[\mathbf{x}\mathbf{x}^H]$. We obtain $\mathbf{R}_{\mathbf{z}}^{(k)}$ by combining the blocks in (A.24):

$$\mathbf{R}_{\mathbf{z}}^{(k)} = \mathbf{M}_{\text{grp}}^{(k)H} (\mathbf{T}\mathbf{T}^H + \sigma^2 \mathbf{I}) \mathbf{M}_{\text{grp}}^{(k)}. \quad (\text{A.25})$$

Finally, using the well-known property of MMSE linear estimator (see e.g. [Hay02]), the weight matrix that minimizes the cost in (3.43) is given by

$$\mathbf{M}_{\text{c,o}}^{(k)} = \mathbf{R}_{\mathbf{z}}^{(k)-1} \mathbf{R}_{\mathbf{zd}}^{(k)} \quad (\text{A.26})$$

$$= [\mathbf{M}_{\text{grp}}^{(k)H} (\mathbf{T}\mathbf{T}^H + \sigma^2 \mathbf{I}) \mathbf{M}_{\text{grp}}^{(k)}]^{-1} \mathbf{M}_{\text{grp}}^{(k)H} \mathbf{T}^{(k)}, \quad (\text{A.27})$$

which completes the proof. \square

A.4 Optimal MMSE linear weights for the single-stage GRP-SIC

Proposition 4. *The solution to (4.6), giving the optimal MMSE weights for the group-based SIC receiver is given by the $NK_j \times NK_j$ matrix*

$$\mathbf{M}_{\text{sic},j} = (\mathbf{R}_j \mathbf{R}_j^H + \tilde{\mathbf{C}}_j \tilde{\mathbf{C}}_j^H + \sigma^2 \mathbf{R}_j)^{-1} \mathbf{R}_j^H, \quad (\text{A.28})$$

where $\mathbf{R}_j = \mathbf{T}_j^H \mathbf{T}_j$ was previously defined in (3.28), and $\tilde{\mathbf{C}}_j$ is given by

$$\tilde{\mathbf{C}}_j \triangleq \mathbf{T}_j^H \tilde{\mathbf{T}}_j, \quad (\text{A.29})$$

where $\tilde{\mathbf{T}}_j$ denotes the columns of \mathbf{T} associated to the users of the groups that have not been detected yet, i.e.:

$$\tilde{\mathbf{T}}_j \triangleq [\mathbf{T}_{j+1}, \dots, \mathbf{T}_G]. \quad (\text{A.30})$$

Proof. This proof is similar to the proofs in Section A.1 and A.2. Assuming perfect symbol estimation and thus using the exact value \mathbf{d}_l instead of the estimate $\hat{\mathbf{d}}_{\text{sic},l}$ in (4.5), the error

signal for group j can be expressed as

$$\boldsymbol{\xi}_j = \mathbf{y} - \mathbf{T}^H \sum_{l=1}^{j-1} \mathbf{T}_l \mathbf{d}_l \quad (\text{A.31})$$

$$= \mathbf{T}^H (\mathbf{T}_j \mathbf{d}_j + \sum_{l=j+1}^G \mathbf{T}_l \mathbf{d}_l + \mathbf{n}) \quad (\text{A.32})$$

$$= \mathbf{T}^H (\mathbf{T}_j \mathbf{d}_j + \tilde{\mathbf{T}}_j \tilde{\mathbf{d}}_j + \mathbf{n}), \quad (\text{A.33})$$

where $\tilde{\mathbf{T}}_j$ contains the columns of \mathbf{T} associated the groups *after* group j as defined in (A.30), and $\tilde{\mathbf{d}}_j$ is defined as

$$\tilde{\mathbf{d}}_j \triangleq [\mathbf{P}_{j+1}, \dots, \mathbf{P}_G]^T \mathbf{d}. \quad (\text{A.34})$$

Using (A.31) in (4.4), the cost function for the GRP-SIC receiver becomes

$$J_{\text{sic},j}(\mathbf{M}) = E(\mathbf{d}_j - \mathbf{M}^H \mathbf{P}_j^T \boldsymbol{\xi}_j)^H (\mathbf{d}_j - \mathbf{M}^H \mathbf{P}_j^T \boldsymbol{\xi}_j) \quad (\text{A.35})$$

$$= \text{tr}[\mathbf{I} - \mathbf{R}_j^H \mathbf{M} - \mathbf{M}^H \mathbf{R}_j + \mathbf{M}^H \mathbf{Q}_{\text{sic},j} \mathbf{M}], \quad (\text{A.36})$$

where (A.36) follows from the statistical independence between the information symbols and the noise, and

$$\mathbf{Q}_{\text{sic},j} \triangleq \mathbf{R}_j \mathbf{R}_j^H + \tilde{\mathbf{C}}_j \tilde{\mathbf{C}}_j^H + \sigma^2 \mathbf{R}_j \quad (\text{A.37})$$

with $\tilde{\mathbf{C}}_j$ defined in (A.29). Through algebraic manipulations, (A.36) can be expressed as

$$J_{\text{sic},j}(\mathbf{M}) = \text{tr}[\mathbf{I} - \mathbf{R}_j \mathbf{Q}_{\text{sic},j}^{-1} \mathbf{R}_j^H + (\mathbf{M} - \bar{\mathbf{M}})^H \mathbf{Q}_{\text{sic},j} (\mathbf{M} - \bar{\mathbf{M}})], \quad (\text{A.38})$$

where $\bar{\mathbf{M}} \triangleq \mathbf{Q}_{\text{sic},j}^{-1} \mathbf{R}_j^H$. It can also be seen that the cost function is minimized when $\mathbf{M} = \bar{\mathbf{M}}$.

Therefore the linear filter minimizing the MMSE cost function in (A.36) can be expressed

as in (A.28) and takes the form

$$\begin{aligned} \mathbf{M}_{\text{sic},j} &= \mathbf{Q}_{\text{sic},j}^{-1} \mathbf{R}_j^H \\ &= (\mathbf{R}_j \mathbf{R}_j^H + \tilde{\mathbf{C}}_j \tilde{\mathbf{C}}_j^H + \sigma^2 \mathbf{R}_j)^{-1} \mathbf{R}_j^H \end{aligned} \quad (\text{A.39})$$

and the minimum cost is given by

$$J_{\text{sic},j}(\mathbf{M}_{\text{sic},j}) = \text{tr}[\mathbf{I} - \mathbf{R}_j \mathbf{Q}_{\text{sic},j}^{-1} \mathbf{R}_j^H]. \quad (\text{A.40})$$

□

Appendix B

Complexity analysis

In this Appendix, the complexity associated to solving a complex linear system with a block Toeplitz and Hermitian structure is derived, in terms of complex floating point operations (CFLOPS). The block Toeplitz system matrix has the following form:

$$\mathbf{A} \triangleq \begin{bmatrix} \mathbf{A}_1 & \mathbf{A}_2^H & \cdots & \mathbf{A}_d^H & & & \\ \mathbf{A}_2 & \mathbf{A}_1 & \ddots & & \ddots & & \\ \vdots & \ddots & \ddots & & & & \mathbf{A}_d^H \\ \mathbf{A}_d & & & & \ddots & & \vdots \\ & \ddots & & \ddots & \ddots & & \mathbf{A}_2^H \\ & & \mathbf{A}_d & \cdots & \mathbf{A}_2 & \mathbf{A}_1 & \end{bmatrix}, \quad (\text{B.1})$$

where $\mathbf{A} \in \mathbb{C}^{NK \times NK}$, $\mathbf{A}_j \in \mathbb{C}^{K \times K}$ for $j = 1, \dots, N$, and \mathbf{A}_1 is Hermitian so that \mathbf{A} is also Hermitian. The system matrix \mathbf{A} has N block rows and columns.

For the last column, when $m = l$, the cost consists of $l - 1$ Hermitian matrix products and additions, and one Cholesky factorization, all of dimension $K \times K$. So the total cost may be approximated as

$$\mathcal{C}_{\text{chol}, l \leq d} \approx \sum_{l=1}^d K^3 l(l+1) + (l-1) \left(K^3 + \frac{K^2}{2} - \frac{K}{2} \right) + (l-1) \frac{K(K+1)}{2} + \frac{K^3}{3} \quad (\text{B.5})$$

$$= \frac{dK^3}{3} + d(d-1) \left[(d+1) \frac{K^3}{3} + \frac{K^3}{2} + \frac{K^2}{2} + \frac{K}{4} \right]. \quad (\text{B.6})$$

Using the same approach, it can be shown that the total cost for the case $l > d$ takes the form

$$\mathcal{C}_{\text{chol}, l > d} \approx (N-d) \left[\frac{K^3}{3} + (d-1) \left((d+1)K^3 + K^2 \right) \right]. \quad (\text{B.7})$$

The total cost for Cholesky factorization of the block Toeplitz matrix with d diagonals in (B.1) can finally be expressed as

$$\mathcal{C}_{\text{chol}} \approx \frac{NK^3}{3} + (d-1) \left[\left(\left(N - \frac{d}{2} \right) (d+1) + \frac{d}{2} \right) K^3 + \left(N - \frac{d}{2} \right) K^2 + \frac{dK}{4} \right]. \quad (\text{B.8})$$

For the special case of a block diagonal matrix ($d = 1$), it can be observed that the cost becomes $NK^3/3$, which is the cost of N Cholesky factorizations of dimension $K \times K$, as expected. Also, for the case $d = 2$, which corresponds to 1 set of block off-diagonal, the cost can be approximated for large N and K as

$$\mathcal{C}_{\text{chol}, 2} \approx \frac{10NK^3}{3}. \quad (\text{B.9})$$

B.2 Block triangular backsubstitution

The backsubstitution allows to efficiently solve the following linear system

$$\mathbf{L}\mathbf{x} = \mathbf{y}, \quad (\text{B.10})$$

where \mathbf{x} is the vector to solve and \mathbf{y} is the data vector. Let \mathbf{x} and \mathbf{y} be partitioned in N blocks of K elements each, such that $\mathbf{x} = [\mathbf{x}_1^T, \mathbf{x}_2^T, \dots, \mathbf{x}_N^T]^T$ and $\mathbf{y} = [\mathbf{y}_1^T, \mathbf{y}_2^T, \dots, \mathbf{y}_N^T]^T$, where each complex vectors \mathbf{x}_l and \mathbf{y}_l for $l = 1, \dots, N$ have dimension K .

Using (B.10), the structure of \mathbf{L} in (B.3) and the vector notation above, it can be shown that for the first $l \leq d$ block, the following equation holds:

$$\mathbf{L}_{l,l}\mathbf{x}_l = \mathbf{y}_l - \sum_{k=1}^{l-1} \mathbf{L}_{l,k}\mathbf{x}_k \quad l = 1, \dots, d. \quad (\text{B.11})$$

The cost associated to solving (B.11) consists of the cost of $l - 1$ $K \times K$ complex matrix-vector product, $l - 1$ vector additions of dimension K , and one backsubstitution of dimension K . The total complexity for $l \leq d$ can thus be expressed as

$$\mathcal{C}_{\text{bs}, l \leq d} \approx \sum_{l=1}^d (2l + 1)K^2 \quad (\text{B.12})$$

$$= d^2 K^2. \quad (\text{B.13})$$

The same approach can be used to calculate the cost for the case $l > d$. The complexity in terms of CFLOPS can be expressed as

$$\mathcal{C}_{\text{bs}, l \geq d} \approx (N - d)(2d - 1)K^2. \quad (\text{B.14})$$

Thus the total cost for solving the system in (B.10) using block backsubstitution, with Cholesky factor \mathbf{L} having d block-diagonals as in (B.3), can finally be expressed as

$$\mathcal{C}_{\text{bs}} = NK^2(2d - 1) - d(d - 1)K^2. \quad (\text{B.15})$$

Again, notice that for $d = 1$, the cost is equivalent to N backsubstitutions, and for the practical case $d = 2$ the cost becomes

$$\mathcal{C}_{\text{bs},2} = K^2(3N - 2) \approx 3NK^2. \quad (\text{B.16})$$

Finally, note that to solve a linear system two backsubstitutions are needed (see e.g.: [GVL96]).

Appendix C

Exact bit-error probability for BPSK

The exact bit error rate can be used to evaluate the performance of the proposed receiver. For each block, N symbols are transmitted per user, with a possibly different probability of error for each. Consider the general case where $\mathbf{z}_{k,n} = \mathbf{m}_{k,n}^H \mathbf{y}$ is the soft estimate for the n^{th} symbol of user k and where $\mathbf{m}_{k,n}$ is the associated total linear filter vector. Then the error probability for BPSK transmission can be expressed as

$$P_e^{(k,n)} = P(\text{Re}(\mathbf{z}_{k,n}) < 0 | b_{k,n} = 1) \quad (\text{C.1})$$

$$= \frac{1}{2^{NK}} \sum_{\substack{\forall \mathbf{b} \\ \mathbf{b}_{k,n}=1}} \text{erfc} \left(\frac{\text{Re}(\mathbf{z}_{k,n})}{\sigma \sqrt{2\mathbf{m}_{k,n}^H \mathbf{T}^H \mathbf{T} \mathbf{m}_{k,n}}} \right), \quad (\text{C.2})$$

where $b_{k,n}$ is the n^{th} symbol transmitted by user k and $\text{erfc}(\cdot)$ is the complementary error function [Pro01]. The BER expression in (C.2) can be used for any linear receiver by replacing the total linear filter $\mathbf{m}_{k,n}$ by the appropriate vector (e.g.: columns of \mathbf{M}_o in (2.27) for the full STMUD receiver).

References

- [3GPa] 3GPP TS 25.102 V7.7.0, “User Equipment (UE) radio transmission and reception (TDD),” (see also <http://www.3gpp.org>).
- [3GPb] 3GPP TS 25.201 V7.3.0, “Physical Layer - General Description,” (see also <http://www.3gpp.org>).
- [And05] J. G. Andrews, “Interference cancellation for cellular systems: a contemporary overview,” *IEEE Wireless Commun. Mag.*, vol. 12, no. 2, pp. 19–29, Apr. 2005.
- [Axe94] O. Axelsson, *Iterative Solution Methods*. Cambridge University Press, 1994.
- [BCMw00] R. M. Buehrer, N. S. Correal-Mendoza, and B. D. Woerner, “A simulation comparison of multiuser receivers for cellular CDMA,” *IEEE Trans. Veh. Technol.*, vol. 49, no. 4, pp. 1065–1085, Jul. 2000.
- [Ber05] D. S. Bernstein, *Matrix Mathematics*. Princeton University Press, 2005.
- [BMV⁺01] D. R. Brown, III, M. Motani, V. V. Veeravalli, H. V. Poor, and C. R. Johnson, Jr., “On the performance of linear parallel interference cancellation,” *IEEE Trans. Inform. Theory*, vol. 47, no. 5, pp. 1957–1970, Jul. 2001.
- [BSZ06] A. Bentrchia, A. U. Sheikh, and A. Zerguine, “A new ordering and grouping algorithm for the linear weighted group matched filter successive interference cancellation detector,” *IEEE Trans. Veh. Technol.*, vol. 55, no. 2, pp. 704–709, March 2006.
- [BZSB07] A. Bentrchia, A. Zerguine, A. U. Sheikh, and M. Benyoucef, “A new linear group-wise SIC multiuser detector,” *IEEE Commun. Lett.*, vol. 11, no. 2, pp. 176–178, Feb. 2007.
- [BZSS03] A. Bentrchia, A. Zerguine, A. U. Sheikh, and W. A. Saif, “A linear group polynomial-expansion successive interference cancellation detector,” in *Proc. IEEE 14th Int. Symposium on Personal, Indoor and Mobile Radio Communications*, vol. 2, Beijing, China, Sep. 2003, pp. 1546–1550.

- [CB04] P. Chitrapu and A. Briancon, *Wideband TDD: WCDMA for the Unpaired Spectrum*. Wiley, 2004.
- [CBW99] N. S. Correal, R. M. Buehrer, and B. D. Woerner, “A DSP-based DS-CDMA multiuser receiver employing partial parallel interference cancellation,” *IEEE J. Select. Areas Commun.*, vol. 17, no. 4, pp. 613–630, Apr. 1999.
- [CP05] C. Comaniciu and H. V. Poor, “Capacity regions and optimal power allocation for groupwise multiuser detection,” *IEEE Trans. Commun.*, vol. 4, no. 2, pp. 349–352, March 2005.
- [DSR98] D. Divsalar, M. K. Simon, and D. Raphaeli, “Improved parallel interference cancellation for CDMA,” *IEEE Trans. Commun.*, vol. 46, no. 2, pp. 258–268, Feb. 1998.
- [ECS+98] R. B. Ertel, P. Cardieri, K. W. Sowerby, T. S. Rappaport, and J. H. Reed, “Overview of spatial channel models for antenna array communication systems,” *IEEE Personal Commun. Mag.*, vol. 5, no. 1, pp. 10–22, Feb. 1998.
- [ETS98] ETSI, “Universal Mobile Telecommunications System (UMTS); Selection procedures for the choice of radio transmission technologies of the UMTS,” European Telecommunications Standard Institute (ETSI), Tech. Rep. TR 101 112, 1998.
- [Fal98] E. Falkenauer, *Genetic Algorithms and Grouping Problems*. John Wiley & Sons, 1998.
- [FFT04] L. Fety, D. Z. Filho, and M. Terre, “A comparison of chip rate MMSE and symbol rate MMSE in multiuser uplink long code DS-CDMA,” in *Proc. IEEE 5th Workshop on Signal Processing Advances in Wireless Communications*, Lisbon, Portugal, Jul. 2004, pp. 497–501.
- [GHB00] B. Göransson, B. Hagerman, and J. Barta, “Adaptive antennas in WCDMA systems - link level simulation results based on typical user scenarios,” in *Proc. IEEE 52nd Veh. Technol. Conf. Fall*, vol. 1, Boston, MA, USA, Sep. 2000, pp. 157–164.
- [GL03] Z. Guo and K. B. Letaief, “Adaptive MMSE receiver with beamforming for DS/CDMA systems,” *IEEE Trans. Wireless Commun.*, vol. 2, no. 4, pp. 605–610, Jul. 2003.
- [God97] L. C. Godara, “Application of antenna arrays to mobile communications, part II: Beam-forming and direction-of-arrival considerations,” *Proc. IEEE*, vol. 85, no. 8, pp. 1195–1245, Aug. 1997.

- [GRSL00] D. Guo, L. K. Rasmussen, S. Sun, and T. J. Lim, "A matrix-algebraic approach to linear parallel interference cancellation in CDMA," *IEEE Trans. Commun.*, vol. 48, no. 1, pp. 152–161, Jan. 2000.
- [GS01] A. Grant and C. Schlegel, "Convergence of linear interference cancellation multiuser receivers," *IEEE Trans. Commun.*, vol. 49, no. 10, pp. 1824–1834, Oct. 2001.
- [GVL96] G. H. Golub and C. F. Van Loan, *Matrix Computations*, 3rd ed. The John Hopkins University Press, 1996.
- [Hat80] M. Hata, "Empirical formula for propagation loss in land mobile radio services," *IEEE Trans. Veh. Technol.*, vol. 29, no. 3, pp. 317–325, Aug. 1980.
- [Hay02] S. S. Haykin, *Adaptive Filter Theory*, 4th ed. Prentice Hall, 2002.
- [HBP03] W. Ha, J. Bae, and J. Park, "Interference cancellation receiver using group-wise decorrelation for W-CDMA downlink," in *Proc. IEEE 14th Int. Symposium on Personal, Indoor and Mobile Radio Communications*, vol. 3, Beijing, China, Sep. 2003, pp. 2125–2129.
- [HJ90] R. A. Horn and C. R. Johnson, *Matrix Analysis*. Cambridge University Press, 1990.
- [HKK⁺00] M. Haardt, A. Klein, R. Koehn, S. Oestreich, M. Purat, V. Sommer, and T. Ulrich, "The TD-CDMA based UTRA TDD mode," *IEEE J. Select. Areas Commun.*, vol. 18, no. 8, pp. 1375–1385, Aug. 2000.
- [HL00] S. H. Han and J. H. Lee, "Performance of multi-rate DS-SS-CDMA system with multi-stage partial parallel interference cancellation," in *Proc. IEEE 51st Veh. Technol. Conf. Spring*, vol. 2, Tokyo, Japan, May 2000, pp. 765–769.
- [HSMTG00] C. Z. W. Hassell Sweatman, B. Mulgrew, J. S. Thompson, and P. M. Grant, "Multiuser detection for CDMA antenna array receivers using spatial equivalence classes," in *IEE Proc. on Communications*, vol. 147, no. 2, Apr. 2000, pp. 105–113.
- [HW05] Y.-T. Hsieh and W.-R. Wu, "Optimal two-stage decoupled partial PIC receivers for multiuser detection," *IEEE Trans. Wireless Commun.*, vol. 4, no. 1, pp. 112–127, Jan. 2005.
- [JR98] A.-L. Johansson and L. K. Rasmussen, "Linear group-wise successive interference cancellation in CDMA," in *Proc. IEEE 5th Int. Symposium on Spread Spectrum Techniques and Applications*, vol. 1, Sun City, South Africa, Sep. 1998, pp. 121–126.

- [KGNH99] S. Kapoor, S. Gollamudi, S. Nagaraj, and Y.-F. Huang, "Adaptive multiuser detection and beamforming for interference suppression in CDMA mobile radio systems," *IEEE Trans. Veh. Technol.*, vol. 48, no. 5, pp. 1341–1355, Sep. 1999.
- [KKB96] A. Klein, G. K. Kaleh, and P. W. Baier, "Zero forcing and minimum mean-square-error equalization for multiuser detection in code-division multiple-access channels," *IEEE Trans. Veh. Technol.*, vol. 45, no. 2, pp. 276–287, May 1996.
- [KYL00] H.-L. Ko, B.-W. Yu, and J. H. Lee, "A switched beamforming system with multiuser detectors," in *Proc. IEEE 51st Veh. Technol. Conf. Spring*, vol. 2, Tokyo, Japan, May 2000, pp. 705–709.
- [LG94] A. Leon-Garcia, *Probability and Random Processes for Electrical Engineering*, 2nd ed. Addison Wesley, 1994.
- [LGH00] G. Lehmann, C. Gessner, and M. Haardt, "Evaluation of link-level performance improvements by using smart antennas for the TD-CDMA based UTRA TDD mobile radio system," in *Proc. IEEE 52nd Veh. Technol. Conf. Fall*, vol. 3, Boston, MA, USA, Sep. 2000, pp. 1328–1332.
- [LLC01] J. Li, K. B. Letaief, and Z. Cao, "A group oriented multiuser detection with beamforming for multicarrier CDMA systems," in *Proc. IEEE Global Telecommunications Conference*, vol. 2, San Antonio, TX, USA, Nov. 2001, pp. 733–737.
- [LLC05] J. Li, K. Letaief, and Z. Cao, "Space-time turbo multiuser detection for coded MC-CDMA," *IEEE Trans. Wireless Commun.*, vol. 4, no. 2, pp. 538–549, March 2005.
- [LPO02] J. H. Lee, J. J. Park, and H. S. Oh, "Comparison of BER performance of WCDMA/TDD based optimum combining and beamforming in angular spread channel," in *Proc. 5th Int. Symposium on Wireless Personal Multimedia Communications*, vol. 1, Honolulu, Hawaii, Oct. 2002, pp. 172–176.
- [LPWL03] K. Luo, K. Pattipati, P. Willett, and G. Levchuk, "Optimal grouping algorithm for a group decision feedback detector in synchronous CDMA communications," *IEEE Trans. Commun.*, vol. 51, no. 3, pp. 341–346, Mar. 2003.
- [LR99] J. C. Liberti Jr. and T. S. Rappaport, *Smart Antennas for Wireless Communications: IS-95 and Third Generation CDMA Applications*. Prentice Hall, 1999.

- [LS03] K.-C. Lai and J. J. Shynk, "Performance evaluation of a generalized linear SIC for DS/CDMA signals," *IEEE Trans. Signal Processing*, vol. 51, no. 6, pp. 1604–1614, June 2003.
- [MG00] J. Ma and H. Ge, "Groupwise successive interference cancellation for multi-rate CDMA based on MMSE criterion," in *Proc. IEEE Int. Conference on Communications*, vol. 2, New Orleans, LA, USA, Jun. 2000, pp. 1174–1178.
- [MH94] U. Madhow and M. L. Honig, "MMSE interference suppression for direct-sequence spread-spectrum CDMA," *IEEE Trans. Commun.*, vol. 42, no. 12, pp. 3178–3188, Dec. 1994.
- [Mos96] S. Moshavi, "Multi-user detection for DS-CDMA communications," *IEEE Commun. Mag.*, vol. 34, no. 10, pp. 124–136, Oct. 1996.
- [MVU01] S. Marinkovic, B. Vucetic, and A. Ushirokawa, "Space-time iterative and multistage receiver structures for CDMA mobile communication systems," *IEEE J. Select. Areas Commun.*, vol. 19, no. 8, pp. 1594–1604, Aug. 2001.
- [PC05] B. Pelletier and B. Champagne, "Group optimal space-time MUD with beamforming," in *Proc. IEEE 61st Veh. Technol. Conf. Spring*, vol. 2, Stockholm, Sweden, May 2005, pp. 1323–1327.
- [PC06a] —, "Group-based block linear successive interference cancellation for DS-CDMA," in *Proc. IEEE Global Telecommunications Conference*, San Francisco, CA, USA, Nov. 2006.
- [PC06b] —, "Group-based linear parallel interference cancellation for DS-CDMA systems," in *Proc. IEEE 64th Veh. Technol. Conf. Fall*, Montréal, Canada, Sep. 2006.
- [PC06c] —, "Group-optimal linear space-time multiuser detection," in *Proc. IEEE Canadian Conference on Electrical and Computer Engineering*, Ottawa, Canada, May 2006, pp. 1761–1765.
- [PC07] —, "Group-based space-time multiuser detection with user sharing," *IEEE Trans. Wireless Commun.*, vol. 6, no. 6, pp. 2034–2039, Jun. 2007.
- [PH94] P. Patel and J. Holtzman, "Analysis of a simple successive interference cancellation scheme in a DS/CDMA system," *IEEE J. Select. Areas Commun.*, vol. 12, no. 5, pp. 796–807, Jun. 1994.
- [PK00] J. W. Park and K. S. Kwak, "Multiuser detection scheme using adaptive antenna array over Rayleigh fading channels," in *Proc. IEEE 51st Veh. Technol. Conf. Spring*, vol. 3, Tokyo, Japan, May 2000, pp. 2157–2161.

- [Pro01] J. G. Proakis, *Digital Communications*, 4th ed. McGraw-Hill, 2001.
- [PTVF92] W. H. Press, S. A. Teukolsky, W. T. Vetterling, and B. P. Flannery, *Numerical Recipes in C*, 2nd ed. Cambridge, 1992.
- [PVBB03] K. Puttegowda, G. Verma, S. Bali, and R. M. Buehrer, "On the effect of cancellation order in successive interference cancellation for CDMA systems," in *Proc. IEEE 58th Veh. Technol. Conf. Fall*, vol. 2, Orlando, FL, USA, Oct. 2003, pp. 1035–1039.
- [Rap02] T. S. Rappaport, *Wireless Communications Principles and Practice*, 2nd ed. Prentice Hall, 2002.
- [RC02] R. Radhakrishnan and J. J. Caffery, "Comparison of codirectional reception using beamforming, switched beams and multiuser detection strategies in WCDMA systems," in *Proc. IEEE 56th Veh. Technol. Conf. Fall*, vol. 2, Vancouver, Canada, Sep. 2002, pp. 651–655.
- [RLJ00] L. K. Rasmussen, T. J. Lim, and A. Johansson, "A matrix-algebraic approach to successive interference cancellation in CDMA," *IEEE Trans. Commun.*, vol. 48, no. 1, pp. 145–151, Jan. 2000.
- [SB93] B. Steiner and P. W. Baier, "Low cost channel estimation in the up-link receiver of CDMA radio systems," *FREQUENZ*, vol. 47, pp. 292–298, Nov./Dec. 1993.
- [SB00a] L. Shao and G. Bi, "A dynamic groupwise successive interference cancellation array receiver scheme for DS-CDMA systems," in *Proc. IEEE Wireless Communications and Networking Conference*, vol. 1, Chicago, IL, USA, Sep. 2000, pp. 343–346.
- [SB00b] —, "A new groupwise successive interference cancellation array receiver scheme for DS-CDMA systems," in *Proc. IEEE 6th Int. Symposium on Spread Spectrum Techniques and Applications*, vol. 1, Parsippany, NJ, USA, Sep. 2000, pp. 11–14.
- [SC00] A. Stéphenne and B. Champagne, "Effective multi-path vector channel simulator for antenna array systems," *IEEE Trans. Veh. Technol.*, vol. 49, no. 6, pp. 2370–2381, Nov. 2000.
- [Sed88] R. Sedgewick, *Algorithms*. Addison-Wesley, 1988.
- [Sk197] B. Sklar, "Rayleigh fading channels in mobile digital communication systems part I: Characterization," *IEEE Commun. Mag.*, vol. 35, no. 9, pp. 136–146, Sep. 1997.

- [TR04] P. H. Tan and L. K. Rasmussen, "Multiuser detection in CDMA – a comparison of relaxations, exact, and heuristic search methods," *IEEE Trans. Wireless Commun.*, vol. 3, no. 5, pp. 1802–1809, Sep. 2004.
- [UM99] Z. A. Uzmi and S. A. Mujtaba, "Performance analysis of a convolutionally-encoded synchronous CDMA system with adaptive beamforming and linear multiuser detection," in *Conf. Rec. 33rd Asilomar Conference on Signals, Systems, and Computers*, vol. 2, Pacific Grove, CA, USA, Oct. 1999, pp. 950–954.
- [Var95] M. K. Varanasi, "Group detection for synchronous Gaussian code-division multiple-access channels," *IEEE Trans. Inform. Theory*, vol. 41, no. 4, pp. 1083–1096, July 1995.
- [Var96] —, "Parallel group detection for synchronous CDMA communication over frequency-selective Rayleigh fading channels," *IEEE Trans. Inform. Theory*, vol. 42, no. 1, pp. 116–128, Jan. 1996.
- [Ver98] S. Verdú, *Multiuser Detection*. Cambridge: Cambridge University Press, 1998.
- [VHG01] M. Vollmer, M. Haardt, and J. Götze, "Comparative study of joint-detection techniques for TD-CDMA based mobile radio systems," *IEEE J. Select. Areas Commun.*, vol. 19, no. 8, pp. 1461–1475, Aug. 2001.
- [Vit90] A. J. Viterbi, "Very low rate convolution codes for maximum theoretical performance of spread-spectrum multiple-access channels," *IEEE J. Select. Areas Commun.*, vol. 8, no. 4, pp. 641–649, May 1990.
- [VT02] H. L. Van Trees, *Detection, Estimation, and Modulation Theory, Part IV, Optimum Array Processing*. John Wiley & Sons, 2002.
- [WHM99] X. Wang and A. Høst-Madsen, "Group-blind multiuser detection for uplink CDMA," *IEEE J. Select. Areas Commun.*, vol. 17, no. 11, pp. 1971–1984, Nov. 1999.
- [WRHR02] G. Woodward, R. Ratasuk, M. L. Honig, and P. B. Rapajic, "Minimum mean-squared error multiuser decision-feedback detectors for DS-SS-CDMA," *IEEE Trans. Commun.*, vol. 50, no. 12, pp. 2104–2112, Dec. 2002.
- [XWLNT99] G. Xue, J. Weng, T. Le-Ngoc, and S. Tahar, "Adaptive multistage parallel interference cancellation for CDMA," *IEEE J. Select. Areas Commun.*, vol. 17, no. 10, pp. 1815–1827, Oct. 1999.

- [YYU02] A. Yener, R. D. Yates, and S. Ulukus, "Combined multiuser detection and beamforming for CDMA systems: Filter structures," *IEEE Trans. Veh. Technol.*, vol. 51, no. 5, pp. 1087–1095, Sep. 2002.
- [ZB03] W. Zha and S. D. Blostein, "Soft-decision multistage multiuser interference cancellation," *IEEE Trans. Veh. Technol.*, vol. 52, no. 2, pp. 380–389, Mar. 2003.